HOKKAIDO UNIVERSITY

Title	Functions, structures, and applications of enzymes acting on trehalose and its derivatives
Author(s)	田口, 陽大
Degree Grantor	北海道大学
Degree Name	博士(農学)
Dissertation Number	甲第14383号
Issue Date	2021-03-25
DOI	https://doi.org/10.14943/doctoral.k14383
Doc URL	https://hdl.handle.net/2115/84509
Type	doctoral thesis
File Information	Taguchi_Yodai.pdf

Hokkaido University Collection of Scholarly and Academic Papers : HUSCAP

Functions, structures, and applications of enzymes acting on trehalose and its derivatives

（トレハロースおよびその誘導体に作用する酵素の構造，機能ならびに応用に関する研究）

Hokkaido University　Graduate School of Agriculture

Division of Applied Bioscience　　Doctor course

Yodai Taguchi

北海道大学　大学院農学院

応用生物科学専攻　博士後期課程

田口　陽大

CONTENTS

1. General introduction 1

1.1. Trehalose and its biosynthesis 1
1.2. Physiological functions of trehalose in plants 3
1.3. Physiological functions of Tre6*P* 4
1.4. Synthesis methods of trehalose and Tre6*P* 8
1.5. Structures and functions of TPS and TPP 10
1.6. Structures and functions of trehalase 12
1.7. Purpose of this study 14

2. Enzymatic synthesis of Tre6*P* and its derivative using the reverse phosphorolysis catalyzed by trehalose 6-phosphate phosphorylase 19

2.1. Introduction 19
2.2. Materials and methods 21
2.2.1. Materials 21
2.2.2. Preparation of β-Glc1*P* 22
2.2.3. Extraction of genomic DNA of *L. lactis* subsp. *lactis* JCM5805 22
2.2.4. Preparation of recombinant LlTrePP 23
2.2.5. Preparation of recombinant β-PGM from *L. lactis* subsp. *lactis* JCM5805 24
2.2.6. Preparation of recombinant hexose phosphatase from *E. coli* 25
2.2.7. Measurement of protein concentration 26
2.2.8. Blue native polyacrylamide gel electrophoresis (BN-PAGE) 26
2.2.9. Standard activity assay of LlTrePP 27
2.2.10. Measurement of activity for the phosphorolysis of Tre6*P* 27
2.2.11. Evaluation of effects of temperature and pH on activity and stability 27
2.2.12. Determination of kinetic parameters for the reverse phosphorolysis of Tre6*P* 28
2.2.13. Analysis of acceptor specificity in reverse phosphorolysis 29
2.2.14. Activity assay of β-PGM 29
2.2.15. Activity assay of hexose phosphatase 29
2.2.16. Structural analysis of oligosaccharide synthesized from β-Glc1*P* and Man6*P* 30
2.2.17. Quantification of carbohydrates 31
2.2.18. Synthesis of Tre6*P* from β-Glc1*P* and Glc6*P* using TrePP 31
2.2.19. Synthesis of Tre6*P* from maltose and Glc6*P* using TrePP and MP 31
2.2.20. Synthesis of Tre6*P* from maltose and inorganic phosphate by TrePP, MP, and β-

PGM 32
2.3. Results 33
2.3.1. Production, purification, and basic properties of recombinant LlTrePP 33
2.3.2. Kinetic analysis of the reverse phosphorolysis of LlTrePP 34
2.3.3. Synthesis and structural analysis of a novel disaccharide phosphate 35
2.3.4. Tre6*P* synthesis from β-Glc1*P* and Glc6*P* by the reverse phosphorolysis of LlTrePP 35
2.3.5. One-pot synthesis of Tre6*P* from maltose and Glc6*P* by LlTrePP and MP 36
2.3.6. One-pot synthesis of Tre6*P* from maltose and inorganic phospahte and effect of inorganic phosphate concentration 36
2.3.7. Efficiency improvement of Tre6*P* synthesis using yeast 38
2.4. Discussion 40

3. Comprehensive evaluation of enzymatic properties of TPP isozymes from *A. thaliana* 62

3.1. Introduction 62
3.2. Materials and methods 62
3.2.1. Plant 62
3.2.2. Sugar phosphates 63
3.2.3. Preparation of expression plasmids 63
3.2.4. Preparation of recombinant AtTPPs 64
3.2.5. Standard enzyme activity assay 65
3.2.6. Effects of temperature and pH on activity and stability of TPP 65
3.2.7. Effect of detergent on activity of TPP 66
3.2.8. Substrate specificity of TPP 66
3.2.9. Determination of kinetic parameters 67
3.3. Results 67
3.3.1. Comparison of primary structures of TPPs. 67
3.3.2. Preparation of recombinant AtTPPs 68
3.3.3. Kinetic analysis of AtTPPs for the Tre6*P*-dephosphorylation 69
3.3.4. Substrate specificity of AtTPPs 70
3.3.5. Influence of detergent on enzymatic activity of AtTPPB 70
3.4. Discussion 70

4. pH-dependent alteration of substrate specificity of plant trehalase and its molecular mechanism 86

4.1. Introduction 86

4.2. Materials and methods 87
4.2.1. Preparation of expression plasmids for recombinant AtTRE1 derivatives and OsTRE1 87
4.2.2. Preparation of AtTRE1 derivatives 88
4.2.3. Preparation of OsTRE1 89
4.2.4. Trehalases from *E. coli* and pig 90
4.2.5. Preparations of trehalose-like disaccharides 90
4.2.6. Measurement of molecular mass by gel filtration column chromatography 94
4.2.7. Measurement of trehalase activity 94
4.2.8. Kinetic analysis of inhibition of dNAtTRE1 reaction by Tris 94
4.2.9. Effects of pH and temperature on activity and stability 95
4.2.10. Evaluation of substrate specificity 96
4.2.11. MS analysis of the reaction products in $H_2{}^{18}O$ 96
4.2.12. Crystallization and data collection 97
4.2.13. Structure solution and refinement 98
4.3. Results 98
4.3.1. Production and basic properties of recombinant AtTRE1 98
4.3.2. pH dependency of kinetic parameters of dNAtTRE1 for trehalose hydrolysis 99
4.3.3. Substrate specificity 100
4.3.4. Comparison of enzymatic characteristics of OsTRE1 with dNAtTRE1 101
4.3.5. Structural analysis of dNAtTRE1 102
4.3.6. Site-directed mutagenesis at the residues on α1→α2 and α11→α12 loops of dNAtTRE1 105
4.4. Discussion 106

5. General discussion 126

6. References 141

Abberebiations

ABA: abscisic acid

AEC: anion exchange column chromatography

Bicine: *N,N*-bis(2-hydroxyethyl)glycine

BN-PAGE: blue native polyacrylamide gel electrophoresis

BSA: bovine serum albumin

CAZy: carbohydrate-active enzymes database

CHES: *N*-cyclohexyl-2-aminoethanesulfonic acid

Col-0: *Arabidopsis thaliana* ecotype Columbia

COSY: correlated spectroscopy

dNAtTRE1: N-terminal truncated AtTRE1

EcTre37A: periplasmic trehalase of *Escherichia coli*

ESI-MS: electrospray ionization mass spectrometry

Fru6*P*: D-fructose 6-phosphate

FT: FLOWERING LOCUS T

FUL: *FRUITFULL*

FW: fresh weight

Gal6*P*: D-galactose 6-phosphate

GH: Glycoside Hydrolase family

α-GF: α-D-glucopyranosyl fluoride

β-GF: β-D-glucopyranosyl fluoride

β-Glc1*P*: β-D-glucose 1-phosphate

Glcα1-1αMan6*P*: α-D-Glc*p*-(1↔1)-α-D-Man*p*6*P*

Glc6*P*: D-glucose 6-phosphate

GRIK1: GEMINIVIRUS REP-INTERACTING KINASE1

GT: Glycosyltransferase family

HAD: haloacid dehalogenase

HEPES: (2-hydroxyethyl) piperazine-1-ethanesulfonic acid

HMBC: heteronuclear multiple bond correlation

HPAEC-PAD: high-performance anion-exchange chromatography equipped with a pulsed amperometric detector

HSQC: heteronuclear single quantum coherence

HSQC-TOCSY: HSQC-total correlation spectroscopy

H2BC: heteronuclear 2 bond correlation

IPTG: isopropyl β-D-1-thiogalactoside

LB: Luria-Bertani

LlTrePP: TrePP of *Lactococcus lactis* subsp. *lactis*

Man6*P*: D-mannose 6-phosphate

MES: 2-morpholinoethanesulfonic acid

MP: maltose phosphorylase

MS: mass spectrometry

MS medium: Murashige and Skoog medium

NMR: nuclear magnetic resonance

NMWL: nominal molecular weight limit

NP-40: nonidet P-40

NR: nitrate reductase

PEPC: phosphoenolpyruvate carboxylase

β-PGM: β-phosphoglucomutase

PxEclTre: trehalase from *Enterobacter cloacae*

ROS: reactive oxygen species

ScNth1: trehalases from *Saccharomyces cerevisiae*

SnRK1: SUCROSE-NON-FERMENTING1-RELATED PROTEIN KINASE1

SOC1: *SUPPRESSOR OF OVEREXPRESSION OF CONTAINS 1*

SPL: *SQUAMOSA PROMOTER BINDING PROTEIN-LIKE*

SPS: sucrose 6-phosphate synthase

Suc6*P*: sucrose 6-phosphate

TbTP: trehalose phosphorylase from *Thermoanaerobacter brokii*

TP: trehalose phosphorylase

TPP: trehalose 6-phosphate phosphatase

TPS: trehalose 6-phosphate synthase

TPS2PD: C-terminal domain of *Cryptococcus neoformans* TPS2

TrePP: trehalose 6-phosphate phosphorylase

TreS: trehalose synthase

TreT: ADP-glucose:D-glucose 1-α-D-glucosyltransferase

TreY: (1→4)-α-D-glucan 1-α-D-glucosylmutase

TreZ: 4-α-D-{(1→4)-α-D-glucano}trehalose trehalohydrolase

Tre6*P*: trehalose 6-phosphate

Tris: tris-hydroxymethyl aminomethane

TsTP: trehalose phosphorylase from *Thermoanaerobacter siderophilus* DSM12299

WRI1: WRINKLED1

1. General introduction

1.1. Trehalose and its biosynthesis

Trehalose (α-D-Glc*p*-(1↔1)-α-D-Glc*p*, Glcα1-1αGlc) is a non-reducing disaccharide that is used as an energy source and compatible solute in microorganisms, insects, and desiccation-tolerant resurrection plants (Benaroudj et al., 2001; Bonini et al., 2004; Elbein, 1974). It stabilizes cell membranes and proteins in dehydrated and frozen states by hydrogen bonding interaction (Richards et al., 2002) and is involved in tolerance against stresses such as osmotic and oxidative stresses in bacteria and fungi (Cao et al., 2008; Ni and Yu, 2007; Purvis et al., 2005). This disaccharide is more resistant to acid hydrolysis and more stable in aqueous solutions at a high temperature than reducing sugars such as maltose (Richards et al., 2002). Sweetness of trehalose is about 50% of sucrose, and trehalose does not cause the Maillard reaction. These properties are preferable for ingredients of foods and cosmetics, and trehalose is widely utilized in various industries.

Five pathways for trehalose biosynthesis are known (Avonce et al., 2006). The universal trehalose synthesis pathway is the TPS-TPP pathways composed of two reactions, catalyzed by two enzymes, the trehalose 6-phosphate synthase (TPS, EC 2.4.1.15) and trehalose 6-phosphate phosphatase (TPP, EC 3.1.3.12) (Fig. 1-1A) (Cabib and Leloir, 1958). Trehalose 6-phosphate (Tre6*P*, α-D-Glc*p*-(1↔1)-α-D-Glc*p*6*P*), is the intermediate which is synthesized by TPS from UDP-glucose and D-glucose 6-phosphate (Glc6*P*) and is dephosphorylated by TPP. Eukaryotes have only this pathway for trehalose synthesis.

The other four pathways are found only in prokaryotes and archaea. Some archaea such as *Thermococcus litoralis* and *Pyrococcus horikoshii* have ADP-glucose:D-glucose 1-α-D-glucosyltransferase (α,α-trehalose synthase, TreT, EC 2.4.1.245) pathway (Fig. 1-1B). TreT catalyzes the reversible formation of trehalose from nucleotide sugar ADP-glucose and D-glucose (Qu et al., 2004; Ryu et al., 2005). In this reaction, trehalose is directly produced from ADP-glucose and D-

glucose.

Some bacteria and archaea such as *Arthrobacter* sp. and *Sulfolobus solfataricus* possess the two-step pathway catalyzed by two enzymes, (1→4)-α-D-glucan 1-α-D-glucosylmutase (maltooligosyl trehalose synthase, TreY, EC 5.4.99.15) and 4-α-D-{(1→4)-α-D-glucano}trehalose trehalohydrolase (maltooligosyltrehalose trehalohydrolase TreZ, EC 3.2.1.141) (Kato et al., 1996a; Kobayashi et al., 1996a; Lama et al., 1990; Maruta et al., 1996; Nakada et al., 1995a, 1995b; De Smet et al., 2000) (Fig. 1-1C). The first enzyme TreY is a mutase but catalyzes intra-molecule transglycosylation. The α1-4 glucosidic linkage at the reducing terminal is cleaved, and the glycan is transferred to the same glucose but to form an α1-1α linkage. Then the terminal trehalose moiety is released through the hydrolysis catalyzed by TreZ (Kato et al., 1996b; Nakada et al., 1995a, 1995b). Some bacteria including *Pimelobacter* sp. and *Corynebacterium glutamicum* have maltose α-D-glucosyltransferase (trehalose synthase, TreS, EC 5.4.99.16) (Kim et al., 2010; Nishimoto et al., 1995, 1996; De Smet et al., 2000; Tsusaki et al., 1996) (Fig. 1-1D). TreS catalyzes a reaction similar to TreY but acts on maltose. Trehalose is directly synthesized through this single intramolecular transglycosylation.

Fungi such as *Aspergillus fumigatus* have trehalose phosphorylase (TP, EC 2.4.1.64) pathway (Puttikamonkul et al., 2010) (Fig. 1-1E). Trehalose is produced from β-D-glucose 1-phosphate (β-Glc1*P*) and D-glucose through the reverse phosphorolysis of TP. In *A. fumigatus*, the TP pathway is thought to be an alternative pathway for trehalose synthesis, because the *TPP*-gene deficient *A. fumigatus* mutant, lacking the TPS-TPP pathway, produces trehalose (Puttikamonkul et al., 2010).

The enzymes involved in these pathways are categorized into Glycoside Hydrolase family (GH) and Glycosyltransferase family (GT) based on their primary structure (Coutinho et al., 2003; Henrissat and Davies, 1997). Enzymes, classified into the same family, generally have a common catalytic domain structure and share a reaction mechanism. Reactions of glycoside hydrolases and

glycosyltransferases are classified into two types: retaining- and inverting-reactions in which the configuration of the anomeric center of the substrate is retained and inverted in the product, respectively (Davies and Henrissat, 1995; McCarter and Withers, 1994; Rye and Withers, 2000; Sinnott, 1990). Retaining glycoside hydrolases catalyze also transglycosylation. A glycosyl residue of a donor glycoside is transferred to a hydroxy group of acceptor compounds such as sugars and alcohols.

1.2. Physiological functions of trehalose in plants

Plants have various defense mechanisms against abiotic stresses such as temperature and drought, since plants cannot move to avoid such stresses. In general, trehalose serves as a compatible solute to deal with abiotic stresses such as osmotic and drought stress. However, its concentration in plants is thought to be too low to function as a compatible solute [*A. thaliana* contains 10.1–22.6 nmol/g fresh weight (FW) of trehalose (Avonce et al., 2004; Van Houtte et al., 2013)]. Various other functions of trehalose and its related compound Tre6*P* have been found since the discovery of genes responsible for the trehalose biosynthesis in *Arabidopsis thaliana* by reverse genetic screens (Blázquez et al., 1998; Leyman et al., 2001; Vogel et al., 1998). *A. thaliana* has genes for 11 TPS-like proteins (*AtTPS1–AtTPS11*) and 10 TPP-like proteins (*AtTPPA–AtTPPJ*) (Lunn et al., 2014), and rice (*Oryza sativa*) has those for 11 TPS-like proteins (Zang et al., 2011) and 10 TPP-like proteins (Pramanik and Imai, 2005). It was observed in various plants such as *A. thaliana*, *O. sativa*, and tobacco (*Nicotiana benthamiana*) that the overexpression of these genes increased endogenous trehalose levels and improved the drought-stress resistance (Avonce et al., 2004; Garg et al., 2002; Miranda et al., 2007; Romero et al., 1997).

In plants, change of trehalose content is thought to be a sign of biotic stresses, because the endogenous level of trehalose is increased by biotic stresses such as the infection with the root-knot disease fungus, *Plasmodiophora brassicae* (Brodmann et al., 2002), and eating damage by an aphid

(*Myzus persicae*) (Hodge et al., 2013; Singh and Shah, 2012). Although functions of trehalose in response to these biotic stresses have not been fully understood, trehalose is regarded as an inducer of reactive oxygen species (ROS). In general, ROS is harmful to plants, but plants sometimes use it for defense signaling in response to both biological and non-biological stresses (Dangl and Jones, 2001; Glazener et al., 1996). By overexpression of *AtTPPE* in *A. thaliana* causes more increase in trehalose and ROS amount than observed in the wild type, and the *AtTPPE*-deficient mutant less (Wang et al., 2020). Induction of ROS accumulation and various defense signaling was observed in tobacco with exogenous trehalose (Shi et al., 2019). Exogenous trehalose induced NADPH oxidase, which catalyzed the reduction of molecular oxygen into ROS. Trehalose would be a key compound for the ROS signaling in plants.

1.3. Physiological functions of Tre6*P*

In plants, Tre6*P* acts as a signal compound controlling growth, flowering, and nutrition flux (Fig. 1-2), although endogenous Tre6*P* content is very low (0.17 nmol/g FW) (Van Houtte et al., 2013). The first one mentioned here is the involvement in the embryo development (Fig. 1-2A). The TPS gene (*AtTPS1*) deficient mutant of *A. thaliana*, which showed lower Tre6*P* levels than the wild type, exhibits a strange cell division pattern of embryo, meaning loss of the ability for the embryo development (Eastmond et al., 2002; Gómez et al., 2006) (Fig. 1-2A). This impotence of the embryo development was rescued by introducing the *TPS* gene (*OtsA*) from *E. coli*. Therefore, a TPS activity, but not the AtTPS1 protein itself, is regarded to be essential for the embryonic development (Schluepmann et al., 2003).

The second thing is controlling the timing of flowering in *A. thaliana* (Schluepmann et al., 2003) (Fig. 1-2B). So far, the flowering time is thought to be controlled by two mechanisms: the photoperiodic flowering pathway and the maturation pathway. Tre6*P* is playing key roles in both

mechanisms. In the photoperiodic flowering pathway, Tre6*P* controls the expression of the transcriptional factor relating to sensing the photoperiod (Wahl et al., 2013). The expression of *FLOWERING LOCUS T* (*FT*: AT1G65480), induced when leaves sensed the photoperiodic changes, was correlated with the Tre6*P* level in diurnal changes. The FT protein bonded to the FD protein, which was a bZip transcription factor, in the shoot apical meristem, causing flower bud formation. *AtTPS1*-deficient mutants, obtained by transient expression of *AtTPS1* using dexamethasone-induced promoter during the embryo development, showed reduced Tre6*P* levels, with a concomitant reduction in *FT* gene expression and delayed flowering. Tre6*P* also seems to cause the maturation in the maturation pathway of *A. thaliana* (Wahl et al., 2013). In this pathway, flowering is controlled by the slow depletion of miR156 and increased expression of *SQUAMOSA PROMOTER BINDING PROTEIN-LIKE* (*SPL*) 3, *SPL*4, and *SPL5* genes (AT2G33810, AT1G53160, and AT3G15270, respectively) during plant aging. The SPL proteins facilitated the expression of the *FT* gene *via SUPPRESSOR OF OVEREXPRESSION OF CONTAINS 1* (*SOC1*, AT2G45660) and *FRUITFULL* (*FUL*, AT5G60910). The expression levels of *SPL*s were repressed by miR156, so that decreased miR156 levels during plant senescence led to increasing *SPL* expression and flower (Wang et al., 2009; Yamaguchi et al., 2009). The Tre6*P* level links to the decrease of miR156. A high level of miR156 in the *AtTPS1* deficient mutant resulted in delaying the flowering (Wahl et al., 2013).

The third role of Tre6*P* is controlling the flux of nutrition, such as sucrose, fatty acids, and amino acids in plants (Fig. 1-2C). Tre6*P*, which increased along with increase of sucrose level (Lunn et al., 2006), was the signal to decrease the sucrose level. Sucrose level decreased by increasing Tre6*P* level through overexpressing the *E. coli OtsA* (Martins et al., 2013; Schluepmann et al., 2003; Yadav et al., 2014). The relationship between sucrose and Tre6*P* in plants is called sucrose-Tre6*P* nexus (Yadav et al., 2014) and seems similar to the that between D-glucose and insulin in mammals. In mammals, elevated blood D-glucose level causes the increase of insulin to suppress the blood D-

glucose level. The inactivation of protein kinases explains this regulation. SUCROSE-NON-FERMENTING1-RELATED PROTEIN KINASE1 (SnRK1) is an important metabolic sensor that is activated when sugars are low (Zhai et al., 2018; Zhang et al., 2009). Tre6*P* inactivates SnRK1 (Zhang et al., 2009). SnRK1 activity in crude enzyme solution prepared from *Arabidopsis* seedlings decreased in a Tre6*P* concentration-dependent manner in the reaction solution. In the presence of 20 μM Tre6*P*, the activity was 50% of that in the absence. This decrease is not seen in purified SnRK1 by anion exchange column chromatography. The addition of a protein solution prepared from *Arabidopsis* seedlings to the reaction mixture of purified SnRK1 reduces activity to 40% in the presence of 1 mM Tre6*P*. This was not observed in the heat-denatured protein solution, suggesting the presence of a protein that regulates the activity of SnRK1. One of these proteins is GEMINIVIRUS REP-INTERACTING KINASE1 (GRIK1) (Zhai et al., 2018). The α-subunit KIN10, which is the catalytic site of SnRK1, interacts with GRIK1 (K_d = 19.5 μM) and is phosphorylated and activated. KIN10 also interacts with Tre6*P* (K_d = 32 μM). In the presence of 50 μM Tre6*P*, the interaction of GRIK1 with KIN10 is weakened (K_d = 67.7 μM). Phosphorylated KIN10 phosphorylates sucrose 6-phosphate synthase (SPS) (Halford and Grahame Hardie, 1998). Dephosphorylated SPS has reduced activity (Huber et al., 1991). Therefore, the sucrose synthesis is negatively regulated by Tre6*P*. Phosphorylated KIN10 also phosphorylates WRINKLED1 (WRI1) (Zhai et al., 2018), which is a transcriptional factor that induces the expression of genes for fatty acid synthesis (Maeo et al., 2009). Phosphorylation of WRI1 by KIN10 results in its proteasomal degradation (Zhai et al., 2017). Therefore, it means that Tre6*P*, which inhibits the phosphorylation of KIN10 followed by the phosphorylation of WRI1, facilitates fatty acid synthesis (Zhai et al., 2018).

Tre6*P* contributes to regulating the production of amino acids and organic acids involved in the TCA cycle (Fichtner et al., 2017; Figueroa et al., 2016), and controls the carbon and nitrogen fluxes needed for plant development. Figueroa *et al.* generated a condition-specific *TPS*-expressing *A.*

thaliana using the ethanol-inducible promoter and quantified the level of amino acids and organic acids in *Arabidopsis* under the TPS induction conditions (Figueroa et al., 2016). Amino acids such as alanine and aspartate and organic acids such as fumaric acid and citric acid are increased by 2–3 folds along with Tre6*P* increase. This phenomenon is explained by the activation of phosphoenolpyruvate carboxylase (PEPC) and nitrate reductase (NR) (Figueroa et al., 2016). The TPS induction increased phosphorylated PEPC and reduced mono-ubiquitinated PEPC [PEPC is activated by the phosphorylation and inactivated by the monoubiquitination (Hartwell et al., 1999; O'Leary et al., 2011)]. NR is phosphorylated by phosphorylated KIN10 (Halford and Grahame Hardie, 1998). KIN10 phosphorylation is suppressed by Tre6*P* as described above, and phosphorylated NR is less active (Su et al., 1996). Therefore, NR activity remains in the presence of Tre6*P*.

Tre6*P*, which controls the carbon and nitrogen fluxes in plants, might be a good target to regulate crop growth and increase crop yields. Applying Tre6*P* analogs to plants increases crop yield (Griffiths et al., 2016). Wheat fed with the Tre6*P* analog has increased grain enlargement and starch content. In this Tre6*P* analog, the phosphate group of Tre6*P* is chemically modified to cancel the electric charge. This modification is removed by UV light. After being taken up by plants, Tre6*P* analogs are converted to Tre6*P* in the body when the plants are exposed to light. The increased Tre6*P* changes the carbon flux and increases the starch content.

Tre6*P* is found in the catabolic pathway of trehalose. In bacteria, Tre6*P* is synthesized from trehalose during the uptake of extracellular trehalose as a carbon source by the phosphotransferase system (Andersson et al., 2001; Boos et al., 1990; Dahl, 2006; Schöck and Dahl, 1996). In *Lactococcus lactis* subsp. *lactis*, generated Tre6*P* is phosphorolyzed to Glc6*P* and β-Glc1*P* by trehalose 6-phosphate phosphorylase (TrePP, EC 2.4.1.216) for further metabolism through glycolysis (Andersson et al., 2001). In *E. coli*, Tre6*P* is hydrolyzed to Glc6*P* and D-glucose by trehalose-6-phosphate hydrolase (EC 3.2.1.93) (Rimmele and Boos, 1994).

Tre6*P* is known to regulate ATP level. In yeast (*Saccharomyces cerevisiae*), Tre6*P* is a competitive inhibitor of hexokinases (HXK1 and HXK2) (Blázquez et al., 1993; Van Heerden et al., 2014). Yeast *TPS* gene-deficient mutant (*cif1*, the altered name was *Δtps1*) did not grow in the presence of D-glucose. This defect was arisen from excess consumption of ATP and accumulation of sugar phosphates, such as Glc6*P* and fructose bisphosphate, due to the loss of inhibition of HXK by Tre6*P* (González et al., 1992; Navon et al., 1979). When ATP is depleted, yeast is thought not to be able to catabolize hexose phosphate through the glycolytic step. The reason is not clear, but it was reported that TPP gene (*tps2*) deficient mutant yeast (*Δtps2*, described as CDV64) showed a similar growth curve to wild type at 27°C, although it accumulated more Tre6*P* than wild type (De Virgilio et al., 1993).

Tre6*P* negatively regulates growth, with an unknown mechanism. In *Mycobacterium tuberculosis*, the *TPP* gene was necessary for growth because of the Tre6*P*-associated toxicity (Korte et al., 2016). TPP is also required for the growth of *A. fumigatus*. A *TPP* deficient mutant displayed severe morphological defects related to asexual reproduction during the growth in the presence of D-glucose (Puttikamonkul et al., 2010). This mutant shows high sensitivity to cell wall perturbing agents, suggesting the relationship between cell wall biosynthesis and Tre6*P* level. In the nematode, accumulation of Tre6*P* causes the lethality (Kormish and McGhee, 2005), because the *TPP* (*gob-1*) deficiency in *Caenorhabditis elegans* gave the lethality, but *TPS* (*tps1* and *tps2*) and *gob-1* deficient triple mutants with less Tre6*P* accumulation was not lethal.

1.4. Synthesis methods of trehalose and Tre6*P*

Trehalose have been prepared by extraction from yeast (Steiner and Cori, 1935; Stewart et al., 1950), organic synthesis (Lemieux and Bauer, 1954), and enzymatic synthesis (Murao et al., 1985). Among them, enzymatic synthesis uses mild reaction conditions (in an aqueous system and no requirement of

harmful substances), produces few by-products, and is easily scaled up.

Of the five trehalose biosynthetic pathways mentioned above, use of the TPS and TreT for trehalose production require sugar nucleotides and are not suitable. Trehalose synthesis using phosphorylases has been reported. Glycoside phosphorylases are classified into GHs 13, 65, 94, 112, and 130, and GTs 4 and 35 in the Carbohydrate-Active enZymes database (CAZy) database (http://www.cazy.org) (Lombard et al., 2014). Unlike hydrolases, in the reaction of inverting phosphorylases, inorganic phosphate attacks the anomeric carbon in a nucleophilic manner to produce a sugar phosphate with the opposite anomeric configuration. This reaction is reversible, and, therefore, oligosaccharides can be synthesized from sugar phosphate (glycosyl donor) and acceptor sugar through the reverse phosphorolysis. TP is able to be applied to the trehalose synthesis from β-Glc1*P* and D-glucose. Since β-Glc1*P* can be supplied by the phosphorolysis of maltose—which is abundantly produced from starch by β-amylase (EC 3.2.1.2)—by maltose phosphorylase (MP, EC 2.4.1.8), combining the reactions of MP and TP provides the synthesis method for trehalose from maltose (yield: 60%) (Murao et al., 1985; Yoshida et al., 1997, 1998).

Trehalose could be also synthesized by the TreY-TreZ pathway. In 1990, Lama *et al.* discovered that a thermophilic archaea *S. solfataricus* produces trehalose from starch (Lama et al., 1990). Since then, various research groups have revealed that this trehalose is produced through the TreY-TreZ pathway (Lama *et al.*, 1990; Kato *et al.*, 1996a; Kato *et al.*, 1996b; Kobayashi *et al.*, 1996a; Kobayashi *et al.*, 1996b). Application of the TreY-TreZ pathway enables the trehalose synthesis from starch, which is an abundant polysaccharide. By combining the reactions of starch debranching enzyme (EC 3.2.1.68) and cyclodextrin glucanotransferase (EC 2.4.1.19) with the reactions of TreY and TreZ, highly efficient trehalose production from starch (yield: 87%) has been improved, and it is currently used for the industrial production of trehalose (Kobayashi et al., 1997; Shibuya and Izawa, 2016).

1.5. Structures and functions of TPS and TPP

As mentioned in section 1.1, TPS and TPP are enzymes comprising the TPS-TPP pathway for biosynthesis of trehalose. In this section, the two enzymes are introduced. TPS is a retaining-type glycosyltransferase and belongs to GT20 together with glucosylglycerol-phosphate synthase (EC 2.4.1.213) (Blázquez et al., 1998; Coutinho et al., 2003; Leyman et al., 2001; Lombard et al., 2014; Vandesteene et al., 2010). Using *E. coli* OtsA, S_Ni reaction mechanism for the retaining-type transglycosylation is proposed (Fig. 1-3A) (Gibson et al., 2002; Lee et al., 2011). In this mechanism, the catalytic reaction proceeds *via* the formation of the ternary complex of the enzyme, the donor substrate (UDP-Glc), and acceptor substrate (Glc6*P*). Glycosidic oxygen of UDP-Glc facilitates the nucleophilic attack by O-1 of Glc6*P* to the anomeric center of D-glucosyl residue of UDP-Glc from the same face. Oxocarbenium ion-like transition state is assumed in this mechanism.

While bacterial TPSs are single-domain proteins, plant TPSs are bi-domain protein consisting of a GT20 domain and a TPP-like domain (Blázquez et al., 1998; Delorge et al., 2015; Van Dijck et al., 2002; Leyman et al., 2001; Pan et al., 2004; Vandesteene et al., 2010). The GT20 domain of some plant TPSs, including *A. thaliana* TPSs such as AtTPS1, AtTPS2, and AtTPS4, conserves the amino acid residues essential for the catalysis, but others such as AtTPS5–AtTPS11 do not (Avonce et al., 2010; Leyman et al., 2001; Yang et al., 2012). In fact, Delorge *et al.* showed that *AtTPS1, AtTPS2*, and *AtTPS4* encode active TPS by the complementation experiment using the *Δtps1* yeast. The *Δtps1* mutant yeast cannot grow in the presence of D-glucose because of disturbance of the glycolysis due to the low level of Tre6*P* as described above (Blázquez et al., 1993, 1998; Delorge et al., 2015; Van Dijck et al., 2002; Vandesteene et al., 2010), but this mutant grows even in the same conditions when the gene encoding TPS is introduced. This complementation of the *TPS1* deficiency was not observed in the transformants, when each of *AtTPS5–AtTPS11* gene was introduced. *AtTPS3* is thought to be a pseudogene because the coding region for 1st α-helix and 2nd β-strand of the GT20 domain lacks

(corresponding to Leu29–Asp50 in *E. coli* OtsA), and the splicing product contains the predicted 1st intron resulting in a premature translation stop (Lunn, 2007; Vandesteene et al., 2010). AtTPS1, AtTPS2, and AtTPS4 are classified into class 1 as active-TPS subfamily and AtTPS5–11 into class 2 as inactive-TPS subfamily.

The second enzyme, TPP belongs to the haloacid dehalogenase (HAD) -like superfamily (Burroughs et al., 2006; Kuznetsova et al., 2006; Lu et al., 2005). The HAD-like superfamily includes ATPases (P-type, EC 7.2.2.-) and β-phosphoglucomutases (β-PGM, EC 5.4.2.6), which catalyze the hydrolysis of phosphoryl esters and the transfer of phosphoryl groups, respectively (Allen and Dunaway-Mariano, 2004; Koonin and Tatusov, 1994; Kuznetsova et al., 2006). HAD-like superfamily phosphatases employ a two-step phosphoaspartyl transferase mechanism involving two catalytic Asp residues (Fig. 1-3B) (Barrozo et al., 2018; Cross et al., 2017a; Farelli et al., 2014; Seifried et al., 2013; Wildberger et al., 2015). In the first step, the Asp, acting as the nucleophile, attacks phosphorus of the phosphoryl group of the substrate to form the phosphoaspartyl enzyme intermediate, while the second catalytic Asp as the general acid protonates the leaving group (trehalose in the reaction of TPP). In the second step, a water molecule, activated by the second catalytic Asp as the general base, nucleophilically attacks phosphorus of the intermediate phosphoryl group to release inorganic phosphate. TPP possesses the four conserved motifs involved in the catalysis and substrate binding. The catalytic domain of TPPs is folded by an α/β domain, which is classified into a hydrolase fold similar to the Rossmann-fold (Kim et al., 2004). TPP also possesses a cap domain, inserted into the Rossman fold-like domain (Farelli et al., 2014) (Fig. 3-3A), and this domain is assumed to open and close during the catalytic process including substrate binding and release (Miao et al., 2016). The structural analysis of *Candida albicans* TPPs complexed with a trehalose-BeF_3 and *Cryptococcus neoformans* TPP inactive mutant complexed with Tre6*P* showed the precise interactions between the substrate and the residues included in the four motifs (Miao et al., 2016).

Plant TPPs such as AtTPPA–AtTPPJ are single-domain proteins as bacterial TPPs and conserve the four motifs. All the AtTPPs was confirmed to be active using *Δtps2* yeast. As described in section 1.3, this mutant yeast does not grow at a high temperature (38°C) because the expression of *tps2*, induced at high temperature, is required for the heat tolerance (De Virgilio et al., 1993). The susceptibility of heat was decreased when the gene encoding TPP is introduced (De Virgilio et al., 1993). The TPP-like domain is also found in class 1 and 2 TPSs as described above, but so far no TPS protein showed TPP activity regardless of the absence and presence of the catalytic Asp residue in class 1 and class 2 proteins, respectively (Ramon et al., 2009; Vandesteene et al., 2010).

1.6. Structures and functions of trehalase

Trehalase (EC 3.2.1.28) catalyzes the hydrolysis of trehalose with net inversion of the anomeric configuration of the substrate (Fig. 1-3C). It is highly specific to trehalose with a few exceptions (Dahlqvist et al., 1960; Hehre et al., 1982; Hey and Elbein, 1968; Mittenbühler and Holzer, 1988; Sasajima et al., 1975). Trehalase also degrades synthetic substrates, α-D-glucopyranosyl fluoride (α-GF) to produce β-D-glucose. It also acts on the other anomeric substrate, β-D-glucopyranosyl fluoride (β-GF) in the presence of D-glucose (Hehre et al., 1982). It looks bizarre because glycoside hydrolases generally do not act on compounds with opposite anomeric configuration to their substrate. In the reaction with β-GF and D-glucose, a slight amount of trehalose was detected. Therefore, this phenomenon is explained by the following two-step reaction, called the "Hehre re-synthesis-hydrolysis": (1) condensation of β-GF and D-glucose to form trehalose; (2) quick hydrolysis of the condensation product.

Trehalase falls into GH15, GH37, and GH65 (Lombard et al., 2014). While trehalase is a minor activity in GH15 and GH65, mainly composed of glucoamylase (EC 3.2.1.3) and various phosphorylases (described in section 2.1 in detail), respectively, GH37 comprises contains only

trehalases. GH37 forms clan GH-G with GH63, GH100, and GH125. *E. coli* has two isozymes of trehalase, the periplasmic and cytosolic trehalases (EcTre37A and TreF, respectively), which are induced by trehalose as a carbon source and a high osmotic environment, respectively (Boos et al., 1987; Gutierrez et al., 1989; Horlacher et al., 1996). The structure of EcTre37A is the first one determined in GH37 members. EcTre37A consists of 565 amino acid residues (30 residues at the N-terminal is a putative signal peptide). This enzyme has an $(\alpha/\alpha)_6$ barrel catalytic domain, formed by twelve α-helices arranged around the funnel-shaped catalytic site, and the N-terminal domain comprised of four α-helices (Gibson et al., 2007). The $(\alpha/\alpha)_6$ barrel structure is also found in various GH enzymes such as the GH15 glucoamylase and the GH65 MP (Egloff et al., 2001). In the catalytic site of these enzymes, some acidic amino acid residues well match topologically, and these are predicted to be the catalytic residues (Aleshin et al., 1992, 1994; Egloff et al., 2001; Gibson et al., 2007). The loop between 5th and 6th α-helices (α5→α6 loop) of the catalytic domain of EcTre37A contains the predicted general acid catalyst (Asp312) (Gibson et al., 2007). The α11→α12 loop covering the active site has the predicted general base catalyst (Glu496). Since the α11→α12 loop completely covers the substrate binding site in the enzyme-inhibitor complex (Adhav et al., 2019; Gibson et al., 2007), it is assumed that this loop opens in the apo-enzyme to bind the substrate and closes in the enzyme-substrate complex. Thus, this loop is called the lid loop. In trehalases of almost all kinds of organisms except for fungi, the α11→α12 loop contains a glycine-rich region, and it is predicted that the loop has high flexibility.

The structure of the N-terminal domain of trehalase from yeast is significantly different from those of trehalase from other organisms. In bacterial trehalases such as enzymes from *E. coli* and *Enterobacter cloacae*, the N-terminal domain locates near the catalytic site, and it looks like a “hood” (Adhav et al., 2019). The hood domain interacts with α11→α12 loop and is thought to affect the structure of the catalytic site. On the contrary, *S. cerevisiae* trehalase possesses a differently oriented

hood domain, and this enzyme also possesses N-terminal extension to interact with 14-3-3 protein, which activates the trehalase (Alblova et al., 2017). Bacterial trehalases are not confirmed to interact with any regulatory proteins.

Only one gene encoding trehalase is identified in the genome of *Arabidopsi*s and rice: *AtTRE1* (AT4G24040) and *OsTRE1* (Os10g0521000), respectively (Van Houtte et al., 2013; Islam et al., 2019; Lunn, 2007; Müller et al., 2001), although plants have multiple genes encoding TPS and TPP. Therefore, the *AtTRE1* deficient mutant shows a drastic phenotypic change. *AtTRE1* deficient plants do not show stomatal closure induced by the plant hormone abscisic acid (ABA) (Van Houtte et al., 2013) and exhibit a drought-susceptible phenotype. This ABA insensitivity of *AtTRE1*-deficient mutant indicates that *AtTRE1* is required for the event. In contrast, the overexpressor of *AtTRE1* results in strong stomatal closure compared to the wild-type plants (width of stomata, wild-type: 4.6 μm, overexpressor: 3.9 μm), and recovered better after a drought stress than the wild type. Trehalose content was low in the overexpressor of *AtTRE1* decreased, so decreasing trehalose content looks to improve drought stress tolerance.

1.7. Purpose of this study

As described above, the contents of Tre6*P* and trehalose have physiologically and metabolically a great impact on plants. However, research on trehalose metabolism in plants has been conducted mainly based on the phenotypic change in overexpressors and deficient mutants of the genes encoding trehalose-metabolizing enzymes. The enzymatic activity was confirmed only by yeast complement assay, and there is little quantitative analysis of the enzymes. The function of many TPP isozymes is unclear, and the enzyme function of trehalase has not been analyzed. The functions and structures of TPP isozymes and trehalase from *A. thaliana* are investigated for better understanding of the trehalose metabolism in plants. For these analyses, various kinds of derivatives of trehalose and Tre6*P* are

required to understand the substrate specificity in detail. However, the usage of these derivatives are limited due to lacking an efficient synthetic method. In this study, an enzymatic synthesis system for Tre6*P* and its derivatives was established. The functions and structures of TPP isozymes and trehalase from *A. thaliana* are investigated for understanding of the trehalose metabolism in plants.

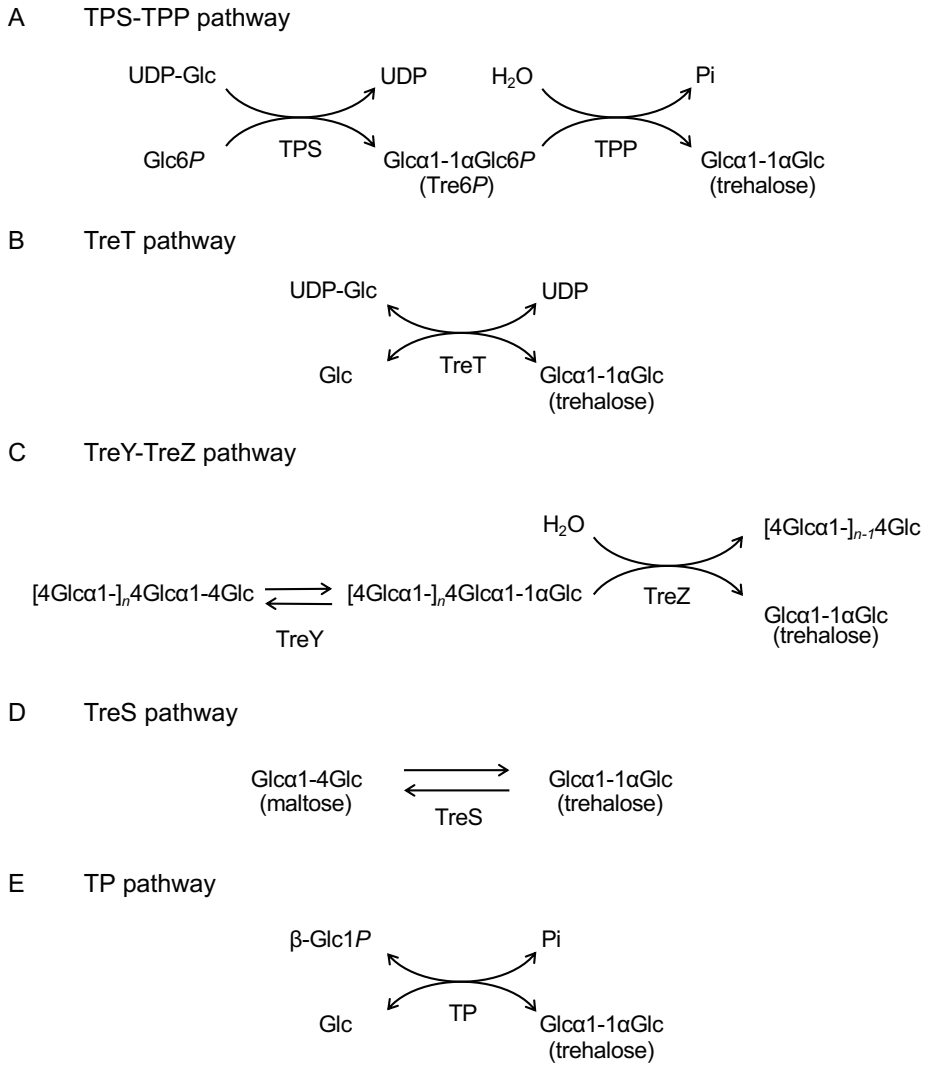

Fig. 1-1. Trehalose biosynthesis pathway.

TPS, trehalose 6-phosphate synthase; TPP, trehalose 6-phosphate phosphatase; TreT, ADP-glucose:D-glucose 1-α-D-glucosyltransferase; TreY, (1→4)-α-D-glucan 1-α-D-glucosylmutase; TreZ, 4-α-D-{(1→4)-α-D-glucano}trehalose trehalohydrolase; TreS, trehalose synthase; TP, trehalose phosphorylase.

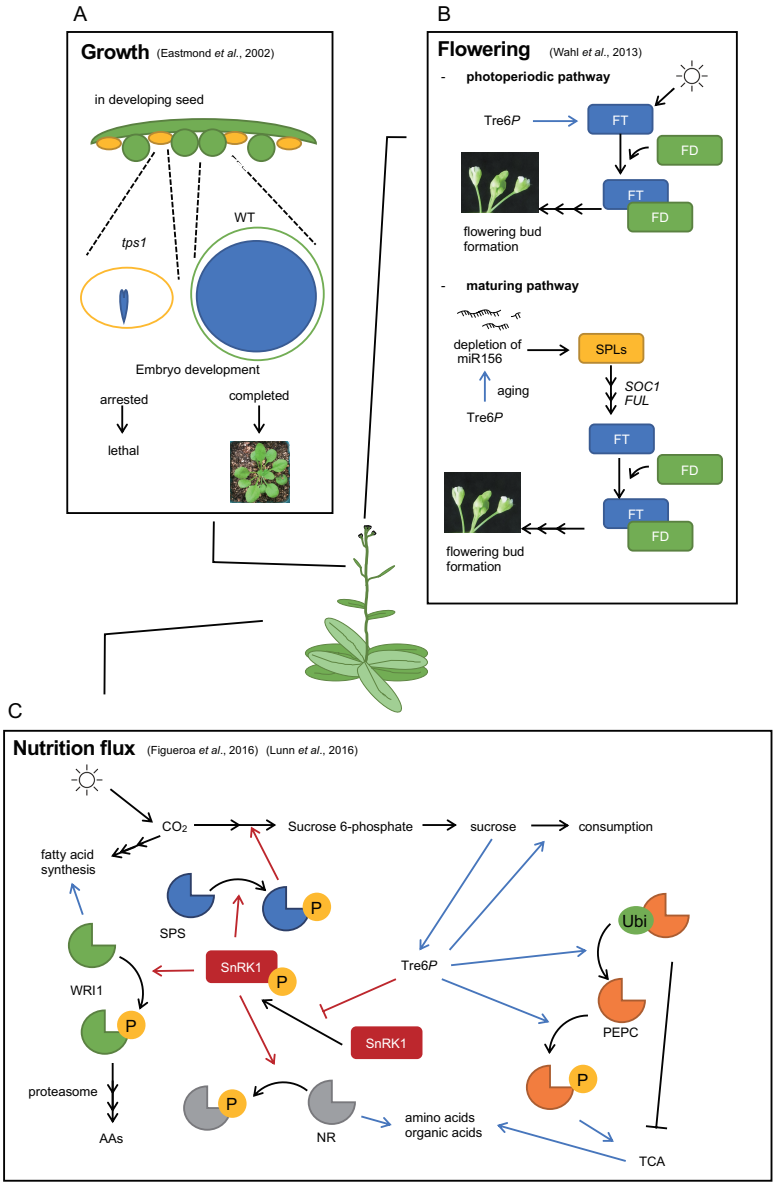

Fig. 1-2. Physiological functions of Tre6*P*.

Physiological functions of Tre6*P* are shown schematically. For detail, see text in section 1.3. (A) Developing *TPS1*/*tps1* heterozygotes seed segregating in a silique. The enlarged view showed mature embryo versus arrested torpedo stage *tps1* embryo. *tps1*: *tps1* deficient mutant of *A. thaliana*, WT: *A. thaliana* Col-0 wild type. (B) The two independent flowering pathways, the photoperiodic pathway, and the maturing pathway. (C) The influence of Tre6*P* on the metabolisms of sucrose and other metabolites. Blue arrows indicate activation by Tre6*P*, and red lines indicate inhibition. FT, *FLOWERING LOCUS T*; *FUL*, *FRUITFULL*; NR, nitrate reductase; PEPC, phosphoenolpyruvate carboxylase; P, phosphoryl group; SPL, *SQUAMOSA PROMOTER BINDING PROTEIN-LIKE*; SPS: sucrose 6-phsphate synthase; *SOC1*, *SUPPRESSOR OF OVEREXPRESSION OF CONTAINS 1*;Ubi, mono-ubiquitin.

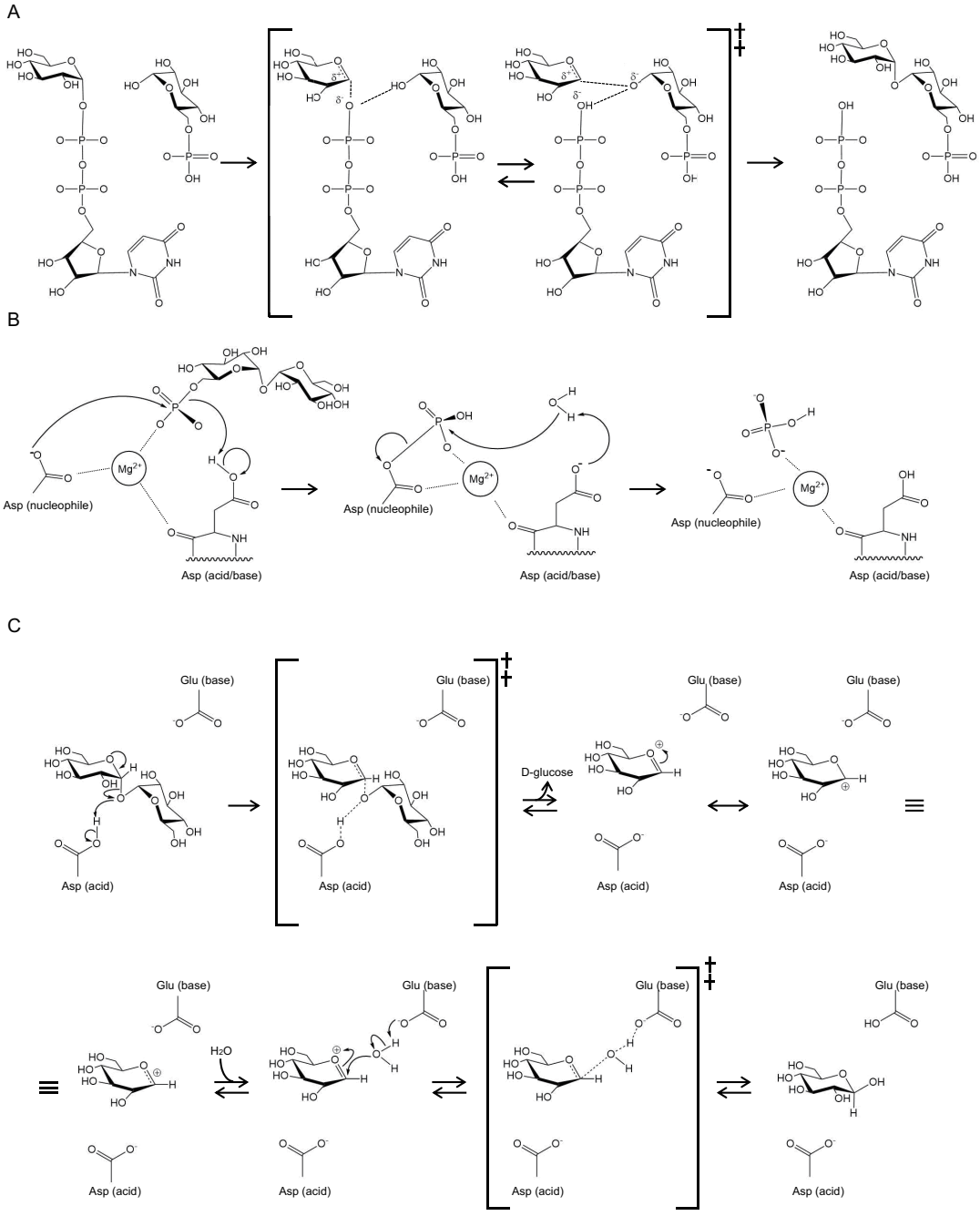

Fig. 1-3. Reaction mechanisms of trehalose-metabolizing enzymes.

The reaction mechanism is quoted from each paper. (A) The reaction mechanism of TPS (Lee et al., 2011). (B) The reaction mechanism of TPP (Barrozo et al., 2018; Wildberger et al., 2015). (C) The reaction mechanisms of trehalase (Hehre et al., 1982; McCarter and Withers, 1994; Mori et al., 2009).

2. Enzymatic synthesis of Tre6*P* and its derivative using the reverse phosphorolysis catalyzed by trehalose 6-phosphate phosphorylase

2.1. Introduction

Tre6*P* has been receiving increasing attention as a signaling molecule in plants. As mentioned in section 1.3, Tre6*P* controls plant physiological conditions. The Tre6*P* derivatives, which are permeable in plants, change sucrose allocation and increases yield of wheat seed (Griffiths et al., 2016). This finding indicates that Tre6*P* has a great potential for agricultural applications to improve crop production. Tre6*P* is also good to target for antibiotic development. In *M. tuberculosis*, the gene of *TPP* which degrade Tre6*P* is essential for growth because of the Tre6*P*-associated toxicity (Korte et al., 2016). Improved access to Tre6*P* would expand the development of new antibiotics using Tre6*P* derivatives.

To understand the physiological functions of Tre6*P*, especially in plants, efficient synthetic methods of Tre6*P* are required to produce a sufficient amount of Tre6*P* for analyses. Tre6*P* is also required to analyzed TPP as a substrate. As mentioned in section 1.2, plants have several TPPs, but their enzymatic functions unclear. To date, Tre6*P* has been reported to synthesized by yeast fermentation (Doi et al., 1998) and organic synthesis (Liu and Mariano, 2015; Rønnow et al., 1994). In the former method, D-glucose provided as the carbon source is converted into Tre6*P* with 11% yield. In the latter method, yield is higher than 50% but several reaction steps, including protection and deprotection of hydroxy groups, and uses of harmful regents including organic solvents are required. In contrast, enzymatic synthesis is simple and environmentally friendly, because it is carried out in aqueous solution under mild conditions.

The reverse phosphorolysis catalyzed by phosphorylases is useful for the production of oligosaccharide. In the reaction, sugar phosphate is used as a glycosyl donor, and the glycosyl group

is transferred to an acceptor molecule. Because the acceptor specificity of phosphorylases is not always strict, various kinds of oligosaccharides are produced by using various acceptor sugars. Generation of sugar phosphate and the reverse phosphorolysis can be coupled in a one-pot reaction. For instance, the phosphorolysis of maltose by MP to produce β-Glc1*P* is coupled with the reverse phosphorolysis of MP using *N*-acetyl-D-glucosamine and L-fucose as acceptors, to produce α-Glc*p*-(1→4)-GlcNAc and α-Glc*p*-(1→4)-L-Fuc*p*, respectively (Nakai et al., 2010). It is also possible to couple reactions of two different phosphorylases. Trehalose can be produced from maltose by the coupled reaction of MP and TP, in which MP phosphorolyzes maltose to β-Glc1*P* and D-glucose, and TP synthesizes trehalose from β-Glc1*P* and D-glucose through the reverse phosphorolysis (Yoshida et al., 1998).

Trehalose 6-phosphate phosphorylase, TrePP phosphorolyzes Tre6*P* to β-Glc1*P* and Glc6*P*. In *L. lactis* subsp. *lactis*, TrePP (LlTrePP) is involved in the trehalose catabolism. Extracellular trehalose is transported into cytosol *via* the phosphotransferase system and phosphorylated (Postma et al., 1986). Tre6*P* produced is phosphorolyzed into β-Glc1*P* and Glc6*P* by LlTrePP, and they are metabolized for the glycolytic pathway (Andersson et al., 2001). TrePP seems to be exclusively responsible for catabolizing Tre6*P* in *L. lactis* because of the absence of any genes coding for other metabolizing enzymes such as TPP, trehalase, and trehalose-6-phosphate hydrolase.

TrePP is found only in GH65. GH65 is mainly composed of α-glucoside phosphorylases including TrePP, MP, TP, kojibiose phosphorylase (EC 2.4.1.230), nigerose phosphorylase (EC 2.4.1.279), 3-*O*-α-glucopyranosyl-L-rhamnose phosphorylase (EC 2.4.1.282), 1,2-α-glucosylglycerol phosphorylase (EC 2.4.1.332), and 1,3-α-oligoglucan phosphorylase (EC 2.4.1.334). In GH65, TrePP is the sole enzyme that phosphorolyzes phosphoryl substrate (Andersson et al., 2001). GH65 enzymes have an $(\alpha/\alpha)_6$-barrel fold catalytic domain, similar to GH15 and GH94 enzymes (Egloff et al., 2001; Hidaka et al., 2004). GH65 enzymes form clan GH-L together with GH15 based on the similarity of

their tertiary structures (Lombard et al., 2014).

In this chapter, a simple and efficient enzymatic synthesis of Tre6*P* from an abundant carbohydrate material using TrePP in combination with some other enzymes is described. Besides, the acceptor preference of LlTrePP in the reverse phosphorolysis is examined in detail, to investigate the possibility of synthesis of other disaccharide phosphates. D-Mannose 6-phosphate (Man6*P*), the sole accepter substrate of LlTrePP except for Glc6*P*, was used as an acceptor substrate, and a Tre6*P* analogue, α-D-Glc*p*-(1↔1)-α-D-Man*p*6*P* (Glcα1-1αMan6*P*), was synthesized.

2.2. Materials and methods

2.2.1. Materials

D-Glucose, D-fructose, L-arabinose, D-sorbose, maltose, lactose, sucrose, and D-glucitol were purchased from Nacalai Tesque (Kyoto, Japan). D-Galactose, D-mannose, D-xylose, methyl α-D-glucopyranoside, and methyl β-D-glucopyranoside were from Wako Pure Chemical Industries (Osaka, Japan). Trehalose was from Hayashibara (Okayama, Japan). D-Glucosamine was from Tokyo Chemical Industry (Tokyo, Japan). Glc6*P* was from Oriental Yeast (Tokyo, Japan). Tre6*P*, Man6*P*, D-galactose 6-phosphate (Gal6*P*), and D-fructose 6-phosphate (Fru6*P*) were from Sigma-Aldrich (St. Louis, MO, USA).

MP from bacteria was purchased from Oriental Yeast. One unit of this MP was defined as the amount of enzyme that produces 1 μmol of D-glucose from 100 mM maltose and 100 mM phosphate buffer (pH 5.6) for 1 min at 30°C. MP from *Bacillus* sp. AHU2001 was prepared according to Gao *et al*. (Gao et al., 2019). β-PGM from *Lactococcus* sp., which was used in section 2.3.5, and 2.3.6, was purchased from Sigma-Aldrich. Glc6*P* dehydrogenase from yeast was from Oriental Yeast. One unit of this enzyme was defined as amount of the enzyme that produces 1 μmol of NADPH from 0.48 mM Glc6*P* and 0.48 mM $NADP^+$ in 80 mM glycylglycine buffer (pH 8.5) containing 19 mM magnesium

chloride for 1 min at 25°C

2.2.2. Preparation of β-Glc1*P*

β-Glc1*P* was prepared from maltose and inorganic phosphate by the phosphorolysis of maltose. A reaction mixture (2 L), composed of 0.3 M maltose, 0.3 M potassium phosphate buffer (pH 8.0), and 25 mg/L MP from *Bacillus* sp. AHU2001 was incubated at 37°C for 96 h. β-Glc1*P* produced was purified by anion exchange column chromatography with Amberjet 4400 (3.6 cm i.d.×90 cm, acetate form; Organo, Tokyo, Japan) according to the method previously described (Hokse, 1983). β-Glc1*P* was concentrated in vacuo and precipitated in 80% ethanol. The precipitate was dissolved in water and passed through a column of cation exchange resin (Dowex 50, H^+ type; Wako Pure Chemical Industries) to remove counter ions of β-Glc1*P*. The pH was adjusted to 8.0 with 6 M KOH, and β-Glc1*P* was precipitated in 80% ethanol. Crystalline β-Glc1*P* was filtered, dried in vacuo, and stored at -20°C. From 0.6 mol maltose, 0.073 mol β-Glc1*P* was obtained, and the yield was 12%. The purity was judged to be 96.3% or more by high-performance anion-exchange chromatography equipped with a pulsed amperometric detector (HPAEC-PAD) as described in section 2.2.17.

2.2.3. Extraction of genomic DNA of *L. lactis* subsp. *lactis* JCM5805

L. lactis subsp. *lactis* JCM5805, the same strain as *L. lactis* subsp. *lactis* ATCC 19435, was inoculated into 2 mL of GAM medium (Nissui Pharmaceutical, Tokyo, Japan) and allowed to stand at 37°C for 18 h under anaerobic conditions (nitrogen: carbon dioxide: hydrogen = 8: 1: 1). The cells were harvested by centrifugation (10,000×g, 4°C, 10 min), suspended in 85 μL of 50 mM NaOH, and kept at 100°C for 10 min. After adding 15 μL of 1 M tris-hydroxymethyl aminomethane (Tris)-HCl buffer (pH 7.0), the supernatant was recovered by centrifugation (10,000×g, 4°C, 10 min).

2.2.4. Preparation of recombinant LlTrePP

The *LlTrePP* gene (GenBank accession number, Y18267.1 ORF3) was obtained from the genomic DNA of *L. lactis* subsp. *lactis* JCM 5805 by PCR with primers (sense, 5′-CATATGACTGAAAAAGATTGGATAATCCA-3′; and antisense, 5′-GCGGCCGCTTTTAAATCAAATTTAGTCTG-3′) and Primestar HS DNA polymerase (Takara Bio, Kusatsu, Japan). The amplified DNA fragment was cloned into pBluescript II SK (+) plasmid (Stratagene, La Jolla, CA, USA). *E. coli* DH5α, used for the propagation of plasmid DNA, was transformed according to the method of Hanahan (Hanahan, 1983), and the plasmid DNA was prepared from *E. coli* transformant by the alkaline SDS method (Sambrook and Russell, 2001). Cloned DNA fragment was cut out from pBluescript II SK (+) derived plasmid by the digestion using *Nde*I and *Not*I, and introduced into pET-23a plasmid (Novagen, Darmstadt, Germany) *via* the same restriction sites. The DNA sequence of inserted fragment was analyzed using a Big Dye Terminator v1.1 Cycle Sequencing Kit (Lifetechnologies, Carlsbad, CA, USA) and an Applied Biosystems 3130 Genetic Analyzer (Applied Biosystems, Foster City, CA).

A transformant of *E. coli* BL21 (DE3), harboring the expression plasmid for LlTrePP, was cultured in 1.0 L of Luria-Bertani (LB) medium containing 100 μg/mL ampicillin at 37°C until A_{600} reached 0.5. Production of the recombinant protein was induced by the addition of 0.1 M isopropyl β-D-1-thiogalactoside (IPTG, Wako Pure Chemical Industries) at a final concentration of 0.1 mM, and the incubation was continued at 18°C for 23 h with vigorous shaking. The *E. coli* cells were harvested by centrifugation (10,000×*g*, 4°C, 10 min), and suspended in 30 mL of 10 mM 2-morpholinoethanesulfonic acid (MES)-NaOH buffer (pH 6.5) containing 0.5 M NaCl and 25 mM imidazole (buffer A). The bacterial cells were disrupted by sonication using a Sonifier 450 (Bronson, Danbury, CT, USA), and the supernatant, obtained by centrifugation (6,000×*g*, 4°C, 10 min), was regarded as the cell-free extract. The cell-free extract was loaded onto a Ni-chelating Sepharose Fast

Flow column (1.6 cm i.d.×2.5 cm, 5 mL, GE Healthcare, Uppsala, Sweden) equilibrated with buffer A. After thorough washing the column with buffer A, adsorbed protein was eluted by a linear gradient from 25 to 500 mM imidazole (total volume, 100 mL). Purity of recombinant LlTrePP in the fractions were analyzed by SDS-PAGE (Laemmli, 1970), and highly purified fractions were pooled. Collected sample was dialyzed against 10 mM MES-NaOH buffer (pH 6.5). The sample was concentrated *via* ultrafiltration using Vivaspin 20 centrifugal concentrators (molecular weight cut off 30,000 Da, Sartorius, Göttingen, Germany), and stored at 4°C.

2.2.5. Preparation of recombinant β-PGM from *L. lactis* subsp. *lactis* JCM5805

The *pgmB* gene encoding a β-PGM (GenBank accession number, AE005176.1) was amplified from the genomic DNA of *L. lactis* subsp. *lactis* JCM 5805 by PCR using primers (sense, 5′-AAAGAAGGTAAAAAGATGTTTAAAGCAGT-3′; and antisense, 5′-TTATTAATTACGAATTATTTTTGCTTTTG-3′) and Primestar HS DNA polymerase. To prepare the expression plasmid of β-PGM, the *pgmB* gene was amplified from the amplified DNA fragment using the primers, 5′-TTAACTTTAAGAAGGAGATATACATATGTTTAAAGCAGTATTGTT-3′ (sense; vector-derived sequence underlined) and 5′-GATCTCAGTGGTGGTGGTGGTGGTG TTTTTGCTTTTGAAGCCAAA-3′ (antisense). Amplified DNA was cloned into pET-23a plasmid using an In-Fusion HD Cloning Kit (Takara Bio). Recombinant β-PGM was produced in *E. coli* BL21 (DE3) transformant and purified by Ni-affinity column chromatography. A transformant of *E. coli* BL21 (DE3) harboring the expression plasmid for β-PGM was cultured in 2.0 L of LB medium containing 100 μg/mL ampicillin at 37°C until A_{600} reached 0.5. Production of the recombinant protein was induced by the addition of 0.1 M IPTG at a concentration of 0.1 mM, and the incubation was continued at 18°C for 19 h with vigorous shaking. The *E. coli* cells were harvested by centrifugation (10,000×*g*, 4°C, 10 min), and suspended in 30 mL of 10 mM (2-hydroxyethyl) piperazine-1-

ethanesulfonic acid (HEPES)-NaOH buffer (pH 7.2) containing 0.5 M NaCl, 5 mM $MgCl_2$, and 25 mM imidazole (buffer B). The bacterial cells were disrupted by sonication and the cell-free extract was obtained by centrifugation (6,000×*g*, 4°C, 10 min). The cell-free extract was loaded onto a Ni-chelating Sepharose Fast Flow column (1.6 cm i.d.×5 cm, 10 mL) equilibrated with buffer B. After thorough washing the column with the same buffer, the adsorbed protein was eluted by a linear gradient from 25 to 500 mM imidazole (100 mL in total). Purity of recombinant β-PGM in the fractions were analyzed by SDS-PAGE (Laemmli, 1970), and highly purified fractions were pooled, and dialyzed against 10 mM HEPES-NaOH buffer (pH 7.2) containing 5 mM $MgCl_2$. The sample was concentrated using Amicon Ultra concentrator [nominal molecular weight limit (NMWL) 10,000 Da, Merck Millipore, Darmstadt, Germany] and stored at 4°C.

2.2.6. Preparation of recombinant hexose phosphatase from *E. coli*

Recombinant hexose phosphatase (EC 3.1.3.23) from *E. coli* (Kuznetsova et al., 2006; Wildberger et al., 2015) was prepared in *E. coli*. The *yidA* gene encoding a hexose phosphatase (GenBank accession number, AP009048.1) was amplified from the genomic DNA of *E. coli* DH5α by PCR using primers (sense, 5′-CTCGGGTGTTGTACTGATTTTTGAG-3′; and antisense, 5′-GTAAACCAATAATCAGTAAGCGGGC-3′) and Primestar HS DNA polymerase. DNA fragment amplified from the PCR product using the primers, 5′-CGCGGCAGCCATATGATGGCTATTAAACTCATTGC -3′ (sense; vector-derived sequence underlined) and 5′-GCGGCCGCAAGCTTGTTAATTCAGCACATACTTCT-3′ (antisense) was cloned into pET-28a plasmid (Novagen) using an In-Fusion HD Cloning Kit. Recombinant YidA was produced in *E. coli* BL21 (DE3) transformant and purified by Ni-affinity column chromatography. A transformant of *E. coli* BL21 (DE3) harboring the expression plasmid for YidA was cultured in 2.0 L of LB medium containing 50 μg/mL kanamycin at 37°C until A_{600} reached 0.8. Production of the

recombinant protein was induced by the addition of 0.1 M IPTG at a concentration of 0.1 mM, and the incubation was continued at 18°C for 23 h with vigorous shaking. The *E. coli* cells were harvested by centrifugation (10,000×*g*, 4°C, 10 min), and suspended in 30 mL of 10 mM HEPES-NaOH buffer (pH 7.0) containing 0.5 M NaCl, 5 mM $MgCl_2$ and 20 mM imidazole (buffer C). The bacterial cells were disrupted by sonication, and cell-free extract was obtained by centrifugation (6,000×*g*, 4°C, 10 min). The cell-free extract was loaded onto a Ni-chelating Sepharose Fast Flow column (1.6 cm i.d.×2.5 cm, 5 mL) equilibrated with buffer C. After thorough washing the column with the same buffer, adsorbed protein was eluted by a linear gradient from 20 to 500 mM imidazole (100 mL in total). Purity of recombinant YidA in the fractions were analyzed by SDS-PAGE (Laemmli, 1970), and highly purified fractions were pooled. Collected sample was dialyzed against 10 mM HEPES-NaOH buffer (pH 7.0) containing 5 mM $MgCl_2$, as described above, and stored at 4°C.

2.2.7. Measurement of protein concentration

Protein concentrations of cell-free extract and fractions from the column chromatography were determined by the Bradford method (Bradford, 1976) and the UV method (A_{280}) (Mach et al., 1995), respectively. Bovine serum albumin (BSA; Nacalai Tesque) was used as the standard protein for the Bradford method. The concentration of the purified enzyme was calculated based on the molar quantities of each amino acid measured using a JLC-500/V (JEOL, Tokyo, Japan) and L-8900 (Hitachi High-Tech Corporation, Tokyo, Japan) after complete acid hydrolysis of the enzyme (6 M HCl, 110°C, 24 h) (Moore and Stein, 1948).

2.2.8. Blue native polyacrylamide gel electrophoresis (BN-PAGE)

The molecular mass of LlTrePP under nondenaturing conditions was determined by blue native PAGE (BN-PAGE) (Schägger et al., 1994). The analytical sample was prepared using a NativePAGE Sample

Prep Kit (Lifetechnologies). Native PAGE Novex 4–16% Bio-Tris Gels (Lifetechnologies) were used, and the electrophoresis was carried out at a constant 150 V for 115 min on ice. Native Mark Unstained Standard (Lifetechnologies) was used to provide protein molecular size standards.

2.2.9. Standard activity assay of LlTrePP

Activity for the synthesis of Tre6*P* from β-Glc1*P* and Glc6*P* was determined by measuring the inorganic phosphate liberated. The velocity for the liberation of inorganic phosphate was regarded as the same as that for the synthesis of Tre6*P*. A reaction mixture (20 μL), composed of an appropriate concentration of enzyme, 105 mM MES-NaOH (pH 5.5), 10 mM β-Glc1*P*, 10 mM Glc6*P*, and 0.5 mg/mL BSA, was incubated at 30°C for 10 min. The reaction was terminated by incubating the sample at 80°C for 5 min. Inorganic phosphate liberated was measured according to the previous publication (Lowry and Lopez, 1946). One unit of enzyme activity was defined as the amount of enzyme which produces 1 μmol of inorganic phosphate in 1 min under these conditions.

2.2.10. Measurement of activity for the phosphorolysis of Tre6*P*

Phosphorolytic activity of LlTrePP to Tre6*P* was measured based on Glc6*P* liberation according to Andersson *et al*. (Andersson et al., 2001). A reaction mixture (150 μL), composed of an appropriate concentration of enzyme, 10 mM potassium phosphate buffer (pH 7.0), 0.667 mM Tre6*P*, 0.8 mM thio-NAD^+, 3.75 U/mL Glc6*P* dehydrogenase, and 0.13 mg/mL BSA, was incubated at 35°C for 10 min. The reaction was terminated by incubating the sample at 80°C for 5 min, and A_{400} was measured. Glc6*P* produced was quantified based on a standard curve of 25–150 μM Glc6*P*. One unit of enzyme activity was defined as the amount of enzyme producing 1 μmol of Glc6*P* in 1 min in these conditions.

2.2.11. Evaluation of effects of temperature and pH on activity and stability

Optimum temperature was determined from activity of Tre6*P* synthesis at 20–50°C. Optimum pH for the synthesis of Tre6*P* was determined from activity at pH 3.5–8.2. As reaction buffers (100 mM), glycine-HCl buffer (pH 3.5), sodium acetate buffer (pH 4.0–5.3), MES-NaOH buffer (pH 5.6–7.2), and HEPES-NaOH (pH 7.2–8.2) were used. For determination of optimum pH for the phosphorolysis of Tre6*P*, potassium phosphate buffers of pH 5.5–8.0 were used as the reaction buffer.

To assess temperature stability, LlTrePP (0.14 μg/mL) was incubated in 10 mM MES-NaOH (pH 5.5) at various temperatures for 15 min, and residual activity was measured by the standard enzyme assay method. Stable range of pH at 4°C and 30°C was assessed based on residual activity after the pH treatment. In the pH treatment at 4°C, LlTrePP (6.9 μg/mL) was kept in 100 mM buffers (sodium acetate buffer, pH 3.0–5.0; MES-NaOH buffer, pH 5.0–7.0; HEPES-NaOH buffer, pH 7.0–8.0; Tricine-NaOH buffer, pH 8.0–8.7; and glycine-NaOH buffer, pH 8.7–11.0) containing 0.5 mg/mL BSA for 24 h. In the pH treatment at 30°C, LlTrePP (0.46 μg/mL) was kept in 20 mM buffers (sodium acetate buffer, pH 4.1–4.7; sodium citrate buffer, pH 4.5–6.3; MES-NaOH buffer, pH 5.7–6.2; HEPES-NaOH buffer, pH 6.5–7.5; *N,N*-bis(2-hydroxyethyl)glycine (Bicine)-NaOH buffer, pH 7.9–8.7; and *N*-cyclohexyl-2-aminoethanesulfonic acid (CHES)-NaOH buffer, pH 8.4–9.2) containing 0.9 mg/mL BSA for 15 min. The ranges of pH and temperature in which the enzyme retained ≥90% of the original activity were regarded as the stable ranges.

2.2.12. Determination of kinetic parameters for the reverse phosphorolysis of Tre6*P*

Kinetic parameters for the reverse phosphorolysis of Tre6*P* were calculated from the initial velocities toward various concentrations of β-Glc1*P* (0.13, 0.20, 0.26, 0.33, and 0.39 mM) and Glc6*P* (3.7, 5.5, 7.2, 9.2, and 11 mM) by fitting to the equation for a sequential bi bi mechanism (Cleland, 1963) (Eq. 2-1).

Eq.2-1 $v = k_{cat}[A][B] / (K_{iA} K_{mB} + K_{mB} [A] + K_{mA} [B] + [A][B])$

A = β-Glc1*P*, B = Glc6*P*

Non-linear regression was performed with Grafit version 7.0.2 (Erithacus Software, East Grinstead, UK).

2.2.13. Analysis of acceptor specificity in reverse phosphorolysis

Acceptor substrates in the reverse phosphorolysis of LlTrePP were screened by measuring activities for inorganic phosphate releasing under the conditions of the standard enzyme assay. Enzyme concentration was 345 μg/mL, and following compounds were tested as acceptor substrates: D-glucose, D-galactose, D-mannose, D-fructose, L-arabinose, D-xylose, D-sorbose, maltose, trehalose, lactose, sucrose, methyl α-D-glucopyranoside, methyl β-D-glucopyranoside, D-glucitol, D-glucosamine, Man6*P*, Gal6*P*, and Fru6*P*.

2.2.14. Activity assay of β-PGM

Activity of β-PGM was measured according to Zhang *et al*. (Zhang et al., 2005). A reaction mixture (150 μL), composed of an appropriate concentration of enzyme, 50 mM HEPES-NaOH buffer (pH 7.0), 6.67 mM β-Glc1*P*, 2 mM magnesium acetate, 0.1 μM α-D-glucose-1,6-bisphosphate (Sigma-Aldrich), 0.8 mM Thio-NAD^+, 3.75 U/mL Glc6*P* dehydrogenase, and 0.13 mg/mL BSA, was incubated at 30°C for 10 min. The reaction was terminated by incubating the sample at 80°C for 5 min. Glc6*P* was quantified as described above. One unit of β-PGM was defined as the amount of enzyme that converts 1 μmol β-Glc1*P* to Glc6*P* per minute under these conditions.

2.2.15. Activity assay of hexose phosphatase

Activity of hexose phosphatase was measured according to Wildberger *et al*. (Wildberger et al., 2015). Liberation of inorganic phosphate from Glc6*P* was measured. A reaction mixture (50 μL), composed

of an appropriate concentration of enzyme, 100 mM HEPES-NaOH buffer (pH 7.0), 20 mM Glc6*P*, 2 mM $MgCl_2$, and 0.2 mg/mL BSA, was incubated at 30°C for 10 min. The reaction was terminated by incubating the sample at 80°C for 5 min. Inorganic phosphate liberated was measured according to the previous publication (Lowry and Lopez, 1946). One unit of enzyme activity was defined as the amount of enzyme producing 1 μmol of inorganic phosphate in 1 min in these conditions.

2.2.16. Structural analysis of oligosaccharide synthesized from β-Glc1*P* and Man6*P*

A reaction mixture, composed of 100 mM β-Glc1*P*, 100 mM Man6*P*, 100 U/mL LlTrePP, 5 mM MES-NaOH (pH 6.5) and 0.5 mg/mL BSA, was incubated at 30°C. Aliquots (20 μL) were taken at 0.5, 1, 2, 4, 8, 16, 24, 36 and 48 h, and kept at 80°C for 5 min to stop the reaction. Inorganic phosphate concentrations, regarded as the same as the product saccharide concentrations, were measured. From 2460 μL of the 48-h reaction mixture, the product was purified by electrodialysis with a Microacylizer G1 (Asahi Kasei Co., Tokyo, Japan). Firstly, inorganic phosphate was removed from the sample by electrodialysis against 30 mL of 0.5 M $NaNO_3$ solution with cartridge AC-110 (molecular mass cutoff 100 Da; Astom, Tokyo Japan) until the current was <0.02 A. The sample was then electrodialyzed against 30 mL of H_2O through cartridge AC-220 (molecular mass cutoff 300 Da; Astom) for 1 h to remove mono-saccharide phosphates obtain the sugar phosphate in the dialysate.

Electrospray ionization-mass spectrometry (ESI-MS) was performed with an Exactive Mass Spectrometer (Thermo Scientific, San Jose, CA, USA). The sample was dissolved in methanol and injected for analysis by flow injection. Methanol was used as the mobile phase solvent. The negative ion was detected in the following conditions: tube lens voltage 80 V, skimmer voltage 30 V.

Nuclear magnetic resonance (NMR) spectra were recorded in D_2O (99.9%; Sigma-Aldrich) using a Bruker AMX500 (500 MHz; Bruker, Billerica, MA, USA). A series of two-dimensional homo- and heteronuclear correlated spectra, i.e. correlated spectroscopy (COSY), heteronuclear single

quantum coherence (HSQC) spectroscopy, HSQC-total correlation spectroscopy (HSQC-TOCSY), heteronuclear 2 bond correlation (H2BC) spectroscopy, and heteronuclear multiple bond correlation (HMBC) spectroscopy were obtained.

2.2.17. Quantification of carbohydrates

Carbohydrates were quantified using HPAEC-PAD (HPAEC-PAD ICS 5000^{+}; Thermo Fisher Scientific, Waltham, MA, USA) on a CarboPac PA1 column (4 mm i.d.×250 mm; Thermo Fisher Scientific). The mobile phase was 200 mM NaOH with a linear gradient of sodium acetate (0–250 mM) in 40 min (flow rate, 0.8 mL/min). The sample injection volume was 10 µL. The standards were 25–200 µM Tre6*P*, 30–120 µM Glcα1-1αMan6*P*, 25–200 µM Glc6*P*, 25–200 µM β-Glc1*P*, 50–400 µM maltose, and 50–400 µM D-glucose. The retention times of D-glucose, maltose, Tre6*P*, Glcα1-1αMan6*P*, β-Glc1*P*, and Glc6*P* were 4, 9, 19, 19, 20, and 26 min, respectively. The concentration of Glcα1-1αMan6*P* solution was verified by the phenol-sulfuric acid method (Dubois et al., 1956).

2.2.18. Synthesis of Tre6*P* from β-Glc1*P* and Glc6*P* using TrePP

A reaction mixture (10 mL), containing 0.2 U/mL LlTrePP, 100 mM β-Glc1*P*, 100 mM Glc6*P*, and 250 mM sodium acetate buffer (pH 5.0), was incubated at 30°C for 36 h. The reaction was stopped by heating the sample at 80°C for 5 min. Inorganic phosphate was measured following the method of Lowry and Lopez (Lowry and Lopez, 1946). The concentration of Tre6*P* after the reaction was determined by HPAEC-PAD. Remaining β-Glc1*P*, Glc6*P*, inorganic phosphate, and sodium acetate were removed from the sample by electrodialysis as described above. ESI-MS and NMR analysis of the oligosaccharide produced was carried out as described in section 2.2.16

2.2.19. Synthesis of Tre6*P* from maltose and Glc6*P* using TrePP and MP

A reaction mixture (1 mL), containing 1.2 U/mL LlTrePP, 3.0 U/mL MP, 100 mM maltose, 100 mM Glc6*P*, and 20 mM sodium phosphate buffer (pH 6.8), was incubated at 30°C. Aliquots (20 μL) were taken at indicated time and heated at 80°C for 5 min to stop the reaction. The concentration of Tre6*P* was determined by HPAEC-PAD.

2.2.20. Synthesis of Tre6*P* from maltose and inorganic phosphate by TrePP, MP, and β-PGM

A reaction mixture (1 mL) containing 1.2 U/mL LlTrePP, 3.0 U/mL MP, 1.0 U/mL β-PGM, 100–120 mM maltose, 20–469 mM sodium phosphate, 1 mM magnesium acetate, and 0.1 μM α-D-glucose 1,6-bisphosphate was incubated at 30°C for 120 h. Aliquots (100 μL) were taken and heated at 80°C for 5 min. β-Glc1*P*, Glc6*P*, Tre6*P*, D-glucose, and maltose were quantified by HPAEC-PAD, and inorganic phosphate was measured by following the method of Lowry and Lopez (Lowry and Lopez, 1946).

Synthesis of Tre6*P* from high concentrations of the substrates (1 M maltose and 0.6 M sodium phosphate buffer, pH 7.0) was performed in the presence of bakery yeast (starting added concentration was 10 mg/mL). A reaction mixture (1 mL), containing the same concentrations of enzyme and magnesium acetate but did not contain α-D-glucose 1,6-bisphosphate. The reaction proceeded under the same conditions as described above. Compounds were quantified as described above. On day 4 of the reaction, 20.6 μL of the enzyme mixture containing 1.2 U LlTrePP, 3.0 U MP, and 3.0 U β-PGM was added, and the incubation was continued.

For Tre6*P* preparation, 100 mL of the reaction mixture containing 1 M maltose, 0.6 M sodium phosphate buffer (pH 7.0), 1 mM magnesium acetate, and 3 U/mL MP from Oriental Yeast was incubated at 30°C. At 48 h of the reaction, 2 mL of the enzyme mixture containing 320 U LlTrePP, 500 U MP, and 590 U β-PGM was added. The reaction was terminated on day 5 by heating at 80°C for 5 min. To remove Glc6*P* and β-Glc1*P*, 208 U YidA was added and incubated at 30°C for 8 h, followed by heating the sample at 80°C for 5 min. The reaction mixture was filtered, and glycine was

added to a concentration of 1 M. This mixture was concentrated at 60°C under reduced pressure. The Maillard reaction proceeded during the concentration procedure. The sample was loaded onto an anion exchange column of Amberjet 4400 resin (4.8 cm i.d.×30 cm, 300 mL, OH^- form), and eluted with 0.25 M potassium acetate buffer (pH 5.0) in accordance with a previously described method (Hokse, 1983). Fractions containing Tre6*P* were collected, and 12 mmol of magnesium acetate and ammonia (three times of the inorganic phosphate content) were added for the formation of struvite precipitation (Ashby et al., 1955; Suzuki et al., 2009). After removing the precipitate of $MgNH_4PO_4$, the pH of the sample was adjusted to 10 with 6 M KOH, and the mixture was concentrated. The mixture was subjected to gel filtration chromatography on a Toyopearl HW-40S column (5.0 cm i.d.×90 cm, 1770 mL, Tosoh, Tokyo, Japan) using water as the eluent (flow rate: 0.9 mL/min). Fractions containing Tre6*P* were collected, and the pooled sample was passed through a column of (Dowex 50 H^+ type) to remove counter ions of Tre6*P*. The pH was adjusted to 8.5 with 6 M KOH and concentrated. Then, Tre6*P* was precipitated in 96% ethanol. The purity was confirmed by HPAEC-PAD and ^{1}H-NMR.

2.3. Results

2.3.1. Production, purification, and basic properties of recombinant LlTrePP

The *TrePP* gene of *L. lactis* subsp. *lactis* JCM 5805 was obtained from the genomic DNA by PCR. The recombinant enzyme with an 11-residue C-terminal extension AAALEHHHHHH was produced in *E. coli* and purified by Ni-affinity column chromatography. From 1.0 L of culture broth of the *E. coli* transformant, 19 mg of LlTrePP was obtained. The specific activity of reverse phosphorolysis to 10 mM β-Glc1*P* and 10 mM Glc6*P* at 30°C was 253 U/mg. The reaction velocity for the phosphorolysis of 0.670 mM Tre6*P* in the presence of 0.1 M inorganic phosphate at 35°C was 36.5 μmol/min/mg protein. SDS-PAGE analysis indicated that the molecular mass of LlTrePP was 90 kDa (Fig. 2-1A), which coincided well with the theoretical mass (88,387 Da). The molecular mass of

LlTrePP in non-denaturing conditions determined by BN-PAGE was 184 kDa (Fig. 2-1B).

For the phosphorolysis of Tre6*P*, the optimum pH was 6.1 (Fig. 2-2A), which is consistent well with the result of the previous study (Andersson et al., 2001). The optimum pH of LlTrePP for the synthesis of Tre6*P* was 4.8 (Fig. 2-2B), which is 1.3 pH units lower than that for the phosphorolysis. The activity of LlTrePP was retained after incubation at pH 4.5–9.0 at 4°C for 24 h (Fig. 2-2C) and pH 5.0–8.0 at 30°C for 15 min (Fig. 2-2D). The optimum pH (pH 4.8) for Tre6P synthesis was outside the stable pH range of LlTrePP at pH 30°C; thus, characterization was carried out at pH 5.5 as the better pH condition within the stable range. The optimum temperature of LlTrePP was 40°C in a 10-min reaction, and LlTrePP retained ≥90% activity up to 30°C for 15 min (Fig. 2-3); thus, the reaction temperature was set at 30°C.

2.3.2. Kinetic analysis of the reverse phosphorolysis of LlTrePP

Initial reaction velocities of LlTrePP were measured for the reverse phosphorolysis at various concentrations of β-Glc1*P* and Glc6*P*. Double reciprocal plots of 1/[β-Glc1*P*] versus 1/*v* at various concentrations of Glc6*P* were linear and crossed at a single point (Fig. 2-4). Thus, this enzyme catalyzes the reactions through a sequential bi bi mechanism involving the formation of a ternary complex, as observed in the phosphorolysis of Tre6*P* (Andersson et al., 2001). Kinetic parameters for the reverse phosphorolysis were: k_{cat} 759 ± 108 s^{-1}, $K_{m\ Glc6P}$ 1.85 ± 0.918 mM, $K_{m\ \beta\text{-}Glc1P}$ 0.413 ± 0.0632 mM, and $K_{i\ \beta\text{-}Glc1P}$ 0.519 ± 0.499 mM (parameter definitions are following section 2.2.12).

The acceptor specificity of LlTrePP was investigated by measuring velocity for the reverse phosphorolysis towards various acceptors (10 mM) in the presence of 10 mM β-Glc1*P* (Table 2-1). LlTrePP showed activity to Man6*P* and Gal6*P* served as an acceptor substrate aside from Glc6*P*. The reaction velocity for Man6*P* and Gal6*P* was 0.134 μmol/min/mg and 0.0663 μmol/min/mg, respectively, which was 0.053% and 0.026% of the value for Glc6*P,* respectively.

2.3.3. Synthesis and structural analysis of a novel disaccharide phosphate

In the synthetic reaction of LlTrePP using 100 mM Man6*P* and 100 mM β-Glc1*P*, release of inorganic phosphate was monitored (Fig. 2-5). At 16 h, the reaction almost reached equilibrium. The concentration of the inorganic phosphate released was 86.6 mM, and the equilibrium constant (K_{eq} = [the product][inorganic phosphate] / [β-Glc1*P*][Man6*P*]) was 41.8. At 48 h, the inorganic phosphate concentration was 81.6 mM. The saccharide product concentration measured by HPAEC-PAD was 83.2 mM, and the total content in 2460 μL of the reaction mixture was 205 μmol. The product was purified through electrodialysis, and 126 μmol of the product was obtained, the yield based on substrate was 51.1%. This product was analyzed by ESI-MS and NMR. The product gave a signal at 421.08 *m*/*z* $[M-H]^-$. The chemical shifts of ^{1}H- and ^{13}C-NMR analyses are summarized in Table 2-2 and Fig. 2-6. Correlation peaks between C1 of the D-glucosyl residue and H1' of the Man6*P* residue, and between H1 of the D-glucosyl residue and C1' of the Man6*P* residue, were observed in the HMBC spectrum (Fig. 2-7), indicating that the glycosidic linkages were formed in the disaccharide between C1 of both residues and O1 of the other residues. Because the $J_{H1, H2}$ value of the Glc was 3.7 Hz, and $J_{H1', C1'}$ of the Man6*P* residue obtained in the HMBC spectrum was 174 Hz (around 170 Hz for α-hexopyranoses) (Bock and Pedersen, 1974), α-anomeric configuration of the both sugar residues were confirmed. Taken together, the reaction product was determined to be a new sugar phosphate, Glcα1-1αMan6*P*.

2.3.4. Tre6*P* synthesis from β-Glc1*P* and Glc6*P* by the reverse phosphorolysis of LlTrePP

LlTrePP was incubated with 100 mM β-Glc1*P* and 100 mM Glc6*P* at 30°C, and released inorganic phosphate was monitored (Fig. 2-8). The concentration of inorganic phosphate was identical to that of the produced Tre6*P* (data not shown). Tre6*P* did not significantly change after 24 h. Tre6*P* attained

91.9 mM in 36 h. From this result, the equilibrium constant of the phosphorolysis of Tre6*P* —K_{eq} = [β-Glc1*P*][Glc6*P*] / [Tre6*P*][inorganic phosphate]— was determined to be 0.0078. The reaction product was purified by electrodialysis and analyzed by ESI-MS and NMR. The product gave a signal at 421.07 *m*/*z* $[M-H]^-$. The chemical shifts detected in the ^{1}H- and ^{13}C-NMR analyses are summarized in Table 2-3. Correlation peaks between C1 of the D-glucosyl residue and H1 of Glc6*P*, and between H1 of the D-glucosyl residue and C1 of Glc6*P*, were observed in the HMBC spectrum, which indicated that double glucosidic linkages had formed between the D-glucosyl residue and Glc6*P* residue. The $J_{H1, H2}$ values of Glc and Glc6*P* were 3.75 Hz and 3.85 Hz, respectively, indicating that both pyranoses were in an α-anomeric configuration. The chemical shifts obtained from the ^{1}H- and ^{13}C-NMR matched those previously reported for Tre6*P* (Liu and Mariano, 2015; Rønnow et al., 1994). Consequently, the reaction product of LlTrePP from β-Glc1*P* and Glc6*P* was confirmed to be Tre6*P*.

2.3.5. One-pot synthesis of Tre6*P* from maltose and Glc6*P* by LlTrePP and MP

Instead of using β-Glc1*P* as a starting material, maltose. Maltose and Glc6*P* were used as starting materials for Tre6*P* synthesis. It was expected that β-Glc1*P* was supplied by phosphorolysis of maltose by MP and used for Tre6*P* production by LlTrePP (Fig. 2-9A). The inorganic phosphate used as a substrate in the MP reaction is released in the reverse phosphorolysis of Tre6*P*. Using 100 mM maltose and 100 mM Glc6*P* in the presence of 20 mM sodium phosphate buffer (pH 6.8) as initial concentrations, Tre6*P* was produced and accumulated to 65 mM in 28 h (Fig. 2-9B). Extending the reaction time after 8 h did not significantly change the Tre6*P* concentration. The yield was 65% based on the maltose concentration (100 mM) and comparable to that of trehalose production from maltose (60%) by the coupled reaction by trehalose phosphorylase and MP (Yoshida et al., 1998).

2.3.6. One-pot synthesis of Tre6*P* from maltose and inorganic phospahte and effect of inorganic

phosphate concentration

Tre6*P* was produced using maltose as a sole carbohydrate source. The expected reaction scheme is shown in Fig. 2-10A. Glc6*P* was not added, but the addition of β-PGM was expected to supply Glc6*P* from β-Glc1*P*. β-PGM has strict anomeric selectivity, and it did not produce α-D-glucose 1-phosphate (data not shown). Tre6*P* was produced from 100–120 mM maltose and 20–469 mM inorganic phosphate. The progress of consumption of the starting materials and reaction products were monitored (Fig. 2-10B–F). During all the reactions, the sum of the substance of the total glucosyl group and the total phosphate in the reaction mixtures were kept within 12%, the total mass balances were kept in all the reactions. In the reaction with 20 mM inorganic phosphate, the reaction reached a plateau rapidly almost in 6 h (Fig. 2-10B). The concentration of Tre6*P* (20 mM), was comparable to the initial concentration of inorganic phosphate. Those of β-Glc1*P* and Glc6*P* were low. This indicates that almost all the inorganic phosphate was incorporated into Tre6*P*. The Tre6*P* yield based on the initial concentration of maltose (100 mM) was 20%; that is, 40% (40 mM) of maltose molecules were used for Tre6*P* synthesis, and 40 mM glucose was released, and the other 40 mM glucose moiety was converted to Tre6*P*. Hereinafter, the percentage of maltose molecules that was used for Tre6*P* synthesis is used as the yield. The K_{eq} ($K_{eq} = K_{TrePP} \times K_{MP}^2 \times K_{\beta\text{-PGM}} = [\text{Tre6}P][\text{glucose}]^2 / ([\text{maltose}]^2[\text{inorganic phosphate}])$ at 12 h was 3.87 ± 0.18, which is close to the theoretical K_{eq} (4.73), calculated from K_{TrePP} [31.3 at 35°C in pH 7.0 (Andersson et al., 2001)], K_{MP} [0.071 at 30°C in pH 7.0 (Aisaka et al., 1996)], $K_{\beta\text{-PGM}}$ [30 at 30°C in pH 7.0 measured in this work; data not shown]. Higher initial inorganic phosphate concentrations up to 224 mM resulted in higher consumption of maltose up to 93% consumption (Fig. 2-10E). The maximum Tre6*P* concentration (33 mM) was attained with 48 h reaction with an initial phosphate concentration of 54 mM (Fig. 2-10C). The yield was 55%. Initial phosphate concentrations higher than 54 mM resulted in lower Tre6*P* production but significant accumulation of Glc6*P*. Under the reaction conditions, the ratio of produced Tre6*P* and Glc6*P* was

not changed by decreasing β-PGM concentration, but just the reaction was delayed (Fig. 2-11). In the 120-h reaction with 469 mM inorganic phosphate, lower consumption of maltose (59% consumption), a higher concentration of β-Glc1*P* than Glc6*P*, and lower production of Tre6*P* (15 mM) were observed (Fig. 2-10F). In the early stage of all reactions, maltose decreased quickly. Concomitantly, β-Glc1*P* was accumulated first and replaced by Tre6*P* and Glc6*P*. The reduction of β-Glc1*P* was delayed depending on inorganic phosphate concentration. Unlike other reactions, β-Glc1*P* was accumulated more than Glc6*P* under 469 mM inorganic phosphate. The concentrations continued to change after 80 h and seemed not to attain equilibrium. The β-PGM reaction took longer to attain equilibrium under a high concentration of inorganic phosphate (data not shown). The β-PGM reaction is considered to be inhibited by inorganic phosphate, which is consistent with the finding that β-PGM activity of *Euglena gracilis* was inhibited by 20% in the presence of 10 mM inorganic phosphate (Belocopitow and Maréchal, 1974). Therefore, the production of Glc6*P* and Tre6*P* did not proceed until the concentration of inorganic phosphate decreased and the β-PGM reaction started. That was the reason why all reactions took a long time despite the high enzyme concentration.

2.3.7. Efficiency improvement of Tre6*P* synthesis using yeast

The reaction from a higher concentration of starting materials, 1 M maltose and 0.6 M inorganic phosphate, was examined (Fig. 2-12A). During the reaction, the sum of the total concentration of D-glucosyl group and phosphate measured were 900–1100 mM and 540–660 mM, respectively, and the total mass balance was kept in the reaction (the errors were within 10%). Maltose concentration decreased to 800 mM and β-Glc1*P* was accumulated in the early stage of the reaction in the presence of remaining inorganic phosphate (Fig. 2-12A). The maltose and β-Glc1*P* concentrations did not change after 2 days. That was because, in the presence of a high concentration of inorganic phosphate, the activity of β-PGM was inhibited by remained inorganic phosphate, and β-PGM might be

deactivated during incubation. After three enzymes, LlTrePP, MP, and β-PGM were added on day 4. Maltose and β-Glc1*P* concentrations decreased, and Tre6*P* and Glc6*P* concentrations increased. Until day 9, 0.7 M maltose was consumed, and 0.7 M glucose and 0.3 M Tre6*P* were produced. The reaction progressed more quickly with addition of yeast in the reaction mixture for reduction of D-glucose, released from maltose by MP (Fig. 2-12B). During the 9-day reaction, the sum of the total D-glucosyl group was decreased to 50% because yeast consumed D-glucose. The error of the sum of the total phosphate was kept within the range of 10%. In this case, maltose and inorganic phosphate concentrations decreased more quickly and β-Glc1*P* accumulated to 0.5 M at day 2. After the addition of LlTrePP, MP, and β-PGM, the Tre6*P* concentration attained 0.4 M in the reaction mixture (the yield was 80%). In either case, Glc6*P* and Tre6*P* were considered not to be produced before the additional supplementation of enzymes. This implies the inactivation of β-PGM during the reaction for day 2.

For the preparation of Tre6*P*, the reaction mixture was up-scaled to 100 mL, which contained 100 mmol maltose, 60 mmol inorganic phosphate, and MP in the presence of yeast (Fig. 2-13, Table 2-4). For the first 2 days, only MP was in the reaction mixture, and LlTrePP, MP, and β-PGM were added at day 2. At day 2 of the incubation, LlTrePP, MP, and β-PGM were added. At day 5, Tre6*P* attained 370 mM (38 mmol). For purification of Tre6*P*, Glc6*P* and β-Glc1*P* were dephosphorylated by *E. coli* hexose phosphatase. Remaining glucose, Glc6*P* were removed by the Maillard reaction followed by the anion exchange column chromatography. They were not difficult to separate by the chromatography without the Maillard reaction (Fig. 2-14), but their Maillard reaction products were removed by it (Fig. 2-14). Most remaining inorganic phosphate was removed by the struvite precipitation. Then, Tre6*P* was further purified by the gel filtration, and 19 mmol (9.4 g) of Tre6*P* was obtained as dipotassium salt with a yield of 38%. The purity was higher than 98%. The NMR spectra of purified Tre6*P* was confirmed (Fig. 2-15B). These spectra were well-matched with the Tre6*P* synthesized from β-Glc1*P* and Glc6*P* (Fig. 2-15A).

2.4. Discussion

LlTrePP was analyzed to apply to the enzymatic synthesis of Tre6*P* and its derivatives. The molecular mass of LlTrePP determined by SDS-PAGE and BN-PAGE were 90 kDa and 184 kDa, respectively (Fig. 2-1). This result indicates that recombinant LlTrePP is a homodimeric protein in non-denaturing conditions although the native LlTrePP was reported to be a monomer (Andersson et al., 2001). Most GH65 enzymes including both native (Aisaka et al., 1996; Chaen et al., 1999a; Kamogawa et al., 1973) and recombinant enzymes are homodimers in solution (Aisaka et al., 1996; Chaen et al., 1999a; Kamogawa et al., 1973; Nakai et al., 2009; Nihira et al., 2012, 2013). The reaction velocity of phosphorolysis of 0.670 mM Tre6*P* in the presence of 0.1 M inorganic phosphate at 35°C was 36.5 μmol/min/mg protein, which was close to the reported velocity of the native enzyme, 32.4 μmol/min/mg, in the same reaction conditions (Andersson et al., 2001). For the phosphorolysis of Tre6*P*, the optimum pH was 6.1 (Fig. 2-2A), which is considered almost the same as previous study (Andersson et al., 2001). Therefore, recombinant LlTrePP was basically the same as native LlTrePP in their catalytic ability in spite of the difference in quaternary structure in solution.

No N-terminal signal peptide was predicted in LlTrePP, it suggesting that is an intracellular enzyme (Andersson et al., 2001). The optimum pH 6.1 for Tre6*P* phosphorolysis also suggests the suitable for the intracellular decomposition of Tre6*P*, since the intracellular pH of bacteria is generally neutral (Booth, 1985). However, the optimum pH of LlTrePP for the synthesis of Tre6*P* was 4.8 (Fig. 2-2B), 1.3 pH units lower than that for the phosphorolysis. Some GH65 enzymes exhibit similar optimum pHs for both phosphorolysis and reverse phosphorolysis (Aisaka et al., 1998; Chaen et al., 1999b, 1999a; Nihira et al., 2013). However, *Lactobacillus acidophilus* MP had a considerably lower optimum pH for the reverse phosphorolysis (pH 3.4) than for the phosphorolysis (pH 6.2) (Nakai et al., 2009), as also observed here for LlTrePP. A lower optimum pH for the reverse phosphorolysis was

also observed for some more trehalose phosphorylases (Aisaka et al., 1996; Kizawa et al., 1995; Marechal and Belocopitow, 1972; Nihira et al., 2012). On the basis of the proposed reaction mechanism for inverting phosphorylases (Egloff et al., 2001; Hidaka et al., 2004), the catalytic acidic residue, acting as a general acid in the phosphorolysis, should be dissociated in the reverse phosphorolysis to act as a general base catalyst that takes the proton from the hydroxy group of the acceptor substrate. Lower pH is, however, unfavorable for the dissociation of the catalytic residue. The fact that LlTrePP showed a lower optimum pH for reverse phosphorolysis might be attributed to some amino acid residue near the active-site and the state of phosphate released.

LlTrePP use Glc6*P* predominantly as acceptor in the reverse phosphorolysis of LlTrePP. But in this work, two more poor acceptor, Man6*P* and Gal6*P* were found (Table 2-1). Some GH65 enzymes acting on D-glucose as acceptors act on D-xylose and even L-fucose as acceptors, i.e. the hydroxymethylene group of D-glucose as acceptor substrate is not essential (Aisaka et al., 1996; Chaen et al., 1999a; Nakai et al., 2009). However, LlTrePP did not use D-xylose, L-arabinose, or D-glucose as acceptors. The acceptor preference of LlTrePP indicates that the phosphate group at the C-6 position is essential in acceptor, which discriminate TrePP from the other GH65 enzymes. The spatial configuration of the phosphate group must be unique for the enzyme in addition with that of the other hydroxy groups.

A Tre6*P* analogue, α-D-Glc*p*-(1↔1)-α-D-Man*p*6*P* (Glcα1-1αMan6*P*), was synthesized. This compound might have the potential to act as a signaling molecule in plants because it structurally mimics Tre6*P*. The function of trehalose and Tre6*P* are described in chapter 1. Besides, an application of plant-permeable analogues of Tre6*P* (1 mM) modulated Tre6*P* levels *in planta*, and increased resilience, and crop yield by 13–20% (Griffiths et al., 2016). These analogs are chemically modified to mask the charge of phosphate. After penetration to the plant, these analogs were converted to Tre6*P* in the plant body by exposure to light because the modification group is released by the light-activation.

These findings imply that other Tre6*P* analogs have potential as bioactive tools. Glcα1-1αMan6*P* might have bioactivity and be applied for further research into Tre6*P* function. The degradation will be mentioned in chapter 3.

The Tre6*P* yield of this enzymatic method was higher than that of the yeast fermentation method (11%) and lower than that of organic synthesis (55%) (Doi et al., 1998; Liu and Mariano, 2015; Rønnow et al., 1994). However, the primary advantage of the enzymatic synthesis method established here is the simple synthesis of Tre6*P* at gram-scale in one-pot reaction from abundantly available starting materials, i.e. maltose and inorganic phosphate.

Table 2-1. Reaction velocity for the reverse phosphorolysis toward various acceptor substrates.

Substrate	Velocity (μmol/min/mg)	Relative activity (%)
Glc6*P**	253	100
Man6*P**	0.134	0.0528
Gal6*P**	0.0663	0.0262
Other substrates*	< 0.0300	< 0.0119
None	< 0.0300	< 0.0119

Inorganic phosphate-releasing velocities from 10 mM β-Glc1*P* 10 mM compounds shown as substrate in the table.

*10 mM

Table 2-2. Chemical shifts of α-D-Glc*p*-(1↔1)-α-D-Man*p*6*P* in ^{1}H and ^{13}C NMR spectra.

Residue	Number	δC (ppm)	δH (ppm)	*J* (Hz)	
α-Glc*p*	1	94.3	5.11	d	3.70
	2	71.6	3.55	m	
	3	73.3	3.65	m	
	4	70.4	3.35	t	9.55
	5	73.3	3.59	m	
	6	61.3	3.67	m	
			3.76	m	
α-Man*p*6*P*	1'	96.0	5.03	d	1.10
	2'	70.9	3.91	m	
	3'	70.8	3.88	m	
	4'	66.9	3.78	m	
	5'	73.5	3.76	m	
	6'	63.5	3.87	m	
			3.92	m	

The prime (') refers to the Man6*P* residue.

Table 2-3. Chemical shifts of Tre6*P* in the ^{1}H- and ^{13}C-NMR spectra.

Residue	Number	δC (ppm)	δH (ppm)	*J* (Hz)	
α-Glc*p*	1'	94.3	5.27	d	3.75
	2'	71.9	3.70	m	
	3'	73.4	3.93	m	
	4'	70.6	3.51	t	9.43
	5'	73.1	3.88	m	
	6'	61.5	3.93	m	
			3.83	m	
α-Glc*p*6*P*	1	94.4	5.25	d	3.85
	2	72.1	3.76	m	
	3	73.2	3.90	m	
	4	70.1	3.66	t	9.60
	5	72.5	3.97	m	
	6	63.9	4.08	m	

The prime (') refers to the nonphosphorylated ring.

Table 2-4. Purification of Tre6*P*.

Process	Tre6*P* mmol	Glc6*P* mmol	β-Glc1*P* mmol	Purity %	Yield**** %
One-pot reaction mixture (100 mL)	38	12	0.23	64	75
YidA treatment*	36	8.5	0.19	73	72
Anion-exchange column chromatography**	25	N.D.	N.D.	86	50
Gel-filtration column chromatography***	19	N.D.	N.D.	98	38

*YidA: hexose phosphatase

** The Maillard reaction with 1 M glycine at 60°C, followed by the chromatography on Amberjet 4400 column.

*** After struvite precipitation, the supernatant was loaded on the Toyopearl HW 40S column.

****The yield was calculated based on the maltose molecules used for Tre6*P* synthesis.

N.D., not detected

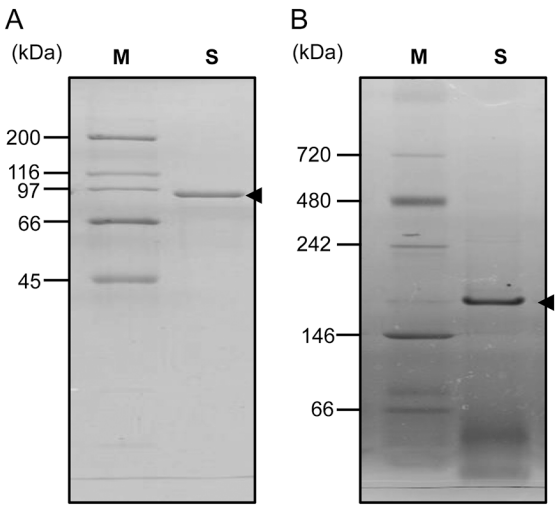

Fig. 2-1. SDS-PAGE and BN-PAGE of purified recombinant LlTrePP.

Purified LlTrePP (1 μg and 3 μg) was analyzed by SDS-PAGE (A) and BN-PAGE (B), respectively. Lane M, size makers; lane S, purified LlTrePP. The molecular masses of the standards are shown on the left. Molecular mass of LlTrePP was estimated to be 90 kDa and 184 kDa by SDS-PAGE and BN-PAGE, respectively.

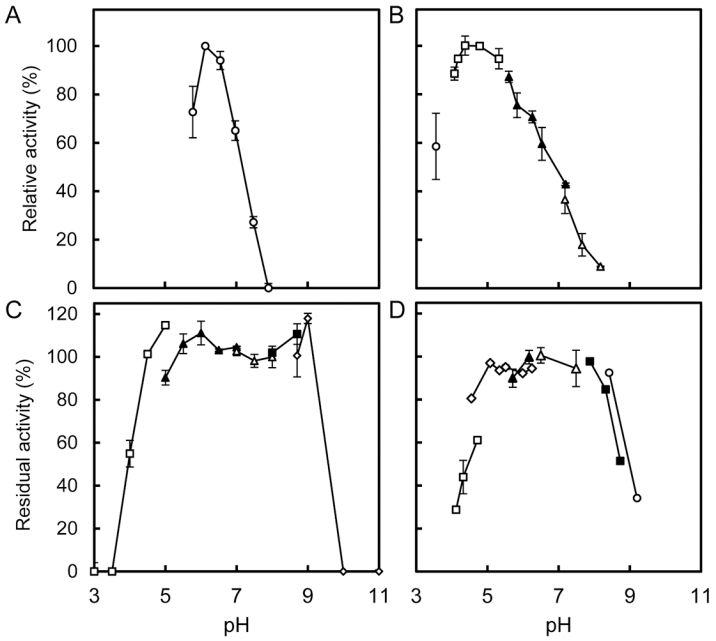

Fig. 2-2. Effects of pH on activity and stability of recombinant LlTrePP.

(A) pH activity curve for the phosphorolytic activity. Glc6*P*-releasing activity was measured with 0.67 mM Tre6*P* in 200 mM potassium phosphate buffer at the indicated pHs at 35°C. (B) pH activity curve for the reverse phosphorolysis. Inorganic phosphate-releasing activity was measured with 10 mM β-Glc1*P* and 10 mM Glc6*P* at the indicated pHs at 30°C. Open circle, glycine-HCl buffer (pH 3.5); open square, sodium acetate buffer (pH 4.0–5.3); filled triangle, MES-NaOH buffer (pH 5.6–7.2); open triangle, HEPES-NaOH buffer (pH 7.2–8.2). (C) pH stability at 4°C. Residual activities after LlTrePP (6.9 μg/mL) was incubated at various pHs at 4°C for 24 h are shown. Open square, sodium acetate buffer (pH 3.0–5.0); filled triangle, MES-NaOH buffer (pH 5.0–7.0); open triangle, HEPES-NaOH buffer (pH 7.0–8.0); filled square, Tricine-NaOH buffer (pH 8.0–8.7); and open diamond, glycine-NaOH buffer (pH 8.7–11.0). (D) pH stability at 30°C. LlTrePP (0.46 μg/mL) was incubated at various pHs at 30°C for 15 min. Open square, sodium acetate buffer (pH 4.1–4.7); open diamond, sodium citrate buffer (pH 4.5–6.3); filled triangle, MES-NaOH buffer (pH 5.7–6.2); open triangle, HEPES-NaOH buffer (pH 6.5–7.5); filled square, Bicine-NaOH buffer (pH 7.9–8.7); and open circle, CHES-NaOH buffer (pH 8.4–9.2). The data are presented as the means of triplicate experiments with standard deviations.

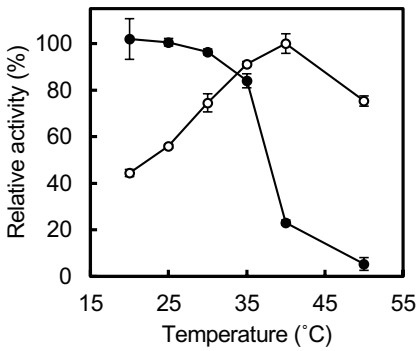

Fig. 2-3. Effects of temperature on activity and stability of recombinant LlTrePP.

Open circles, activities at pH 5.5 in a 10-min reaction. Filled circles, residual activity after incubation at pH 5.5 for 15 min. The data are presented as the means of triplicate experiments with standard deviations.

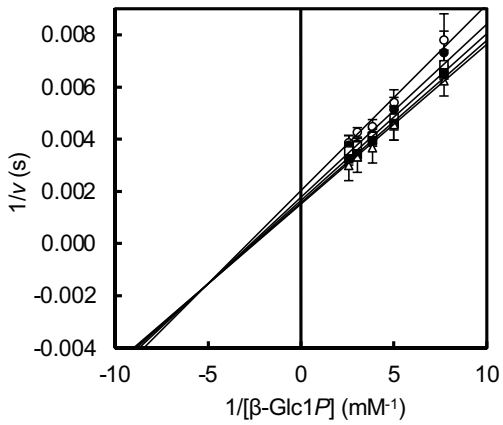

Fig. 2-4. Double reciprocal plots for reverse phosphorolysis of LlTrePP.

Double reciprocal plots for synthesis of Tre6*P*. The concentrations of Glc6*P* were: open circle 3.7 mM, filled circle 5.5 mM, open square 7.2 mM, filled square 9.2 mM, and open triangle 11 mM. The lines were obtained by fitting the data to an equation for a sequential bi bi mechanism. The data are presented as the means of triplicate experiments with standard deviations.

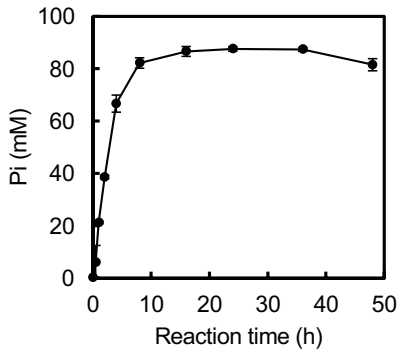

Fig. 2-5. Time course of the reaction of LlTrePP with 100 mM Man6*P* and 100 mM β-Glc1*P*.

Liberated inorganic phosphate, which was produced at an equimolar concentration with the product of the reverse phosphorolysis by LlTrePP, was measured. The data are presented as the means of triplicate experiments with standard deviations.

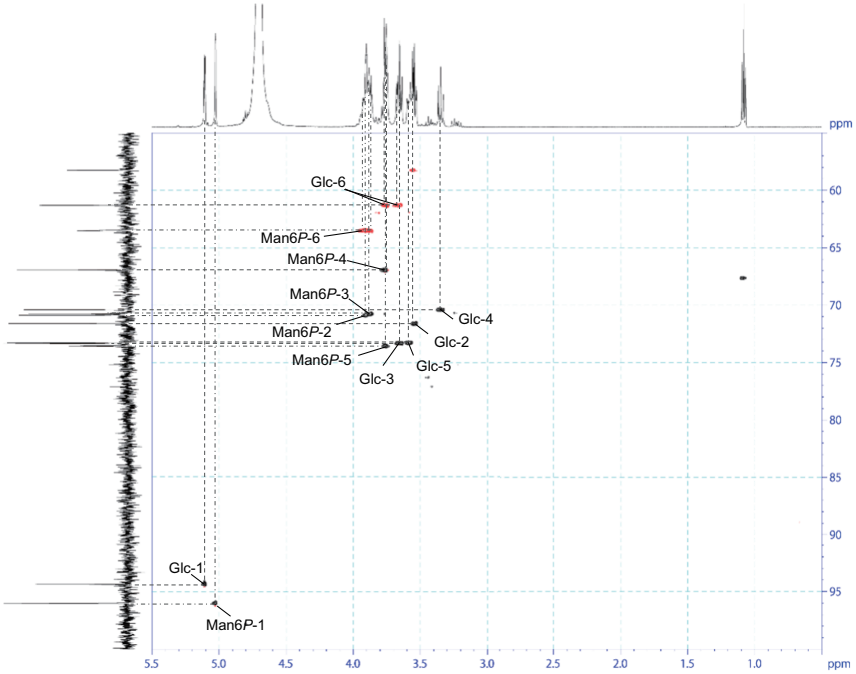

Fig. 2-6. HSQC-spectrum of α-D-Glc*p*-(1↔1)-α-D-Man*p*6*P*.

HSQC spectrum of a novel sugar phosphate, α-D-Glc*p*-(1↔1)-α-D-Man*p*6*P* is shown. Each number shown after the residue indicates the number of the carbon and proton. The dotted lines show the correlation between carbon and proton.

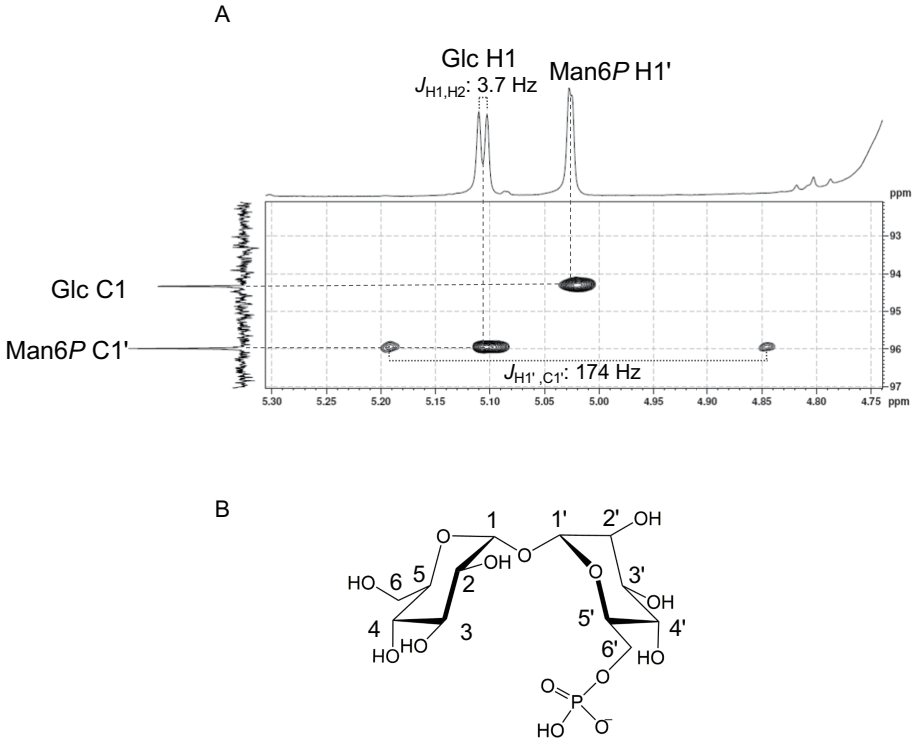

Fig. 2-7. HMBC analysis of the product from β-Glc1*P* and Man6*P* in the reverse phosphorolysis.

(A) The signals for the anomeric protons and carbons of the product in the HMBC analysis are shown. Dotted lines indicate correlations between Glc H1 and Man6*P* C1', and between Glc C1 and Man6*P* H1'. The coupling constants of Glc H1 $J_{H1,H2}$ and Man6*P* H1' $J_{H1',C1'}$ were 3.7 and 174 Hz, respectively.

(B) The carbon numbers are followed as Table 2-2

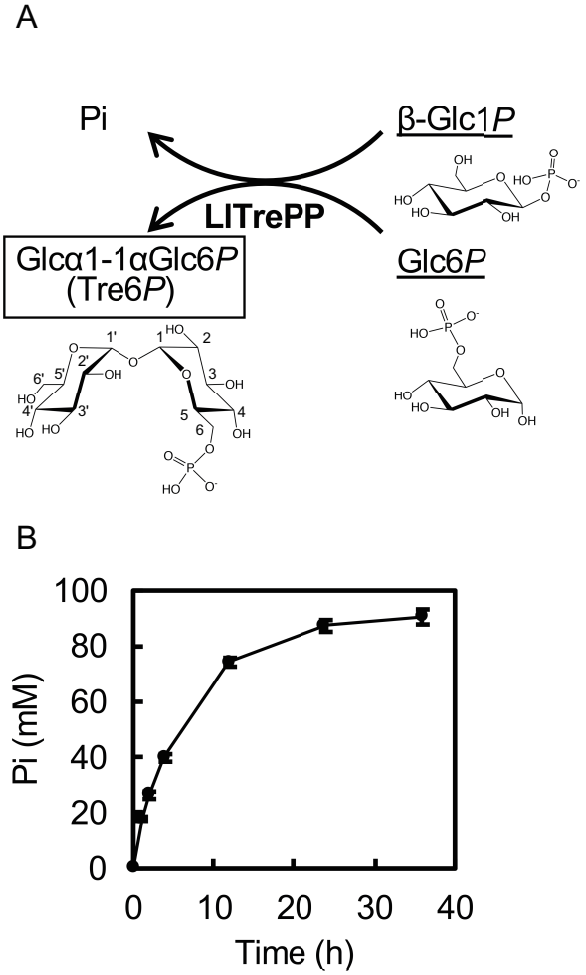

Fig. 2-8. Time course of Tre6*P* formation from 100 mM β-Glc1*P* and 100 mM Glc6*P* by LlTrePP.

(A) Expected reaction scheme. LlTrePP, Tre6*P* phosphorylase from *L. lactis* subsp. *lactis*. The carbon numbers are followed as Table 2-3. (B) Time course of accumulation of Tre6*P*. Starting materials were Glc6*P* (100 mM), and β-Glc1*P* (100 mM). Liberated inorganic phosphate was measured following the method of Lowry and Lopez (Lowry and Lopez, 1946). At 36 h, Tre6*P* was quantified by HPAEC-PAD. The concentration of inorganic phosphate was identical to that of the produced Tre6*P*. Data are means of triplicate experiments with standard deviations in three independent reactions. Glc6*P* in solution is a mixture of α- and β-anomer. α-Glc6*P* is used as a substrate for LlTrePP, and β-Glc6*P* is converted to α-Glc6*P* by mutarotation.

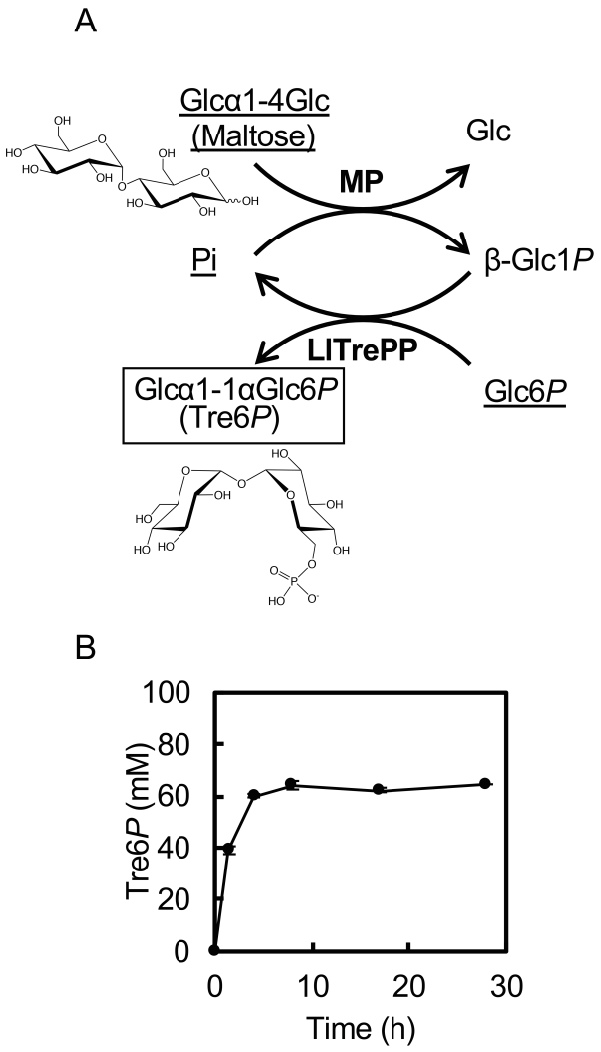

Fig. 2-9. One-pot synthesis of Tre6*P* from maltose and Glc6*P* by LlTrePP and MP.

(A) Expected reaction scheme. LlTrePP, Tre6*P* phosphorylase from *L. lactis* subsp. *lactis*; MP, maltose phosphorylase. (B) Time course of accumulation of Tre6*P*. Starting materials were Glc6*P* (100 mM), maltose (100 mM), and 20 mM inorganic phosphate. Tre6*P* was quantified by HPAEC-PAD. Data are means of triplicate experiments with standard deviations in three independent reactions.

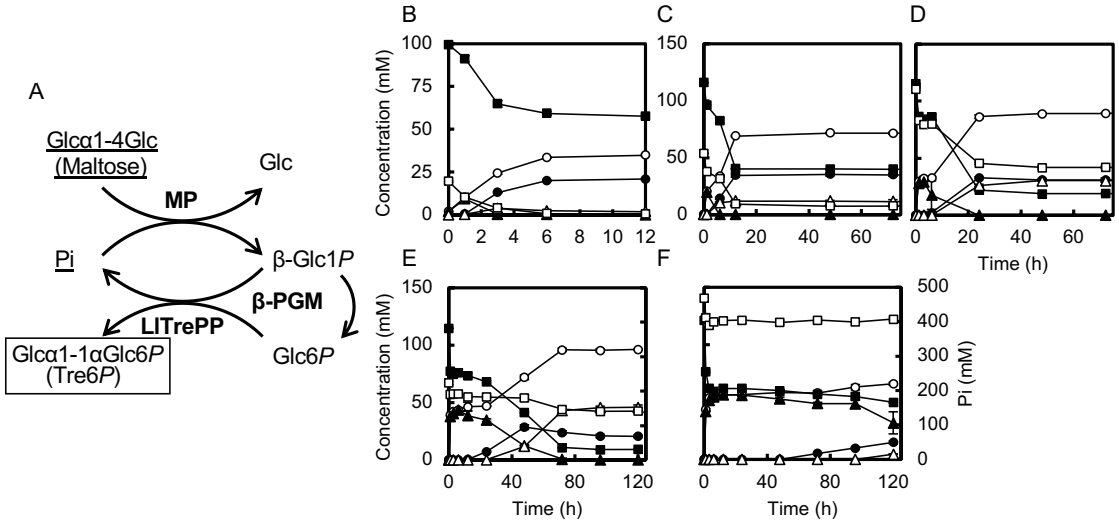

Fig. 2-10. Production of Tre6*P* using maltose as a single carbohydrate source.

(A) Expected reaction scheme. An additional enzyme, β-phosphoglucomutase (β-PGM), was added. (B–F) Time course of accumulation of Tre6*P* synthesized from 100–120 mM maltose and inorganic phosphate (B: 20 mM, C: 54 mM, D: 110 mM, E: 224 mM, F: 469 mM). Tre6*P* and the other carbohydrates were quantified. Maltose (filled square), inorganic phosphate (open square), Tre6*P* (filled circle), glucose (open circle), Glc6*P* (open triangle), and β-Glc1*P* (filled triangle). [Pi]: right side axis in E and F. Data are means of triplicate experiments with standard deviations in three independent reactions.

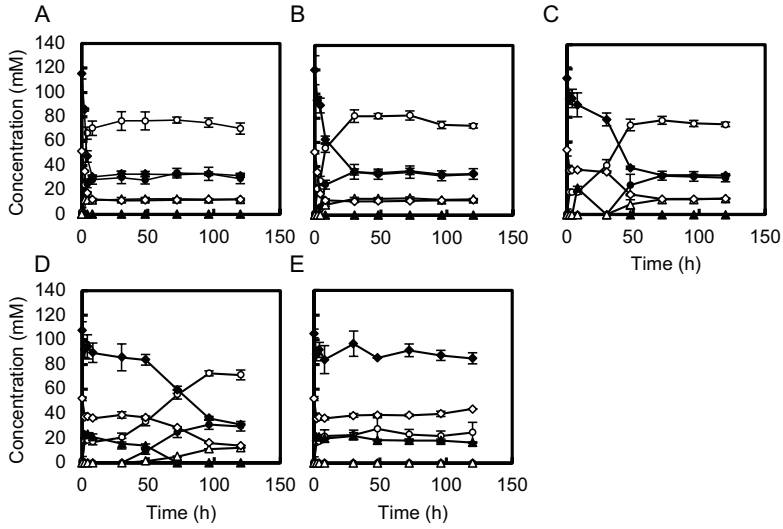

Fig. 2-11 Effect of the β-PGM concentration to the production of Tre6*P* using maltose as a single carbohydrate source.

(A–E) Time course of accumulation of Tre6*P* synthesized from 100–120 mM maltose and 50–54 mM inorganic phosphate in the presence of β-PGM (A: 1 U/mL, B: 0.5 U/mL, C: 0.1 U/mL, D: 0.05 U/mL, E: 0.01 U/mL). Tre6*P* and the other carbohydrates were quantified. Maltose (filled square), inorganic phosphate (open square), Tre6*P* (filled circle), glucose (open circle), Glc6*P* (open triangle), and β-Glc1*P* (filled triangle). Data are means of triplicate experiments with standard deviations in three independent reactions.

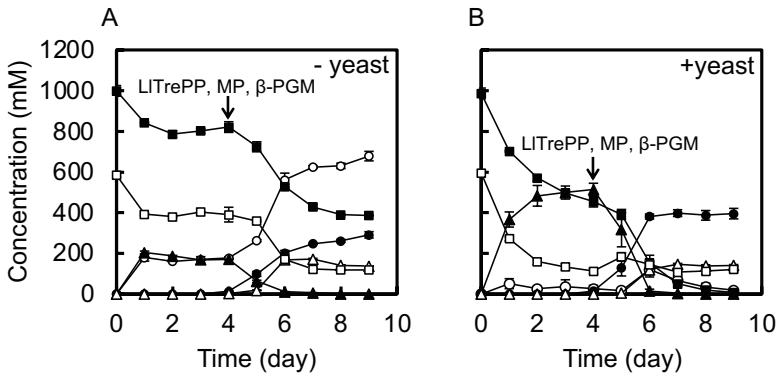

Fig. 2-12. Time course of Tre6*P* synthesis from 1 M maltose and 0.6 M inorganic phosphate.

Time course of Tre6*P* synthesis reactions without yeast (A) and with yeast (B) are shown. The enzymes were supplemented at day 4. Symbols are the same as shown in Fig. 2-10B. Data are means of triplicate experiments with standard deviations in three independent reactions.

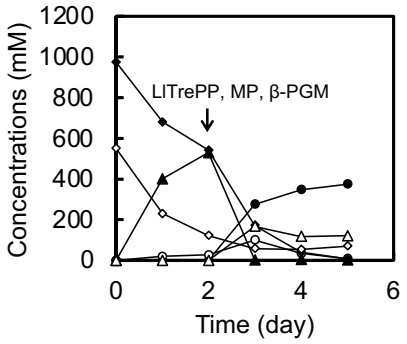

Fig. 2-13. Time course of large-scale (100 mL) synthesis of Tre6*P*

Tre6*P* was synthesized in a 100-mL reaction mixture containing 1 M (100 mmol) maltose, 0.6 M (60 mmol) sodium phosphate was monitored. As enzymes, only MP was present in the reaction mixture. The enzymes were supplemented at day 2. Symbols are the same as shown in Fig. 2-10B.

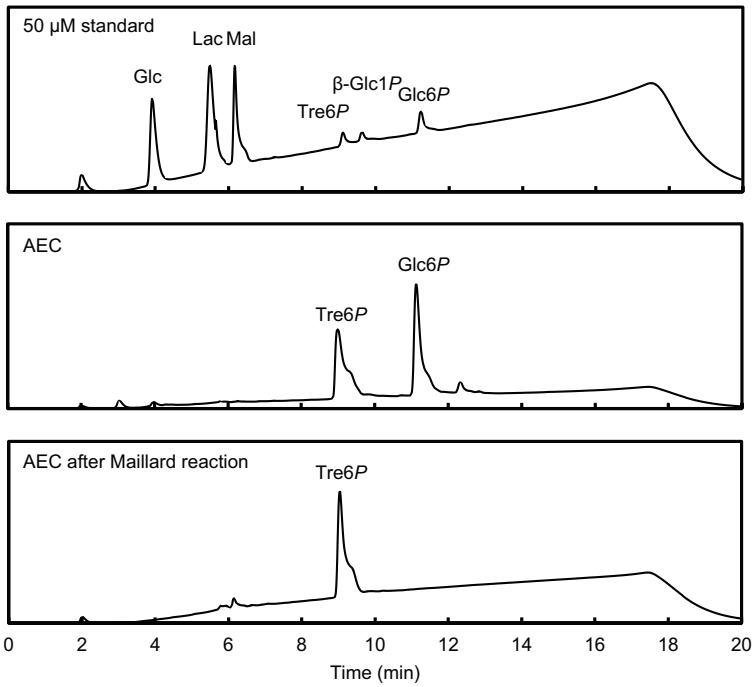

Fig. 2-14 HPAEC-PAD analysis of the mixture after anion exchange column chromatography.

The sample separated by anion exchange column chromatography (AEC) was analyzed by HPAEC-PAD.

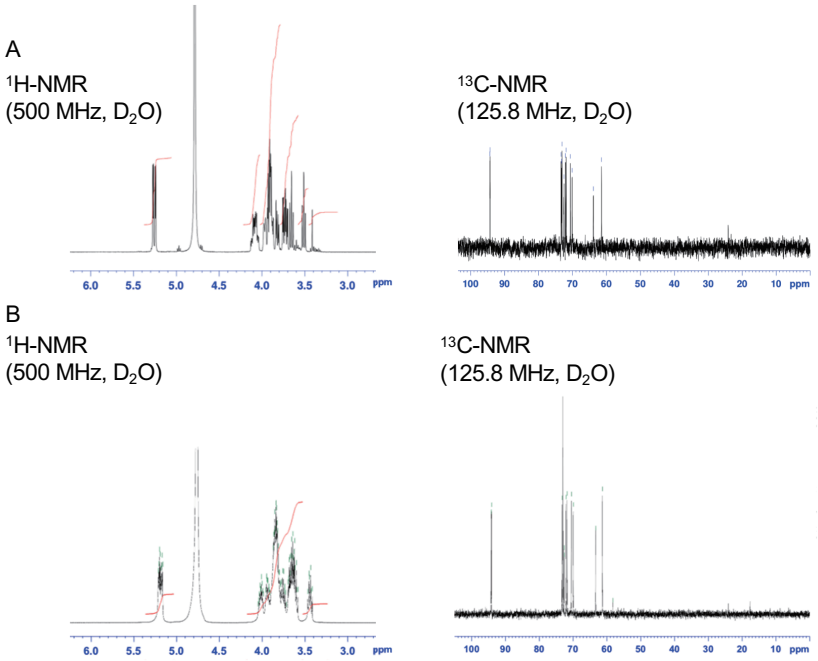

Fig. 2-15. ^{1}H- and ^{13}C-NMR spectra of synthesized Tre6*P*.

The synthesized Tre6*P* from (A) β-Glc1*P* and Glc6*P*, and (B) maltose and inorganic phosphate were analyzed by ^{1}H- and ^{13}C- NMR.

3. Comprehensive evaluation of enzymatic properties of TPP isozymes from *A. thaliana*

3.1. Introduction

TPP catalyses the hydrolysis of the phosphoryl ester of Tre6*P* to release phosphate and trehalose. TPP is a member of HAD-like superfamily as described in chapter 1 (Allen and Dunaway-Mariano, 2004; Koonin and Tatusov, 1994; Kuznetsova et al., 2006).

In plants, Tre6*P* acts as a bioactive compound. The specific TPP proteins have distinct tissue-specific expression patterns during development and in response to various environmental stimuli (Fig. 3-1). These facts indicate that the level of Tre6*P* is strictly regulated by multiple-enzyme system of TPS and TPP at various growth stages and organs. The TPP from *Arabidopsis*, AtTPPE and AtTPPI, are shown to be involved in the drought stress response mediated by ABA (Lin et al., 2020; Wang et al., 2020). Overexpression of the genes encoding these TPPs shows higher tolerance against drought stress, and deletion of the genes increases stomatal aperture. AtTPPD, localized in chloroplast, positively regulates tolerance against high salinity stress through accumulation of soluble sugars (Krasensky et al., 2014). This isozyme known to be reversibly inactivated through oxidation of the Cys residues. In rice, *OsTPP1* and *OsTPP2*, are considered to be the major TPP genes based on their expression levels in the normal conditions (Shima et al., 2007). Their expression is increased by abiotic stresses such as chilling (Pramanik and Imai, 2005; Shima et al., 2007).

Although some plant TPP isozymes were demonstrated to have important physiological functions in stress responses, biochemical characteristics of TPP isozymes have not been fully investigated thus far. In this study, enzymatic properties of all TPP isozymes from *Arabidopsis* are analyzed using recombinant enzymes produced in *E. coli*

3.2. Materials and methods

3.2.1. Plant

A. thaliana ecotype Columbia (Col-0) was used for TPP cDNA cloning. Sterilized seeds were planted to Murashige and Skoog medium [MS medium; 4.4g/L Murashige and Skoog Plant Salts Mixture (Wako Pure Chemical Industries), 5 mg/L nicotinic acid, 500 μg/L pyridoxine hydrochloride (Kanto), 3 mg/L thiamin hydrochloride (Wako Pure Chemical Industries), 20 g/L sucrose, and 3 g/L gellan gum (Wako Pure Chemical Industries)] and cultivated in a 16-h light/8-h dark photoperiod at 40 μmol/m^2/s light intensity at 60% humidity (standard growth condition). As KNO_3 treatment, 12-day-old seedling grown on the MS medium plate was placed on the MS medium plate containing 200 mM KNO_3 for 2 h under the standard growth condition. As NaCl treatment, 12-day-old seedling was placed on the MS medium plate containing 150 mM NaCl for 8 h under the standard growth condition. As chilling treatment, 12-day-old seedling was kept at 4°C for 24 h in darkness. The whole seedlings were collected by snap-frozen with liquid nitrogen and kept at -80°C.

3.2.2. Sugar phosphates

α-Glc1*P* and Fru6*P* were purchased from Nacalai Tesque. Sucrose 6-phosphate (Suc6*P*, Glc*p*α1-2βFru*f*6*P*) was purchased from Sigma-Aldrich. Tre6*P* and Glcα1-1αMan6*P* were prepared as described in chapter 2 (Taguchi et al., 2017, 2020).

3.2.3. Preparation of expression plasmids

Collected plant samples were crashed in liquid nitrogen using Multi-beads shocker (Yasui Kikai, Osaka, Japan). Total RNA was extracted from powdery plant samples using Total RNA Extraction Kit Mini YRP50 (RBC Bioscience, New Taipei City, Taiwan). For cDNA synthesis, Superscript IV First-Strand Synthesis System for RT-PCR (Invitrogen, Foster city, CA, USA) was used. Total RNA and random hexamer were used as template and primer, respectively.

The cDNA of AtTPPs were amplified by PCR. Primer sequences were decided based on the

registered gene sequences, which are registered under the following NCBI accession numbers: AtTPPA, NM_001344937.1; AtTPPB, NM_106458.4; AtTPPC, NM_102071.2; AtTPPD, NM_103289.5; AtTPPE, NM_127787.3; AtTPPF, NM_117313.2; AtTPPG, NM_118385.4; AtTPPH, NM_120140.3; AtTPPI, NM_121048.3; and AtTPPJ, NM_125913.5. Sequence of the primers used are listed in Table 3-1, and the oligonucleotides were synthesized by Macrogen (Seoul, Korea). Primestar GXL DNA polymerase (Takara Bio, for AtTPPA, AtTPPB, AtTPPC, AtTPPE, AtTPPF, AtTPPH, and AtTPPJ) or KOD FX Neo (Toyobo, Osaka, Japan, for AtTPPD, AtTPPG, and AtTPPI) was used. The PCR product were reamplified using primers containing the short sequence of pET-28a. For AtTPPA, AtTPPB, AtTPPD, AtTPPF, and AtTPPI, the PCR products were inserted into pET-28a using In-Fusion HD Cloning Kit. In the cases of AtTPPC, AtTPPE, AtTPPG, AtTPPH, and AtTPPJ, the PCR product was cloned into the *Eco*RV site of pBluescript II SK (+) and sequenced. In the preparation of the expression plasmid for these AtTPPs, the pBluescript II SK (+) derived plasmid harboring the cording region of AtTPPs was digested with *Nde*I and *Sac*I, and the resulting DNA fragment was cloned into the same restrict enzyme sites of pET-28a using DNA Ligation Kit Mighty Mix (Takara Bio). The DNA sequence of inserted fragment and flanking regions was analyzed using an Applied Biosystems 3130 Genetic Analyzer and a Big Dye Terminator v1.1 Cycle Sequencing Kit.

3.2.4. Preparation of recombinant AtTPPs

Transformants of *E. coli* BL21 (DE3) harboring the AtTPP-expression plasmids were cultured in 1.0–2.0 L of LB medium containing 50 μg/mL kanamycin at 37°C until A_{600} reached 0.4–0.9. Production of the recombinant proteins was induced by the addition of 0.1 M IPTG at a final concentration of 0.1 mM, and the incubation was continued at 18°C for 24 h with vigorous shaking. The cells were recovered by centrifugation (6,000×g, 4°C, 5 min), suspended in 30 mL of buffer A (50 mM Tris-HCl buffer (pH 7.0) containing 0.5 M NaCl, 40 mM imidazole, and 10 mM $MgCl_2$), and disrupted by

sonication. Cell-free extract was obtained by centrifugation (10,000×g, 4°C, 10 min), and was separated on a Ni-chelating Sepharose Fast Flow column (1.6 cm i.d.×2.5 cm, 5 mL), equilibrated with buffer A. After washing the column with 100 mL of buffer A, adsorbed proteins were eluted with a 40–500 mM imidazole linear gradient (100 mL). The collected fractions were pooled, and stored at 4°C (AtTPPA, AtTPPB, and AtTPPF), and -80°C (the others). These enzymes are inactivated in the absence of imidazole and NaCl. The concentration of proteins was measured as in section 2.2.7.

3.2.5. Standard enzyme activity assay

Phosphatase activity on Tre6*P* was measured by quantified inorganic phosphate released under the following conditions. A reaction mixture (50 μL), containing enzyme, 10 mM Tre6*P*, 50 mM HEPES-NaOH buffer (pH 7.0), 10 mM Tris-HCl buffer (pH 7.0), 100 mM imidazole, 100 mM NaCl, 12 mM $MgCl_2$, 10 mM Tre6*P*, and 0.2 mg/mL BSA, was incubated at 30°C for 10 min. The reaction was terminated by incubating the sample at 100°C for 2 min. Released inorganic phosphate was quantified according to Lowry and Lopez (Lowry and Lopez, 1946) or using Biomol Green reagent (Enzo Life Sciences, NY, USA) (Cross et al., 2017a, 2017b; Krasensky et al., 2014; Shima et al., 2007). The amount of enzyme that releases 1 μmol of inorganic phosphate from Tre6*P* in 1 min under the described conditions was defined as 1 U.

3.2.6. Effects of temperature and pH on activity and stability of TPP

Optimum temperature was determined from the activity to Tre6*P* at 20–50°C. Optimum pH was determined from the activity to Tre6*P* at pH 4.1–8.8. Following buffers were used as reaction buffers: 80 mM sodium acetate buffer (AtTPPA–AtTPPC: pH 4.1–4.7, and AtTPPD–AtTPPJ: pH 4.7–6.3), 80 mM sodium citrate buffer (pH 4.8–6.4, and pH 5.2–6.8), 100 mM MES-NaOH buffer (pH 6.2–7.0, and pH 6.6–6.9), 100 mM HEPES-NaOH buffer (pH 7.0–8.0, and pH 6.9–7.3), and 200 mM Bicine-

NaOH buffer (pH 8.0–8.8, and pH 7.6–8.3). The reaction mixture of AtTPPA–AtTPPC did not contain 10 mM Tris-HCl buffer (pH 7.0), 100 mM imidazole, and 100 mM NaCl.

To determine a stable range, in which the enzyme retained ≥90% of the original activity, residual activity after the heat and pH treatments was measured by the standard enzyme assay. As the heat treatment, 0.186–1.10 μM AtTPPs were incubated in 50 mM Tris-HCl buffer (pH 7.0) containing 0.5 M NaCl, 0.5 M imidazole, and 10 mM $MgCl_2$ at various temperatures for 15 min. As the pH treatment, 1.86 μM AtTPPB was kept in following buffers: 250 mM sodium acetate buffer (pH 4.7–6.8), 250 mM MES-NaOH buffer (pH 6.7–7.0), 250 mM HEPES-NaOH buffer (pH 6.9–7.3), 250 mM Bicine-NaOH buffer (pH 8.0–9.0), and 1 M glycine-NaOH buffer (pH 9.0–11) at 30°C for 15 min. The sample was diluted 10-fold with 50 mM Tris-HCl buffer (pH 7.0) containing 0.5 M NaCl, 0.5 M imidazole, 10 mM $MgCl_2$, and 1 mg/mL BSA for the activity measurement.

3.2.7. Effect of detergent on activity of TPP

The whole seedlings of 4-week-old Col-0 plants were collected by snap-frozen and crushed as section 3.2.3. The crushed sample (242 mg) was suspended in 25 mM Tris-HCl buffer (pH 6.8) containing 150 mM NaCl, 1 mM EDTA, 1% Nonidet P-40 (NP-40, Nacalai Tesque), and 5% glycerol (extraction buffer), and kept at 4°C for 15 min with gentle shaking. Plant extract was obtained by centrifugation (10,000×g, 4°C, 10 min). The plant extract was added to the reaction mixture, and the activity was measured as section 3.2.5. The extraction buffer did not effect on the inorganic phosphate measuring.

TPP activity was measured in the presence of 0.05–1% NP-40, Triton X-100 (Nacalai Tesque), and Tween 20 (ICN Biomedicals Inc., CA, USA).

3.2.8. Substrate specificity of TPP

The phosphatase reaction of AtTPPs on various sugar phosphates was carried out according to the

standard activity assay (3.2.5) but 24-h reaction in a 5-μL reaction mixture. As substrates, α-Glc1*P*, β-Glc1*P*, Glc6*P*, Man6*P*, Gal6*P*, Fru6*P*, Tre6*P*, Glcα1-1αMan6*P*, and Suc6*P* were used. One μL of the sample was spotted on a silica gel plate (TLC Silica gel 60 F_{254} aluminum sheet, Merck) and developed by acetonitrile: ethyl acetate: 1-propanol: water = 85: 20: 50: 60 (v/v/v/v). Sugars were detected by spraying a detection reagent (acetic acid: sulfuric acid: anisaldehyde = 100: 2: 1, v/ v/ v)] onto the plate, followed by heating the plate in an oven.

3.2.9. Determination of kinetic parameters

Inorganic phosphate-releasing rates were measured under the same conditions as the standard activity assay but at various concentrations of Tre6*P* and Glcα1-1αMan6*P* (0.1–10 mM). Kinetic parameters were calculated by fitting the Michaelis-Menten equation to the reaction rates on the s-*v* plots by non-linear regression using Grafit version 7.0.2.

3.3. Results

3.3.1. Comparison of primary structures of TPPs.

The primary structures of AtTPPA–AtTPPJ were compared with those of well-studied TPPs—the C-terminal domain of *C. neoformans* TPS2 (TPS2PD) and OtsB of *E. coli*— (Fig. 3-2A) (Miao et al., 2016). Multiple alignment of the amino acid sequences and phylogenetic analysis were performed using MAFFT v7 with the automatic method (Katoh et al., 2019) (Fig. 3-2). AtTPPs have an elongation of 50–100 residues at N-terminus compared with OtsB. It is the longest in AtTPPA and shortest in AtTPPC. The loop between 4th and 5th β-strands (β4→β5 loop) of AtTPPA and AtTPPG is longer than the other AtTPPs by 14 and 15 residues, respectively (AtTPPA: Ser197–Gln211, AtTPPG: Asn184–Glu199).

The four motifs of TPPs, which contain essential residues for the catalysis and substrate binding,

are conserved well in all the AtTPPs. Two catalytic Asp residues that act as nucleophilic catalysts and general acid/base catalysts, respectively, are included in the DXD motif (motif I), located on β1→α2 loop. These residues are also involved in the binding to Mg^{2+} and phosphoryl groups of the substrate. Ser in the SGR motif (motif II) on β2→α3 loop and Lys in the KG motif (motif III) on 6th α-helix are responsible for binding to the phosphoryl group of the substrate. AtTPPB, AtTPPD, AtTPPI, and AtTPPJ have Thr at the Ser position in motif II. First Asp in the GDDXTDE motif (motif IV) on the β10→α7 loop interacts with Mg^{2+}. Some residues, which are not included in the conserved motifs but are responsible for substrate binding in TPS2PD, are substituted in AtTPPs. AtTPPs possess Asn or His at the position of Lys133 of TPS2PD on the β6→β7 loop (Fig. 3-2A), which is suitably located at the position to form a hydrogen bond with 3-O of 6-phospho-D-glucosyl residue of Tre6*P* (Fig. 3-3). Asn178 of TPS2PD on the 9th β-strand, which forms a hydrogen bond with 2-O of D-glucosyl residue of Tre6*P* (Fig. 3-3), is substituted with Val in all AtTPPs (Fig. 3-2A).

In the phylogenetic tree of TPPs including AtTPPA–AtTPPJ and OsTPP1–OsTPP10 (Fig. 3-2B), TPPs from nematode (BmGOB1 and CeGOB1) were apparently apart from others. Bacterial TPPs (EcOtsB and MtOtsB) are similar to plant TPPs. AtTPPs could be classified into two groups: group 1 consisted of AtTPPA, AtTPPF, and AtTPPG; and group 2 of the other enzymes. OsTPP1, which is one of the major TPPs in rice (Shima et al., 2007), was divided into different groups from AtTPPs, while OsTPP2, another major TPP in rice, was fallen into group 1.

3.3.2. Preparation of recombinant AtTPPs

The cDNA of AtTPPs except for AtTPPC, AtTPPD, AtTPPG, and AtTPPI were obtained by reverse transcription PCR from the RNA prepared from aboveground parts of normally grown Col-0 plants. The genes of AtTPPC, AtTPPD, and AtTPPI are expressed at a low level according to a database (Schmid et al., 2005), so the cDNA of these genes were prepared from Col-0 plants with various

treatments below. The cDNA of AtTPPC were from the seedling of *A. thaliana* Col-0 after the KNO_3 treatment. The cDNA of AtTPPD and AtTPPG were from the root of Col-0 after the cold treatments. The cDNA of AtTPPI were from the root of Col-0 after the NaCl treatment.

Recombinant AtTPPs as N-terminal His-tag fusion protein were produced in *E. coli* transformant carrying the expression plasmid. The N-terminal extension of Met-Gly-Ser-Ser-His-His-His-His-His-His-Ser-Ser-Gly-Leu-Val-Pro-Arg-Gly-Ser-His was attached to the first methionine in the AtTPPs coded by the start codon ATG. Recombinant enzymes were purified by Ni-affinity column chromatography. From 1.0–2.0 L of culture broth of the *E. coli* transformant, 1.2–23 mg of purified AtTPPA–AtTPPJ were obtained. SDS-PAGE analysis indicated that the molecular mass of these enzymes was 37–46 kDa, consistent with the molecular mass estimated from the sequence (Table 3-2, Fig. 3-4). AtTPPs except for AtTPPI showed 0.789–18.9 U/mg of specific activity to 10 mM Tre6*P* at pH 7.0 at 30°C (Table 3-2). The pH optimum of these AtTPPs was pH 6.6–7.0 (Table 3-2, Fig. 3-5). All active AtTPPs showed high activity under neutral pH conditions. AtTPPs were stable at pH 7.0 for 15 min up to 30°C (AtTPPA and AtTPPD), 34°C (AtTPPJ), 40°C (AtTPPB, AtTPPC, and AtTPPE) or 45°C (AtTPPF, AtTPPG, and AtTPPH) (Table 3-2).

3.3.3. Kinetic analysis of AtTPPs for the Tre6*P*-dephosphorylation

Kinetic parameters for the dephosphorylation of Tre6*P* were measured (Table 3-3). The k_{cat}/K_m values of AtTPPA and AtTPPB, 18.9 and 23.0 $s^{-1}mM^{-1}$, respectively, were higher than the others. Although AtTPPA and AtTPPB belong to different groups as describe above (sequence identity: 47%), k_{cat} and K_m of these enzymes were similar to each other. AtTPPJ, which shows highest sequence identity (71%) with inactive AtTPPI, showed the lowest k_{cat}/K_m among AtTPPs analyzed. The k_{cat}/K_m values of AtTPPF, AtTPPG, and AtTPPH, 7.54–9.65 $s^{-1}mM^{-1}$, were moderate among AtTPP isozymes. Because of low k_{cat}, the k_{cat}/K_m of AtTPPD and AtTPPE (1.05 and 1.40 $s^{-1}mM^{-1}$, respectively) were much lower

than the others except for AtTPPJ. AtTPPC had the highest k_{cat} of all TPPs, and also had higher K_m than the others except for AtTPPJ.

3.3.4. Substrate specificity of AtTPPs

The enzymes were incubated with α-Glc1*P*, β-Glc1*P*, Glc6*P*, Fru6*P*, Man6*P*, Tre6*P*, Glcα1-1αMan6*P*, and Suc6*P*, and products were analyzed by TLC (Fig. 3-6). AtTPPs except for AtTPPI produced the reaction product, which showed higher migration on TLC than the substrate, in the reactions with Glcα1-1αMan6*P* and Tre6*P*. A slight spot of the reaction product of AtTPPJ was confirmed. Glcα1-1αMan6*P* also served as substrate of AtTPPs. Using AtTPPB showing the highest specific activity, kinetic parameters to Glcα1-1αMan6*P* were analyzed. The k_{cat}, K_m, and k_{cat}/K_m values were 2.31 ± 0.04 s^{-1}, 3.02 ± 0.20 mM, and 0.768 ± 0.041 $s^{-1}mM^{-1}$, respectively. The k_{cat}/K_m value to Glcα1-1αMan6*P* was 30 times lower than to Tre6*P* because of low k_{cat} and high K_m.

3.3.5. Influence of detergent on enzymatic activity of AtTPPB

Tre6*P* in plants level must be strictly controlled, so the TPP activity might be regulated with some compounds. To find such compounds, the extract from *A. thaliana* with a buffer containing NP-40 was prepared, and effect of that on activity of AtTPPB was measured. The extract increased its activity 1.5-fold, but the extraction buffer itself increased it 1.8-fold. Therefore, the enhancement of activity was depending on the buffer. Effects of NP-40 was examined. The activity increased up to 174% depending on NP-40 concentration in the range of 0–0.4% (Fig. 3-7). At higher NP-40 than 0.4%, the degree of increase in activity was lower: 120% at 1% NP40. Triton X-100 and Tween 20 did not activate AtTPPB (Fig. 3-7).

3.4. Discussion

TPP is the enzyme that dephosphorylates Tre6*P* to produce trehalose in various organisms. The enzymatic characteristics of TPPs from microorganisms and nematode are mentioned well thus far (Cross et al., 2017a, 2018; Klutts et al., 2003; Kushwaha et al., 2011; Pan et al., 2004), but plant TPPs are scarcely characterized. In this study, enzymatic characteristics of 10 *Arabidopsis* TPP isozymes were investigated using recombinant enzymes. AtTPPs showed a variety of dephosphorylation activity to Tre6*P.* Enzyme activity of AtTPPI was not detectable under the analytical conditions, and other isozymes showed 0.789–18.9 U/mg of TPP activity. The TPPs with low or no activity also conserve the motifs as described above. The kinetic parameters of TPPs to Tre6*P* significantly differed even among those showing high sequence identity. AtTPPE and AtTPPH, belonging to the group 2 (Fig. 3-2B), show the sequence identity 76%, but AtTPPH had 6.9 times higher k_{cat}/K_m than TPPE (Table 3-3). AtTPPB and AtTPPC in group 2 (sequence identity, 65%) showed a largely different K_m value (Table 3-3). On the contrary, AtTPPA and AtTPPB fall into different groups (Fig. 3-2B), but they showed similar k_{cat}/K_m value. These facts suggest that activity of TPP could not be easily predicted from overall sequence identity.

The reason for the low activity of TPP isozymes can be explained by a precise comparison of amino acid sequences and known structure of TPP (Miao et al., 2016) (Fig. 3-8). Amino acid sequence alignment of AtTPPs suggests that Cys on β7→α5 loop is conserved in TPPs with low or no activity (Fig. 3-8A). TPP of *C. neoformans* and other AtTPPs with high TPP activity possessed Asn, Gln, or Arg at the position. According to the structure of *C. neoformans* TPP, the equivalent of Asn143 is next to Arg142, which is located on the cap domain and could interact with the substrate (Fig. 3-3B and Fig. 3-8A). Besides, the equivalent of Asn143 could interact with the carbonyl oxygen of Lys34 on β1→α2 loop of the catalytic domain (Miao et al., 2016). A cap domain is assumed to open and close during the catalytic process including substrate binding and release as described in section 1.5 (Miao et al., 2016). The cap domain and the catalytic domain predicted to interact *via* the hydrogen bond

interaction between Lys34 and Asn143 in *C. neoformans* TPP (Miao et al., 2016). The substitution of this Asn with Cys is assumed to less stabilize the closed conformation. For catalysis, the closed conformation is important because of the interaction between substrate and cap domain. Therefore, AtTPPs with Cys at this position would show low activity.

AtTPPJ especially showed low activity, and the activity of AtTPPI was not detectable (Table 3-2, Table 3-3). These isozymes possess Phe at the position corresponding to Leu179 of *C. neoformans* TPP. Leu179 of *C. neoformans* TPP is located next to Glu180, which could interact with the substrate (Fig. 3-3B). Leu is involved in the formation of hydrophobic core of the cap domain together with surrounding hydrophobic residues (Fig. 3-3C). It might be more difficult for the cap domain structure to take a suitable structure for catalysis than the known structure when Leu in the hydrophobic region of the cap domain becomes was substituted with Phe.

In previous studies, TPPs from bacteria and fungi are found to be specific to Tre6*P* (Klutts et al., 2003; Kushwaha et al., 2011). A small-scale substrate screening in this study suggests that AtTPPs act only on the substrates with α1-1α glucosidic linkage, including Tre6*P* and Glcα1-1αMan6*P* but not sucrose 6-phosphate and other monosaccharide phosphates. This indicates that AtTPPs are basically specific to Tre6*P*, and its derivative (Fig. 3-6). According to the available structure of the fungal TPP (Miao et al., 2016), the D-glucosyl group of Tre6*P* interacts with the cap domain (Fig. 3-8B). The results that AtTPPs did not show the activity to Glc6*P* indicates that the non-phosphorylated D-glucosyl group of Tre6*P* is necessary for the catalysis. Perhaps the D-glucose part has interaction with the cap domain of TPP, and the interaction is indispensable for the catalysis. Considering that the phosphorylated D-glucose residue can be concluded to be important but not indispensable. Catalytic activity of AtTPPB showed lower activity to Glcα1-1αMan6*P* than Tre6*P*, the 2-OH of Man6*P* would not cause steric hindrance upon binding to the substrate binding site, although Arg on the β2→α3 loop is predicted to be close proximity to 2-OH of Man6*P* residue (Fig. 3-8C). The

k_{cat}/K_m to Glcα1-1αMan6*P* was smaller than that of Tre6*P* because of lacking the hydrogen bond formed between 2-OH of the Glc6*P* residue of Tre6*P* and the Glu on the cap domain in the catalytic AtTPPs (Fig. 3-8C).

The biochemical analysis of AtTPPI showed that this isozyme did not have detectable TPP activity, although this isozyme could recover the growth of *Δ*tps2 yeast and *AtTPPI* gene-deficient and overexpressor *Arabidopsis* decreased and increased the survival rate under drought stress, respectively (Lin et al., 2020). Overexpression of *AtTPPI* did not enhance the expression of SnRK1-induced genes, which are negatively regulated by Tre6*P* (Zhang et al., 2009), while the overexpression of catalytically active *E. coli* OtsB in *Arabidopsis* decreased Tre6*P* level and enhanced SnRK1-induced genes. As the expression of an active TPP decreases Tre6*P* level and should lead to enhancing the expression of SnRK1-induced genes, the fact that AtTPPI does not have a TPP activity *in vitro* is consistent with no change of expression of SnRK1-induced genes with overexpression of *AtTPPI*. Change of tolerance against drought stress through modification of expression level of *AtTPPI* in *Arabidopsis* might be explained by some other function of AtTPPI protein or RNA. In fact, Claeys *et al*. show that even the inactive *TPP* gene (mutant of the catalytic aspartate) could complement the phenotype of *TPP*-deficient maize, which showed the abnormal development of meristem (Claeys et al., 2019; Satoh-Nagasawa et al., 2006). They showed that the plant TPP might have a "moonlight" function in addition to the degradation of Tre6*P*.

Since endogenous level of Tre6*P* is very low, the k_{cat}/K_m, an indicator of reaction rate at low concentration of substrate, can be utilized to evaluate the intracellular activity of AtTPPs. Based on the k_{cat}/K_m values for Tre6*P*, AtTPPA and AtTPPB were thought to be major proteins for dephosphorylation of Tre6*P*. In addition, the genes encoding AtTPPA and AtTPPB are highly expressed in various upper organs and root, respectively (Fig. 3-1). Thus, these isozymes are presumably responsible for dephosphorylation of Tre6*P* at the upper ground and root, respectively.

Since AtTPPF, AtTPPG, and AtTPPH showed moderate k_{cat}/K_m (k_{cat}/K_m: 7.54–9.65 $s^{-1}mM^{-1}$) and expressed at relatively high level in various organs including vegetative tissues and root, these TPPs could also contribute to the regulation of Tre6*P* level.

Table 3-1. Sequences of primers used in this study.

Name	Sequence (5′ to 3′)	Purpose
AtTPPA_fw	GTTAAACCGCAGAGCTTCTTCTATC	cloning
AtTPPA_rv	TGTCTTGAATTAATCCGGAGATGGA	cloning
pET28a_AtTPPA_fw	TGCCGCGCGGCAGCCATATGGACATGAAATCTGGTCACTC	preparation of expression plasmid
pET28a_AtTPPA_rv	TGGTGGTGGTGGTGCTCGAGTTAACCCATTGATCTCTTCC	preparation of expression plasmid
AtTPPB_fw	GTCTTCTCTCTGTCTCAACGAGAAT	cloning
AtTPPB_rv	CACCCTCCAGGCATCTACTAATTTA	cloning
pET28a_AtTPPB_fw	TGCCGCGCGGCAGCCATATGACTAACCAGAATGTCATCGT	preparation of expression plasmid
pET28a_AtTPPB_fw	TGGTGGTGGTGGTGCTCGAGTCACTCTTCTCCCACTGTCT	preparation of expression plasmid
AtTPPC_fw	GCTTCTGTGTTACTCTTACCTCTCT	cloning
AtTPPC_rv	GTCCCATATATTTCAGGACGGGTTA	cloning
pET28a_AtTPPC_fw	TGCCGCGCGGCAGCCATATGAAGATTACGGATATTTCCGG	preparation of expression plasmid
pET28a_AtTPPC_rv	TGGTGGTGGTGGTGCTCGAGTTATTCTCCAAGTGTTTGTT	preparation of expression plasmid
AtTPPD_fw	GCCCCTAATGACAAACCATAATGCC	cloning
AtTPPD_rv	GTCAGGAAATTGGCTATCTTCCTC	cloning
pET28a_AtTPPD_fw	TGCCGCGCGGCAGCCATATGACAAACCATAATGCCTTAAT	preparation of expression plasmid
pET28a_AtTPPD_rv	TGGTGGTGGTGGTGCTCGAGCTATCTTCCTCTTAGTGACA	preparation of expression plasmid
AtTPPE_fw	AACAACCCACATTCACTCTCATTTC	cloning
AtTPPE_rv	CATGGATAGCAACAAACGACTAGTC	cloning
pET28a_AtTPPE_fw	TGCCGCGCGGCAGCCATATGGTTAGATTCATCGAAGAAAA	preparation of expression plasmid
pET28a_AtTPPE_rv	TGGTGGTGGTGGTGCTCGAGTCATGCCCCACACCTTGACT	preparation of expression plasmid
AtTPPF_fw	GTTCTTGCATTGAAGCATTGGTTTT	cloning
AtTPPF_rv	GTTGAGCTCCAAGGAAAAAGTCTTT	cloning
pET28a_AtTPPF_fw	TGCCGCGCGGCAGCCATATGGATTTAAACTCAAACCACAA	preparation of expression plasmid
pET28a_AtTPPF_rv	TGGTGGTGGTGGTGCTCGAGTCAAAAACCAGTAGAATTCT	preparation of expression plasmid
AtTPPG_fw	GACAGTTCAACAACAAGCAGTGATA	cloning
AtTPPG_rv	TGAAGCTTCTGATTCTCCTACACAA	cloning
pET28a_AtTPPG_fw	TGCCGCGCGGCAGCCATATGGATTTGAATATAAACAAGAC	preparation of expression plasmid
pET28a_AtTPPG_rv	TGGTGGTGGTGGTGCTCGAGTCAAAAACTTGTTTTTGAAC	preparation of expression plasmid
AtTPPH_fw	ACACACTCATTCTCACTCTGTTTCT	cloning
AtTPPH_rv	CGCGTTGAGTACAATATATGAGAGC	cloning
pET28a_AtTPPH_fw	TGCCGCGCGGCAGCCATATGGTTAGATTCATAGAAGAAAA	preparation of expression plasmid
pET28a_AtTPPH_rv	TGGTGGTGGTGGTGCTCGAGTCATGCTCCAGATCTCAATT	preparation of expression plasmid
AtTPPI_fw	CTCAAATGGTGCGTTTTGTCGTGG	cloning
AtTPPI_rv	CACATTCTTGGCTGCATTTGTTTCC	cloning
pET28a_AtTPPI_fw	TGCCGCGCGGCAGCCATATGGTGCGTTTTGTCGTGGAAAA	preparation of expression plasmid
pET28a_AtTPPI_rv	TGGTGGTGGTGGTGCTCGAGTCACATTCTTGGCTGCATTT	preparation of expression plasmid
AtTPPJ_fw	TCCTAGTTTCTCGTTTGGTCTCATT	cloning
AtTPPJ_rv	CCCTTTCCCTTACAATAGCCTAACT	cloning
pET28a_AtTPPJ_fw	TGCCGCGCGGCAGCCATATGGTGAGCCAAAACGTCGTCGT	preparation of expression plasmid
pET28a_AtTPPJ_rv	TGGTGGTGGTGGTGCTCGAGTTATTGCTGCATCTGTTTCC	preparation of expression plasmid

The sequences underlined were the sequence of pET-28a.

Table 3-2. Basic properties of recombinant AtTPPs.

	Molecular mass* kDa	Specific activity U/mg	Optimum pH pH	The stability range of temperature °C
AtTPPA	45 (45)	17.8	7.0	≤30
AtTPPB	45 (45)	18.9	7.0	≤40
AtTPPC	37 (39)	17.7	7.0	≤40
AtTPPD	43 (44)	2.79	6.8	≤30
AtTPPE	43 (42)	1.50	6.9	≤40
AtTPPF	45 (44)	7.22	6.6	≤45
AtTPPG	46 (45)	11.14	6.6	≤45
AtTPPH	40 (42)	4.72	6.6	≤45
AtTPPI	44 (45)	<0.1	N.A.	N.A.
AtTPPJ	43 (44)	0.789	6.9	≤34

*Molecular masses were estimated from the SDS-PAGE analysis. The values in parentheses indicate theoretical values from the amino acid sequences. N.A., not analyzed.

Table 3-3. Kinetic parameters of AtTPPs to Tre6*P*.

	k_{cat}*	K_m*	k_{cat}/K_m*
	s^{-1}	mM	$s^{-1}mM^{-1}$
AtTPPA	12.0 ± 0.15	0.637 ± 0.03	18.9 ± 1.2
AtTPPB	12.1 ± 0.3	0.526 ± 0.04	23.0 ± 1.3
AtTPPC	14.6 ± 0.2	4.61 ± 0.33	3.18 ± 0.19
AtTPPD	1.73 ± 0.12	1.65 ± 0.11	1.05 ± 0.01
AtTPPE	0.947 ± 0.03	0.778 ± 0.266	1.40 ± 0.55
AtTPPF	5.44 ± 0.12	0.693 ± 0.071	7.93 ± 0.85
AtTPPG	9.14 ± 0.65	1.25 ± 0.27	7.54 ± 1.16
AtTPPH	3.50 ± 0.10	0.364 ± 0.022	9.65 ± 0.50
AtTPPJ	1.14 ± 0.20	10.1 ± 1.41	0.113 ± 0.002

*The kinetic parameters were measured at 30°C and pH 7.0. The data are presented as the means of triplicate experiments with standard deviations.

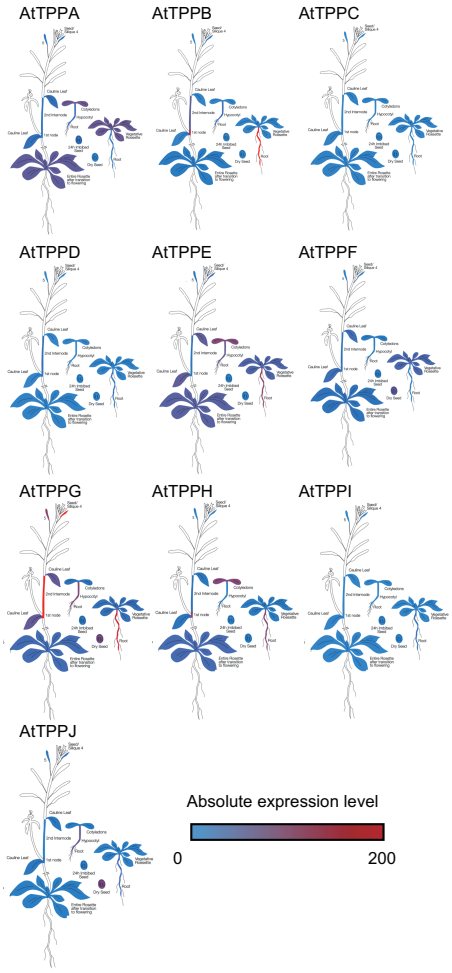

Fig. 3-1. Expression pattern of AtTPPs.

The expression patterns of each *AtTPP* gene during normal growth in the *Arabidopsis* gene expression database, eFP Browser 2.0 (Winter et al., 2007), are shown. The scale bar means the absolute expression level, and expression level increases depending on the color (blue→red).

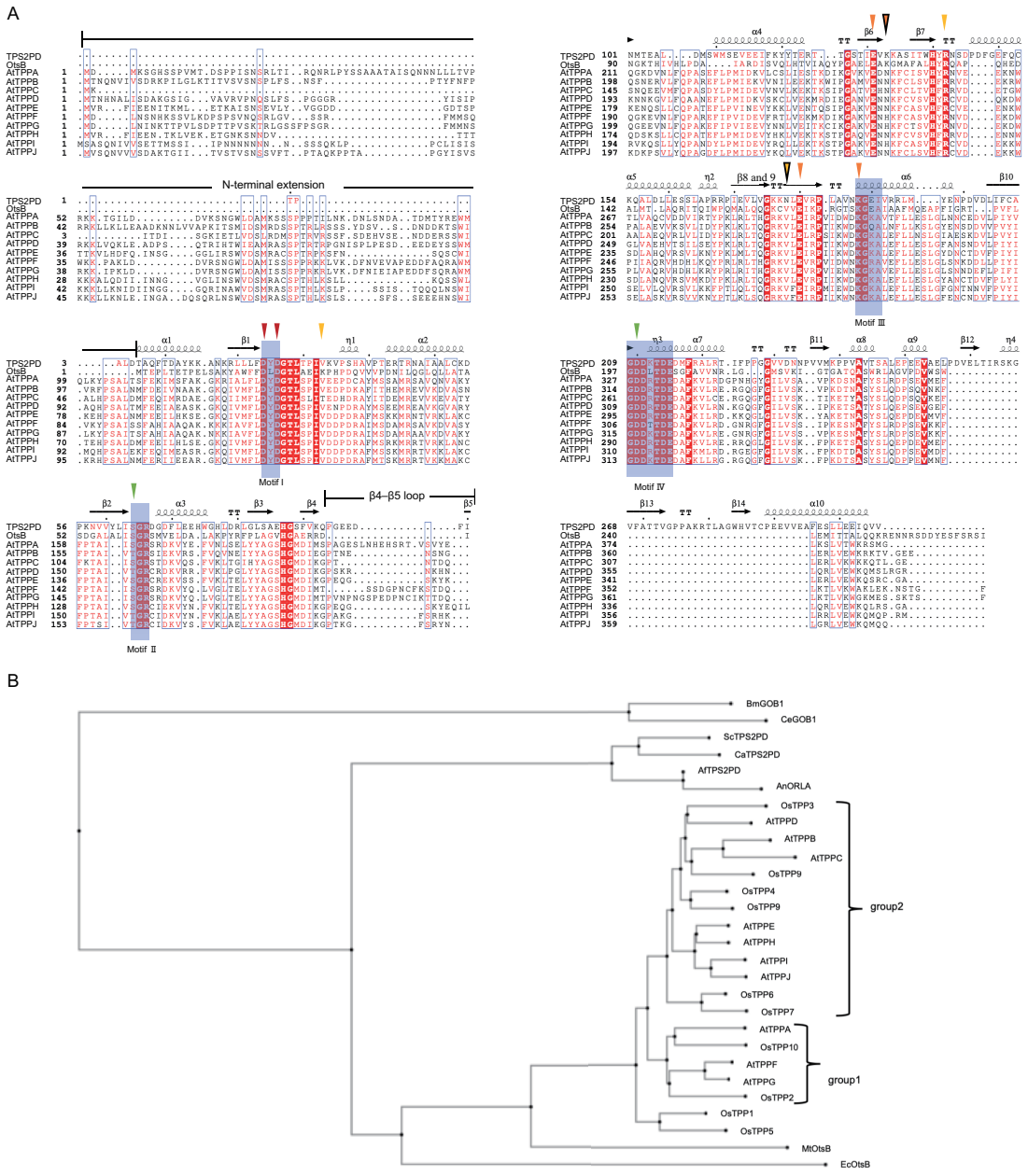

Fig. 3-2 Analysis of primary structure of AtTPPs.

(A) Multiple alignment of the amino acid sequences of C-terminal domain (TPP domain) of TPS2 of *C. neoformans* (TPS2PD), *E. coli* OtsB, and AtTPPs. It was made by MAFFT v7 with automatic method (Katoh et al., 2019). Secondary structures of TPS2PD are shown on the top of the sequence. Based on the known structure (Miao et al., 2016), residues responsible for the catalysis, substrate binding, and metal binding are shown by inverted arrowheads (red: catalytic residues, yellow: residues interacting with D-glucosyl residue, orange: residues interacting with 6-phospho-glucosyl residue, green: residues interacting with Mg^{2+}). Inverted triangles surrounded by lines indicate residues that are known to interact with the substrate but are not conserved by AtTPP. The conserved sequences are shaded. (B) The phylogenetic tree of TPPs. TPPs from various organisms such as bacteria, (*E. coli* and *M. tuberculosis*), fungi (*S. cerevisiae*, *C. albicans*, *A. fumigatus*, *and A. nidulans*), nematode (*Brugia malayi*, and *C. elegans*), and plants (*A. thaliana*, and *O. sativa*) were used for the constriction of phylogenetic tree, made by Phylo.io v1.0.0 (Robinson et al., 2016).

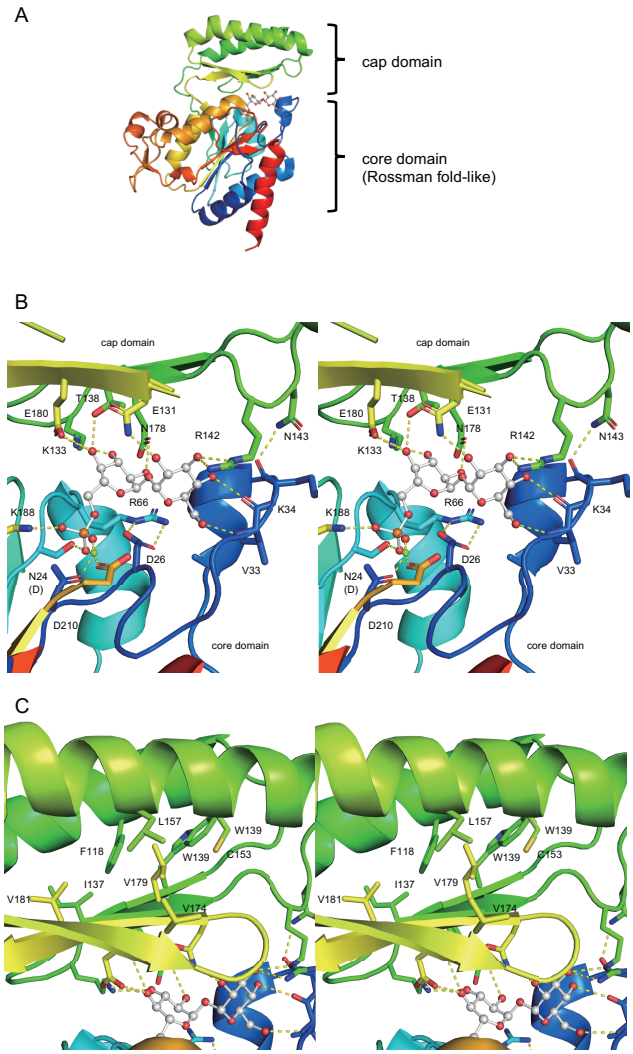

Fig. 3-3 The structure of the C-terminal domain (TPP domain) of TPS2 of *C. neoformans*.

The structural data is from Miao *et al*. (PDBID: 5DX9). The structure is shown as cartoons and colored rainbow (N: blue-C: red). Panel A showed the whole structure. Panel B showed the stereo view of the substrate binding site. Panel C showed the hydrophobic region of the cap domain. The residues around 4 Å of Val179 was shown as stick.

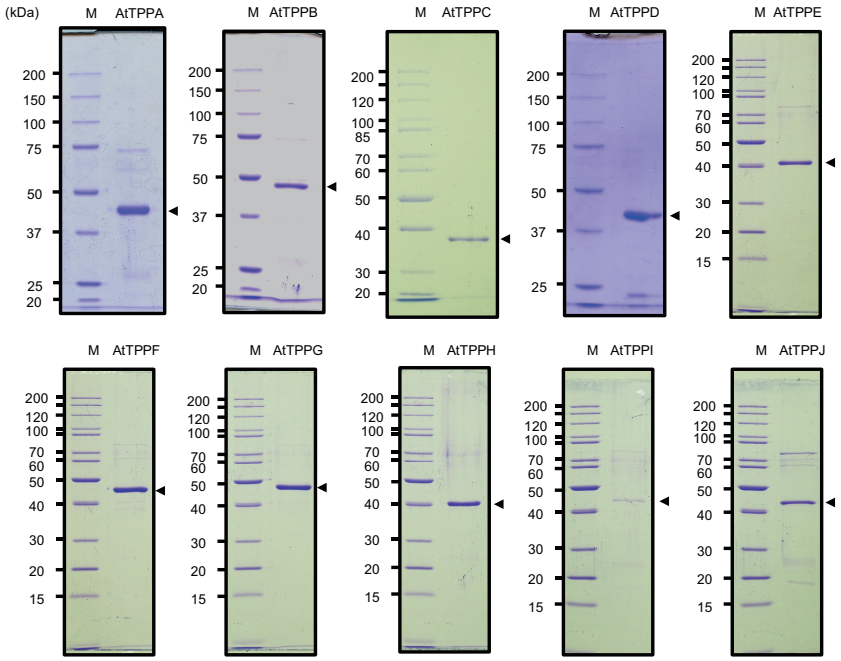

Fig. 3-4. SDS-PAGE of purified recombinant enzymes.

Purified AtTPPA–AtTPPJ were analyzed by SDS-PAGE. The molecular masses of the standard proteins are shown on the left. Black arrows showed the purified AtTPPs. Molecular masses are as follows: AtTPPA, 45 kDa; AtTPPB, 45 kDa; AtTPPC, 37 kDa; AtTPPD, 43 kDa; AtTPPE, 43 kDa; AtTPPF, 45 kDa; AtTPPG, 46 kDa; AtTPPH, 40 kDa; AtTPPI, 44 kDa; AtTPPJ, 43 kDa.

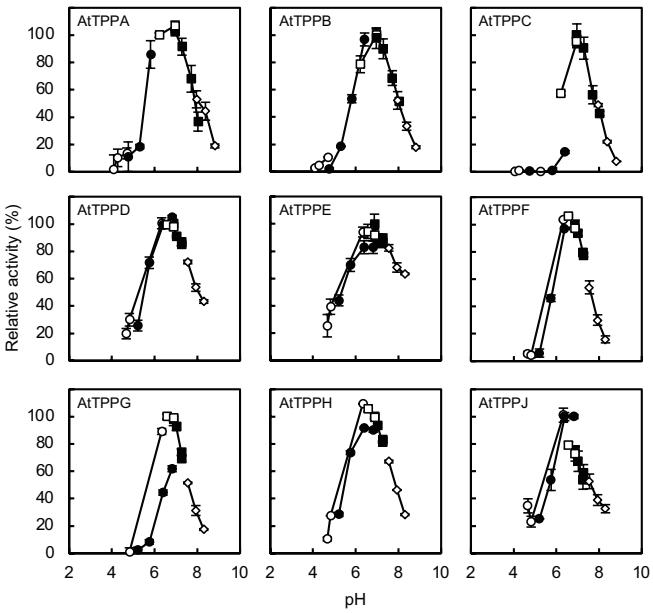

Fig. 3-5. Effects of pH on dephosphorylation activity of recombinant AtTPPs to Tre6*P*.

Inorganic phosphate-releasing activity was measured with 10 mM Tre6*P* at the indicated pHs at 30°C. Open circle, sodium acetate buffer (pH 4.0–6.3); filled circle, sodium citrate buffer (pH 4.8–6.4); open square, MES-NaOH buffer (pH 6.2–7.0); filled square, HEPES-NaOH buffer (pH 7.0–8.0), open diamond, Bicine-NaOH buffer (pH 7.6–8.8). The data are presented as the means of triplicate experiments with standard deviations.

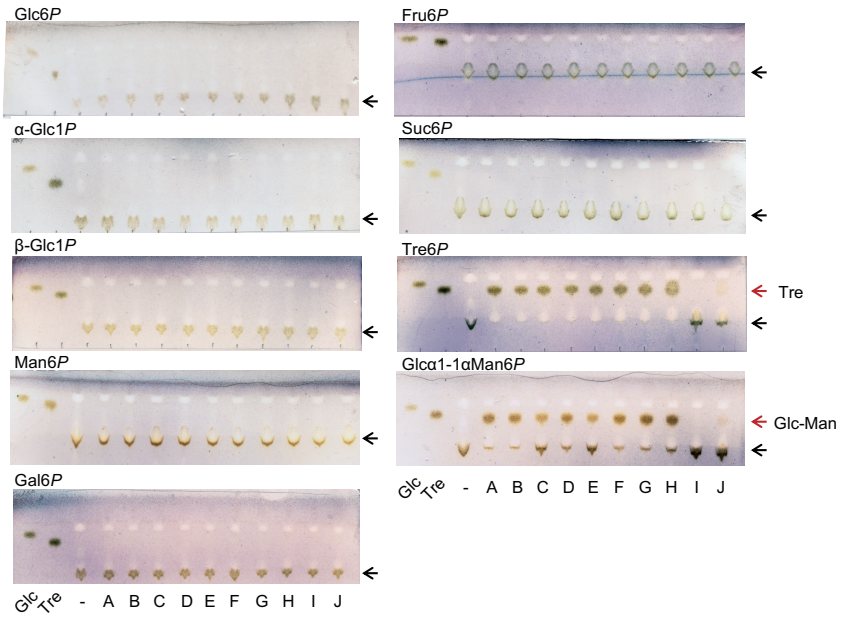

Fig. 3-6. TLC analysis of dephosphorylation reaction catalyzed by AtTPPs.

AtTPPs were incubated with 10 mM each substrate in 50 mM HEPES-NaOH buffer (pH 7.0) at 30°C for 24 h. Black and red arrows showed the substrates and reaction products, respectively. Minus symbol means the sample without the enzyme, and A–J indicate enzyme names. The sample was developed by acetonitrile: ethyl acetate: 1-propanol: water = 85: 20: 50: 60 (v/v/v/v).

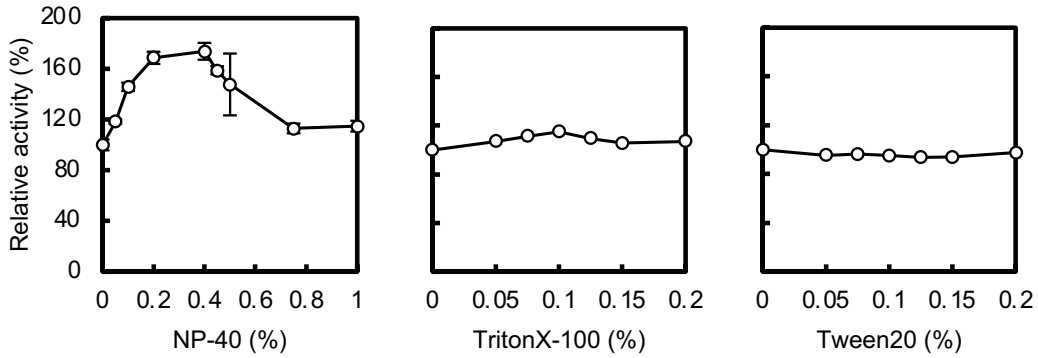

Fig. 3-7. Effect of detergents to the phosphatase activity of AtTPPB.

The relative TPP activity in the presence of the indicated concentration of various detergents are shown. The data of NP-40-effect are presented as the means of triplicate experiments with standard deviations, and others are from single result.

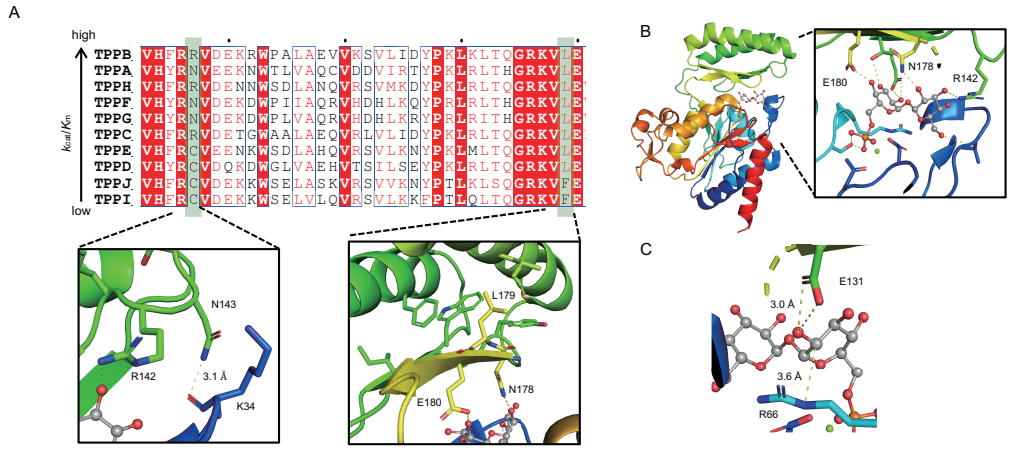

Fig. 3-8. Comparison of structures between AtTPPs and *C. neoformans* TPP.

(A) Amino acid sequence alignment of AtTPPs in the order of k_{cat}/K_m. Conserved residues are shown in red. Residues conserved only in AtTPPs with low or no activity are shown in green shade, and the structures of *C. neoformans* TPP (Miao et al., 2016) around the residues shown in green shade are shown in enlarged view. (B) Structure of *C. neoformans* TPP inactive mutant in complex with Tre6*P* (Miao et al., 2016). Close-up view of substrate binding site is shown. (C) The enlarged view of residues around 2-OH of Glc6*P* residue of Tre6*P*.

4. pH-dependent alteration of substrate specificity of plant trehalase and its molecular mechanism

4.1. Introduction

Arabidopsis and rice possess only one trehalase AtTRE1 and OsTRE1, respectively, both of which belong to GH37 (Van Houtte et al., 2013; Lunn, 2007; Müller et al., 2001). The trehalase activity of AtTRE1 was demonstrated by the functional complementation of trehalase deficiency in yeast (Frison et al., 2007). AtTRE1 is anchored to plasma membrane of stomatal guard cells with the N-terminal membrane-spanning domain (Met1–Leu63) (Frison et al., 2007; Van Houtte et al., 2013). On the other hand, OsTRE1 does not have such a membrane-spanning domain nor a signal peptide in the deduced amino acid sequence, and it is thought to be localized in the cytosol (Islam et al., 2019). As described in chapter 1, overexpression of the *AtTRE1* gene gave ABA-mediating stomatal closure and its resultant drought tolerance because of higher sensitivity to ABA, and *AtTRE1*-deficient plants do not show the stomatal closure (Van Houtte et al., 2013). This ABA insensitivity in the deficient mutant indicates that AtTRE1 is required for the acceptance of ABA signaling in the guard cells. Besides, *OsTRE1* gene is induced by stresses such as salt, drought, and chilling (Islam et al., 2019). *OsTRE1* overexpressors exhibited enhanced salt tolerance, suggesting the involvement of OsTRE1 in salt stress tolerance in rice (Islam et al., 2019).

As described in section 1.6, *E. coli* trehalase Tre37A (EcTre37A) was characterized structurally as GH37 trehalase. Based on the structure of EcTre37A in complex with the inhibitors, 1-thiatrehazolin and validoxylamine A (Gibson et al., 2007), two catalytic residues were predicted: Asp on the loop between 5th and 6th α-helices (α5→α6 loop) as the catalytic acid; and Glu on α11→α12 loop as the catalytic base. Contribution of carboxy groups in the reaction of trehalase was kinetically confirmed (Lee et al., 2001). Since α11→α12 loop, called “lid loop”, completely covers the substrate binding site

in the enzyme-inhibitor complex, this loop is assumed to open in the apo-enzyme to bind substrate and closes in the enzyme-substrate complex. This structural feature is commonly observed in trehalases from *E. cloacae* (PxEclTre) and *S. cerevisiae* (ScNth1) (Adhav et al., 2019; Alblova et al., 2017).

Although some physiological functions of plant trehalases has been discussed, its biochemical function and structure have not been fully mentioned thus far. In this study, function and structure of AtTRE1 were investigated through biochemical, mutational, and structural analysis, and compared with trehalases from other origins.

4.2. Materials and methods

4.2.1. Preparation of expression plasmids for recombinant AtTRE1 derivatives and OsTRE1

The cDNA of AtTRE1 was amplified by RT-PCR. cDNA was prepared from *A. thaliana* Col-0 as the same manner as section 3.2.1. For DNA fragments of *AtTRE1* (At4g24040) and 5′-region-truncated *AtTRE1* (*dNAtTRE1*, 189 nucleotides from 5′-terminal were deleted), following primers were used: 5′-ATGAAATCATACAAACTTAATAACC-3′ (sense) and 5′-AAAACTCGAGGG CTTCAATGCTAAGATGA-3′ (antisense) for *AtTRE1*; and 5′-AAAACATATGGACT CGGACACAGACACGG-3′ (sense) and 5′-AAAACTCGAGGGCTTCAATGCTAAGATGA-3′ (antisense) for *dNAtTRE1*. Primestar HS DNA polymerase was used. The PCR product was cloned into the *Eco*RV site of pBluescript II SK (+) and sequenced. To prepare the expression plasmid of full-length AtTRE1, the *AtTRE1* gene was amplified from the pBluescript II SK (+)-derived plasmid using the primers (5′-TTAACTTTAAGAAGGAGATATACATATGAAATCATACAAACTTAA-3′ (sense; sequence from pET-23a underlined) and 5′-GATCTCAGTGGTGGTGGTGGTGGTG GGCTTCAATGCTAAGATG AG-3′) (antisense). Amplified DNA was cloned into pET-23a using In-Fusion HD Cloning Kit. In the preparation of the expression plasmid for dNAtTRE1, the pBluescript

II SK (+)-derived plasmid harboring cDNA of dNAtTRE was digested with *Nde*I and *Xho*I, and the resulting DNA fragment was cloned into the *Nde*I and *Xho*I sites of pET-23a using DNA Ligation Kit Mighty Mix (Takara Bio). Expression plasmids of mutated dNAtTRE1 were prepared using Primestar Mutagenesis Basal Kit (Takara Bio). Primers used are as following: for D102A, 5′-ACGCCTGCCCCCAAATCCTACATTGAT-3′ (sense, mutation site was shown underlined) and 5′-TTTGGGGGCAGGCGTTTGTTTTTTAGG-3′ (antisense); for S223G, 5′-CCCGG TGGCAGATTCAGAGAAGTCTAT-3′ (sense) and 5′-GAATCTGCCACCGGGAATGATAACCGG-3′ (antisense); for R224A, 5′-GGTTCGGCTTTCAGAGAAGTCTATTAC-3′ (sense) and 5′-TCTGAAAGCCGAACCGGGAATGATAAC-3′ (antisense); for D380A, 5′-GGATGCGCTTTCAGCACGCGATGGATG-3′ (sense) and 5′-GCTGAAAGCGCATCCTGATTCAGCAGC-3′ (antisense); for E595A, 5′-GGAGGA GCATATATGCCACAGACCGGA-3′ (sense) and 5′-CATATATGCTCCTCCACCACCATATTC-3′ (antisense); for T600D, 5′-CCACAGGACGGATTCGGATGGTCAAAT-3′ (sense) and 5′-GAATCC GTCCTGTGGCATATATTCTCC-3′ (antisense).

The *OsTRE1* gene was obtained according to Islam *et al*. (Islam et al., 2019). To prepare the expression plasmid of OsTRE1, PCR was performed using primers, 5′-AGAAAAGAGAGGCTGAAGCTATTCACATGGCGCCCACCGC-3′, (sense, sequence from pPICZα underlined), and 5′- TCTGAGATGAGTTTTTGTTCGCAGTCTATCTTCTTGTCCT-3′ (antisense). Amplified DNA was cloned into the pPICZαA expression vector (Novagen) at the sites between *Pml*I and the *c-myc* epitope sequence (GAACAAAAACTCATCTCAGAAGAGGATCTG) using the In-Fusion HD Cloning Kit.

4.2.2. Preparation of AtTRE1 derivatives

A transformant of *E. coli* BL21 (DE3) harboring the expression plasmid for the dNAtTRE1 derivatives

was cultured in 1.0 L of LB medium containing 100 μg/mL ampicillin at 37°C until A_{600} reached 0.5. Protein production was induced by the addition of IPTG at 0.1 mM, and the induction culture was continued at 18°C for 23 h with vigorous shaking. The *E. coli* cells were harvested by centrifugation (10,000×g, 4°C, 10 min), and suspended in 30 mL of 50 mM sodium phosphate buffer (pH 6.5) containing 0.5 M NaCl and 25 mM imidazole. The bacterial cells were disrupted by sonication using a Sonifier 450, and the cell-free extract was obtained by centrifugation (6,000×g, 4°C, 10 min). The cell-free extract was loaded onto a Ni-chelating Sepharose Fast Flow column (1.6 cm i.d.×2.5 cm, 5 mL) equilibrated with 50 mM sodium phosphate buffer (pH 6.5) containing 0.5 M NaCl and 25 mM imidazole. After thoroughly washing the column with the same buffer, adsorbed protein was eluted with a linear gradient from 25 to 500 mM imidazole (100 mL in total). Eluted fractions were analyzed by SDS-PAGE, and fractions containing highly purified enzyme were pooled. The collected sample was dialyzed against 10 mM potassium phosphate buffer (pH 7.0), concentrated to 1.99 mg/mL using Amicon Ultra concentrator (NMWL 10,000 Da), and stored at 4°C. The concentration of proteins was determined following section 2.2.7.

4.2.3. Preparation of OsTRE1

The expression plasmid of OsTRE1, linearized by *Sac*I digestion, was introduced into *Pichia pastoris* strain X-33 by electroporation using a Gene Pulser (Bio-Rad, Hercules, CA). Transformant, grown on a YPDSZ plate [10 mg/mL of yeast extract (Nacalai Tesque), 20 mg/mL of peptone (Difco, Detroit, MI, USA), 20 mg/mL of D-glucose, 1 M D-glucitol, 20 mg/mL of agar (Nacalai Tesuque), and 100 μg/mL of Zeocin (Thermo Fisher Scientific), was inoculated into 170 mL of BMGY medium [10 mg/mL of yeast extract, 20 mg/mL of peptone, 13.4 mg/mL of yeast nitrogen base without amino acid with ammonium sulfate (Invitrogen), 4 mg/L of D-biotin, 10 mg/mL of glycerol, and 0.1 M potassium phosphate buffer (pH 6.0)], and incubated at 30°C for 16 h with vigorous shaking. Cells were collected

by centrifugation, suspended in 500 mL of BMMY medium [10 mg/mL of glycerol in BMGY was changed to 2% (v/v) methanol], and incubated at 30°C for 96 h. Protein production was maintained by the addition of methanol at concentration of 2% (v/v) every 24 h. Produced enzyme was purified from the culture supernatant by Ni-affinity column chromatography and conserved as the same manner as dNAtTRE1.

4.2.4. Trehalases from *E. coli* and pig

Recombinant EcTre37A was produced in *E. coli*. The *tre37A* gene (GenBank accession No.: AAC74281.1) was obtained from the genomic DNA of *E. coli* DH5α by PCR in which primers (sense, 5'-TGCCTGACAGTTCGCAGAAT-3'; antisense, 5'-AATCGCCGGGTGATGAAAGT-3') and Primestar HS DNA polymerase were used. The nucleotide sequence of the gene was the same as the reregistered. To prepare the expression plasmid of EcTre37A, the *tre37A* gene was amplified using the first PCR DNA fragment as template and the primers, 5′-AAGAAGGAGATATACATATGGAAGAAACACCGGTAACACC-3′ (sense; vector-derived sequence underlined) and 5′- CAGTGGTGGTGGTGGTGGTGAGGTGTGGGTTGTGCCTCTT-3′ (antisense). The amplified DNA was cloned into pET-23a plasmid using In-Fusion HD Cloning Kit. This plasmid was introduced into *E. coli* BL21(DE3), and the transformant was cultured in 1 L of LB medium containing 100 μg/mL ampicillin at 37°C until A_{600} reached 0.5. Protein expression was induced, and the recombinant protein was purified by Ni affinity column chromatography as described in section 4.2.2.

Trehalase from porcine kidney was purchased from Sigma-Aldrich.

4.2.5. Preparations of trehalose-like disaccharides

Tre6*P*, Glcα1-1αMan6*P* were synthesized as described in chapter 2 (Taguchi et al., 2017, 2020).

Glcα1-1αGal, Glcα1-1αXyl, and Glcα1-4-L-Ara were synthesized by the reverse phosphorolysis of TP from *Thermoanaerobacter siderophilus* DSM12299 (TsTP; locus tag, *ThesiDRAFT1_1928*; GenBank accession number, EIW00805.1). For preparation of N-terminal His-tagged protein, TsTP gene was amplified from the genomic DNA of *T. siderophilus* DSM12299 with primers: 5′-ATGGCCAACAAAACGAAGAAACCAA-3′ (sense) and 5′-TTAATTTTTGCGACTTTCTACTTTA-3′ (antisense). The first PCR DNA fragment (2343 bp) was used as template for the second PCR, with primers; 5′-TGCCGCGCGGCAGCCATATGGCCAACAAAACGAAGAA-3′ (sense) and 5′-GCGGCCGCAAGCTTGTCGACTTAATTTTTGCGACTTTCTA-3′ (antisense). pET-28a harboring the DNA fragment was prepared using In-Fusion HD Cloning Kit and cloned. The DNA sequence of inserted fragment and flanking regions was analyzed using an Applied Biosystems 3130 Genetic Analyzer. This plasmid was introduced into *E. coli* BL21 (DE3), and transformant harboring the plasmid was cultured in 1 L of LB medium containing 50 μg/mL kanamycin at 37°C until A_{600} reached 0.5. Protein production was induced with 0.1 M IPTG at 0.1 mM, and the induction was done at 18°C for 24 h with vigorous shaking. The *E. coli* cells were harvested by centrifugation (10,000×g, 4°C, 10 min), and suspended in 30 mL of 20 mM imidazole-HCl buffer (pH 8.0) containing 0.5 M NaCl. The bacterial cells were disrupted by sonication using a Sonifier 450, and the cell-free extract was obtained by centrifugation (6,000×g, 4°C, 10 min). This extract was loaded onto a Ni-chelating Sepharose Fast Flow column (1.6 cm i.d.×2.5 cm, 5 mL) equilibrated with 20 mM imidazole-HCl buffer (pH 8.0) containing 0.5 M NaCl (buffer A). After thoroughly washing the column with buffer A, the adsorbed proteins were eluted with a linear gradient from 20 to 300 mM of buffer A (100 mL in total). Eluted fractions were analyzed by SDS-PAGE, and fractions containing highly purified enzyme were pooled. The collected sample was dialyzed against 10 mM MES-NaOH buffer (pH 6.5) and stored at 4°C. Concentration of protein were determined following section 2.2.7, but TsTP was quantified based on

calculated specific coefficient (138730 A_{280}/mol/cm) according to Pace *et al*. (Pace et al., 1995).

Trehalose phosphorylase activity was measured as below: a reaction mixture (50μL), containing enzyme, 4 mM trehalose, and 40 mM sodium phosphate buffer (pH 7.3), was incubated at 50°C for 10 min. The reaction was stopped by incubating the sample at 100°C for 5 min, and D-glucose produced was measured by the glucose oxidase peroxidase method (Miwa et al., 1972). One unit of enzyme activity was defined as the amount of enzyme to phosphorolyze 1 μmol of trehalose in 1 min under these conditions.

275 U of trehalose phosphorylase activity was confirmed in the cell free-extract. 10 mg of purified TsTP showing 9.38 U/mg was obtained by Ni affinity column chromatography. TsTP showed 97.5% of sequence identity to TP from *Thermoanaerobacter brokii* (TbTP). TbTP showed 21.8 U/mg to 29 mM trehalose and 50 mM inorganic phosphate (much higher than K_m) at pH 7.0 and 50°C, and there was little difference in specific activity between pH 7.0 and 7.5 (Chaen et al., 1999a). TsTP showed approximately half specific activity compared with TbTP.

A reaction mixtures (75 mL), containing 7.0 U/mL TsTP, 40 mM β-Glc1*P*, 40 mM acceptor monosaccharide, was incubated at 50°C for 98 h. The pH of the reaction mixture was adjusted to pH 6.0 with 6 M HCl without addition of any buffer. As acceptor monosaccharide, D-xylose, D-galactose (Nacalai Tesque), and L-arabinose (Kanto Chemical, Tokyo, Japan) were used. At 50 h, inorganic phosphate was precipitated by the addition of 495 mg of $(NH_4)_2SO_4$ and 1.85 g of $MgSO_4 \cdot 7H_2O$ (concentration of $(NH_4)_2SO_4$ and $MgSO_4$ were 50 and 100 mM, respectively). The reaction was stopped by boiling. The supernatant was obtained after centrifugation and was desalted with Amberlite MB-4 (Organo) and evaporated to 7 mL. The reaction product was subjected to gel filtration column chromatography using Bio-Gel P2 (1.6 cm i.d. × 200 cm, 400 mL, equilibrated with water, Bio-Rad). The fractions, containing the purified reaction product, were collected and lyophilized. Yield of Glcα1-1αGal, Glcα1-1αXyl, and Glcα1-4-L-Ara were 642, 637, and 549 mg, respectively.

The chemical structure of these products was confirmed by ESI-MS and NMR as described in section 2.2.16.

Glcα1-1αGal: ESI-MS, *m*/*z* 365.11 $[M+Na]^+$; ^{1}H-NMR (D_2O) δ 5.24 (d, J = 4.0 Hz, Gal H-1), 5.23 (d, J = 3.9 Hz, Glc H-1), 4.09 (t, J = 6.1 Hz, Gal H-5), 4.03 (m, Gal H-3), 4.03 (m, Gal H-4), 3.93 (m, Gal H-2), 3.87 (m, Glc H-3), 3.87 (m, Glc H-6), 3.84 (m, Glc H-5), 3.78 (m, Glc H-6), 3.76 (m, Gal H-6), 3.67 (dd, J = 3.8, 9.9 Hz, Glc H-2), 3.47 (t, J = 9.4 Hz, Glc H-4); ^{13}C-NMR (D_2O) δ 96.1 (Gal C-1), 95.9 (Glc C-1), 75.3 (Glc C-3), 74.9 (Glc C-5), 74.1 (Gal C-5), 73.9 (Glc C-2), 72.5 (Glc C-4), 72.1 (Gal C-4), 71.8 (Gal C-3), 70.7 (Gal C-2), 64.0 (Gal C-6), 63.3 (Glc C-6).

Glcα1-1αXyl: ESI-MS, *m*/*z* 335.10 $[M+Na]^+$; ^{1}H-NMR (D_2O) δ 5.19 (d, J = 3.8 Hz, Glc H-1), 5.19 (d, J = 3.8 Hz, Xyl H-1), 3.90 (m, Glc H-3), 3.88 (m, Glc H-6), 3.86 (m, Glc H-5), 3.83 (m, Xyl H-3), 3.79 (m, Glc H-6), 3.73 (m, Xyl H-5), 3.71 (m, Xyl H-5), 3.69 (m, Xyl H-4), 3.68 (m, Glc H-2), 3.68 (m, Xyl H-2), 3.48 (t, J = 9.5 Hz, Glc H-4); ^{13}C-NMR (D_2O) δ 96.3（Xyl C-1）, 96.2 (Glc C-1), 75.5 (Xyl C-3), 75.4 (Glc C-3), 75.0 (Glc C-5), 73.9 (Glc C-2), 73.9 (Xyl C-2), 72.5 (Glc C-4), 72.3 (Xyl C-4), 64.4 (Xyl C-5), 63.3 (Glc C-6).

Glcα1-4-L-Ara: ESI-MS, *m*/*z* 335.10 $[M+Na]^+$; ^{1}H-NMR (D_2O) δ 5.29 (d, J = 3.4 Hz, β-Ara*p* H-1), 5.10 (d, J = 3.8 Hz, Glc H-1), 4.61 (d, J = 7.6 Hz, α-Ara*p* H-1), 4.11 (dd, J = 2.2, 13.5 Hz, α-Ara*p* H-5), 4.09 (m, α-Ara*p* H-4), 4.06 (m, β-Ara*p* H-3), 4.05 (m, β-Ara*p* H-4), 4.01 (m, β-Ara*p* H-5), 3.99 (m, Glc H-5), 3.95 (m, β-Ara*p* H-2), 3.88 (m, Glc H-6), 3.86 (m, β-Ara*p* H-5), 3.85 (m, Glc H-3), 3.81 (m, Glc H-6), 3.81 (m, α-Ara*p* H-3), 3.65 (m, α-Ara*p* H-2), 3.64 (m, α-Ara*p* H-5), 3.61 (m, Glc H-2), 3.47 (t, J = 9.3 Hz, Glc H-4); ^{13}C-NMR (D_2O) δ 99.6 (α-Ara*p* C-1), 98.6 (Glc C-1), 95.3 (β-Ara*p* C-1), 76.5 (β-Ara*p* C-4), 76.3 (α-Ara*p* C-4), 75.7 (Glc C-3), 74.7 (Glc C-5), 74.6 (α-Ara*p* C-3), 74.5 (α-Ara*p* C-2), 74.3 (Glc C-2), 72.4 (Glc C-4), 71.4 (β-Ara*p* C-2), 71.0 (β-Ara*p* C-3), 65.1 (α-Ara*p* C-5), 63.3 (Glc C-6), 61.7 (β-Ara*p* C-5).

4.2.6. Measurement of molecular mass by gel filtration column chromatography

Molecular mass of dNAtTRE1 was measured by gel filtration. Superdex 200 10/300 GL High-Performance column (1.0 cm i.d.×30 cm, 24 mL, GE Healthcare), equilibrated with 10 mM MES-NaOH buffer (pH 6.5) containing 150 mM NaCl, was used at room temperature. dNAtTRE1 (398 μg was loaded. Flow rate was 0.5 mL/min. The protein was detected by measuring A_{254}. Molecular mass was calibrated with Gel Filtration Standard (Bio-Rad).

4.2.7. Measurement of trehalase activity

Trehalase activity was determined by measuring D-glucose liberated from trehalose. A reaction mixture (50 μL), composed of an appropriate concentration of enzyme, 102 mM potassium phosphate buffer (pH 7.0), 10 mM trehalose, and 0.4 mg/mL BSA, was incubated at 37°C for 10 min. The reaction was terminated by adding 25 μL of 4 M Tris-HCl (pH 7.0) or incubating the sample at 100°C for 2 min. The concentration of D-glucose liberated was measured by the glucose oxidase peroxidase method (Miwa et al., 1972). One unit of enzyme activity was defined as the amount of enzyme hydrolyzing 1 μmol of trehalose i.e., the formation of 2 μmol of glucose in 1 min under these conditions. For the evaluation of glycerol, 2.5–20% glycerol was added to a reaction mixture, and BSA concentration was changed to 0.2 mg/mL.

The kinetic parameters for the hydrolysis of trehalose were determined by fitting the reaction rates at various concentrations (0.05–6.4 mM) of trehalose to the Michaelis-Menten equation by non-linear regression using Grafit version 7.0.2. The reaction conditions were the same for the activity assay, but with 0.05–6.4 mM trehalose and 0.722 nM dNAtTRE1, and trehalose-hydrolytic velocity was regarded as half as glucose-releasing velocity.

4.2.8. Kinetic analysis of inhibition of dNAtTRE1 reaction by Tris

Reaction rates in the presence or absence of Tris were measured. A reaction mixture (50 μL), containing enzyme, 0.05–6.4 mM trehalose, 0–20 mM Tris-HCl buffer (pH 7.0), 102 mM potassium phosphate buffer (pH 7.0), and 0.2 mg/mL BSA, was incubated in the same manner as the standard enzyme assay. Kinetic parameters were calculated by fitting the rate equation for the mixed type inhibition (Eq. 4-1) to the obtained velocities. Non-linear regression with the Eq.4-1 was performed on the s-*v* plots using Grafit version 7.0.2.

Eq.4-1 $v = k_{cat}[S]/[K_s (1+ [I]/K_i)+(1+ [I]/K'_i)[S]]$

K_i, dissociation constant of inhibitor and free enzyme; K'_i, dissociation constant of inhibitor and enzyme-substrate complex

4.2.9. Effects of pH and temperature on activity and stability

Stable range for pH and temperature was evaluated by measuring residual activity after the pH and heat treatment, respectively. As the pH treatment, 10.3 μM dNAtTRE1 or 5.6 μM OsTRE1 was kept in 100–160 mM Briton-Robinson buffer (pH 2.5–12.4) at 4°C for 24 h. As the heat treatment, 8.18 nM dNAtTRE1 or 2.23 nM OsTRE1 was incubated in 10 mM potassium phosphate buffer (pH 7.0) containing 1.0 mg/mL BSA at various temperatures for 15 min. The ranges of pH and temperature, in which the enzyme retained ≥90% of the original activity, were regarded as the stable ranges. Effect of pH on dependence of the kinetic parameters was evaluated by measuring the kinetic parameters at various pH values. The reaction conditions and determination of kinetic parameters were the same as section 4.2.7, but buffer and pH was changed. As the reaction buffer, 100 mM Britton Robinson buffer (pH 2.5–12.4), 100 mM glycine-HCl buffer (pH 2.7–3.1), 100 mM sodium acetate buffer (pH 3.5–6.1), 100 mM sodium phosphate buffer (pH 5.4–8.0), 100 mM MES-NaOH buffer (pH 6.0–6.8), and 100 mM HEPES- NaOH buffer (pH 6.9–7.8) were used.

4.2.10. Evaluation of substrate specificity

To examine the hydrolytic activity of dNAtTRE1 and OsTRE1 against various disaccharides, these enzymes (41 U/mL: dNAtTRE1, 4.49 μM; OsTRE1, 3.35 μM) was incubated in 50 μL of a reaction mixture containing 10 mM α-glucosides [trehalose, kojibiose (Glcα1-2Glc, Wako Pure Chemical Industries), nigerose (Glcα1-3Glc, Wako Pure Chemical Industries), maltose, isomaltose (Glcα1-6Glc, Tokyo Chemical Industry), Tre6*P*, Glcα1-1αMan6*P*, neotrehalose (Glcα1-1βGlc, Hayashibara), sucrose (Glcα1-2βFru, Nacalai Tesque), Glcα1-1αXyl, Glcα1-1αGal, and Glcα1-4-L-Ara] and 100 mM reaction buffer at 37°C for 24 h. For dNAtTRE1, 100 mM sodium acetate buffer (pH 3.6) and 100 mM potassium phosphate buffer (pH 7.0) were used as reaction buffer, and for OsTRE1, 100 mM sodium acetate buffer (pH 4.5) was used. The reaction was stopped by heating the sample at 80°C for 5 min. The reaction product was analyzed by TLC using Silica gel 60 F_{254} aluminum sheet. For the analysis of the reaction products from trehalose, Glcα1-1αXyl, and Glcα1-1αGal, 2-propanol: 1-butanol: water = 2: 2: 1 (v/v/v) was used as developing solvent; for the reaction product from Glcα1-4-L-Ara, isopropanol: acetone: 0.1 M lactic acid = 4: 4: 2 (v/v/v) was used; and for the products from the other substrates, acetonitrile: ethyl acetate: 1-propanol: water = 85: 20: 50: 60 (v/v/v/v) was used. Carbohydrate was detected by praying the detection solution (acetic acid: sulfuric acid: anisaldehyde = 100: 2: 1, v/v/v) and heating the plate.

Kinetic parameters for the hydrolysis of Glcα1-1αXyl, Glcα1-1αGal, Glcα1-4-L-Ara, and Tre6*P* were determined from the reaction velocity at various concentrations of the substrates in the same manner as the reaction with trehalose.

4.2.11. MS analysis of the reaction products in $H_2{}^{18}O$

A reaction mixture (20 μL), containing 0.28 mg/mL dNAtTRE1, 10 mM substrate, 100 mM Briton Robinson buffer (pH 3.5), and 2 mM potassium phosphate buffer (pH 7.0), was incubated at 37°C.

Tre6*P*, Glcα1-4-L-Ara, and Glcα1-1αGal were used as substrate. For all the solvents except for enzyme, $H_2{}^{18}O$ (Sigma-Aldrich) was used. At reaction 10 and 60 min, the reaction was stopped by keeping the sample at 80°C for 5 min. The mass of the product was measured using ESI-MS as described in section 2.2.16.

4.2.12. Crystallization and data collection

dNAtTRE1 wild type and D380A purified by Ni-chelating Sepharose Fast Flow column and anion exchange column chromatography using a Toyopearl DEAE 650M column (1.6 cm i.d.×2.5 cm, 5 mL, Tosoh) equilibrated with 10 mM sodium phosphate buffer (pH 7.0). In the anion exchange column chromatography, the adsorbed protein was eluted with a linear gradient of NaCl from 0 to 0.5 M (total elution volume, 100 mL) after thorough washing the column with 10 mM sodium phosphate buffer (pH 7.0). Purified dNAtTRE1 wild type and D380A were dialyzed against 10 mM potassium phosphate buffer (pH 7.0) and concentrated to 4.6–25 mg/mL using Amicon Ultra concentrator (NMWL 10,000 Da): wild type for substrate-free structure, 4.6 mg/mL; D380A for co-crystallization with trehalose, 22 mg/mL; and D380A for co-crystallization with Tre6*P*, 25 mg/mL. These proteins were crystallized by the sitting-drop vapor-diffusion method, in which 0.75 μL of protein solution was mixed with an equal volume of reservoir solution. Crystals were obtained at 20°C with following reservoir solutions: wild type, 0.1 M sodium acetate and 200 g/L PEG3400; D380A and trehalose complex, 10 mM trehalose, 0.1 M sodium fluoride and 200 g/L PEG3400; and D380A substrate free, 10 mM Tre6*P*, 0.1 M sodium chloride and 200 g/L PEG3400.

For X-ray diffraction experiments, the crystals were picked up from the crystallization solution and flash cooled. Diffraction data were collected under a stream of liquid nitrogen at 100 K on beamline BL-44XU at SPring-8 (Hyogo, Japan) for the wild type and D380A-trehalose complex, and BL-5A at Photon Factory (Tsukuba, Japan) for D380A-Tre6*P* complex. The data set was indexed,

integrated, scaled and merged using the *XDS* program suite (Kabsch, 2010). The asymmetric unit of dNAtTRE1 apo, D380A with trehalose, and D380A with Tre6*P* contained two or four molecules, corresponding to a Matthews coefficient of 2.1, 2.5, and 4.1 $Å^3$/Da, respectively, and an estimated solvent content was 42.5%, 51.1%, and 70.1%, respectively. The data collection and processing statistics are summarized in Table 4-1.

4.2.13. Structure solution and refinement

The structure of dNAtTRE1 was determined by the molecular replacement method with the program *AutoMR* in the *Phenix* program package (Adams et al., 2010; McCoy et al., 2007), using the structure of EcTre37A (PDB entry: 2JG0) as the search model. Several rounds of refinement were performed using the program *Phenix.refine* in the *Phenix* program suite, alternating with manual fitting and rebuilding, based on $2F_o$-F_c and F_o-F_c electron density using *COOT* (Emsley and Cowtan, 2004; McCoy et al., 2007). The final refinement statistics and geometry defined by *MolProbity* (Chen et al., 2010) are shown in Table 4-1. All figures of structures were generated by the *PyMol* molecular graphics system version 2.2.0 (Schrdöinger, LLC, New York, NY, USA).

4.3. Results

4.3.1. Production and basic properties of recombinant AtTRE1

Recombinant AtTRE1 was prepared using an *E. coli* expression system. Full-length AtTRE1 with a His-tag at C-terminal (eight residues extension, Leu-Glu-His-His-His-His-His-His, was attached) was not produced in *E. coli* (data not shown), and thus a predicted N-terminal transmembrane region (Met1–Leu63) was eliminated. N-terminal truncated AtTRE1 (dNAtTRE1) was successfully produced in *E. coli* as soluble protein. From 2 L of the culture broth of the *E. coli* transformant, 21 mg of purified dNAtTRE1 was obtained by immobilized Ni affinity column chromatography. The specific activity of

the purified dNAtTRE1 to 10 mM trehalose at pH 7.0 at 37°C was 139 U/mg.

Purified dNAtTRE1 showed a single band of 63 kDa on SDS-PAGE (Fig. 4-1A). This molecular mass was consistent well with estimated molecular masses from the amino acid sequence (65 kDa) and from size exclusion column chromatography (62 kDa) (Fig. 4-1B), indicating that dNAtTRE1 was a monomeric protein under nondenaturing conditions. The stable temperature and pH ranges of dNAtTRE1, in which >90% of the original activity was retained after the heat and pH treatments, respectively, were ≤50°C (for 15 min) and pH 5.0–10.0 (at 4°C for 24 h), respectively (Fig. 4-2). Tris inhibited the dNAtTRE1 reaction. The reaction rates at various concentrations of trehalose in 0–20 mM Tris obeyed the rate equation for the mixed inhibition well (Fig. 4-3). The rate parameters determined at pH 7.0 were as follows: k_{cat} = 143 ± 2 s^{-1}, K_s = 1.39 ± 0.03 mM, K'_s = 19.1 ± 7.1 mM K_i = 1.03 ± 0.09 mM, and K'_i = 13.8 ± 4.1 mM.

4.3.2. pH dependency of kinetic parameters of dNAtTRE1 for trehalose hydrolysis

Kinetic parameters of dNAtTRE1 for trehalose hydrolysis were determined at various pH values (Britton Robinson buffer was used as reaction buffer). The reaction rates at various concentrations of trehalose followed the Michaelis-Menten equation well. In the pH-k_{cat} curve, dNAtTRE1 showed two peaks at pH 3.7 and pH 6.9 (Fig. 4-4A), while in the pH-k_{cat}/K_m curve, it showed a single peak at pH 4.5 (Fig. 4-4B). The k_{cat} and K_m values of dNAtTRE1 at pH 3.7 were 274 ± 3 s^{-1} and 2.44 ± 0.06 mM, respectively; those at pH 4.5 were 147 ± 7.8 s^{-1} and 0.395 ± 0.023 mM, respectively; and those at pH 6.9 were 134 ± 1 s^{-1} and 1.08 ± 0.05 mM, respectively. The lowest K_m value (0.34 mM) was obtained at pH 5.0 (Fig. 4-4C). This value was 7.2- and 3.2-fold lower than the values at pH 3.7 and pH 6.9, respectively. Two peaks in the pH-k_{cat} curve were also observed, when other buffers, glycine-HCl buffer, sodium acetate buffer, sodium phosphate buffer, MES-NaOH buffer, and HEPES-NaOH buffer, were used as the reaction buffer (Fig. 4-4D). Compared with the specific activity in sodium

phosphate buffer at pH 7.0, the specific activity of dNAtTRE1 in MES-NaOH buffer and HEPES-NaOH buffer increased by 8% and 11%, respectively.

4.3.3. Substrate specificity

Substrate specificity of dNAtTRE1 was examined based on hydrolytic activity to various α-glucosides. The formation of products at pH 3.7 and pH 6.9 were analyzed by TLC (Fig. 4-5). Products were observed in the reaction with from trehalose, Glcα1-1αXyl, Glcα1-1αGal, Glcα1-4-L-Ara, and Tre6*P* except the one on Tre6*P* at pH 6.9. Kojibiose, nigerose, maltose, isomaltose, Glcα1-1αMan6*P*, neotrehalose, and sucrose did not serve as substrate of dNAtTRE1.

The kinetic parameters of dNAtTRE1 for Glcα1-1αXyl, Glcα1-1αGal, Glcα1-4-L-Ara, and Tre6*P* were measured at pH 3.7 and 6.9 (Table 4-2). For all the substrates, the reaction rates followed the Michaelis-Menten equation well. The k_{cat}/K_m values for them were much lower than for trehalose. The k_{cat}/K_m values for Glcα1-4-L-Ara, Glcα1-1αGal, and Glcα1-1αXyl at pH 6.9 were higher than at pH 3.7. The k_{cat}/K_m values to Glcα1-4-L-Ara and Glcα1-1αGal were similar to each other at pH 3.7, but k_{cat}/K_m to Glcα1-4-L-Ara was 1.9-fold higher than to Glcα1-1αGal at pH 6.9. The k_{cat}/K_m to Tre6*P* was the lowest among the tested substrates at both pH values, but the k_{cat}/K_m obtained at pH 3.7 was 21 times higher than at pH 6.9. The pH dependency of the hydrolysis of Tre6*P* by dNAtTRE1 was analyzed (Fig. 4-4E and F). Unlike the hydrolysis of trehalose, the pH-k_{cat} curve has a single peak at pH 3.9 (1.27 s^{-1}, Fig. 4-4E). The pH-k_{cat}/K_m curve was almost the same shape as the pH-k_{cat} curve, and the maximum value was 0.0986 s^{-1} mM^{-1} at pH 4.2 (Fig. 4-4F). Tre6*P*-hydrolyzing velocity of dNAtTRE1 was compared with trehalases from *E. coli* (EcTre37A) and pig (Table 4-3). The velocity of dNAtTRE1, EcTre37A, and pig trehalase to 10 mM Tre6*P* was 0.303 μmol/min/mg, 0.0285 μmol/min/mg, and $<1.7\times10^{-4}$ μmol/min/mg, respectively. The velocity of dNAtTRE1 was much higher than trehalases from the other origins.

The cleavage linkages of Glcα1-1αXyl, Glcα1-4-L-Ara, and Tre6*P*, were analyzed by ESI-MS analysis of ^{18}O-labeled products (Fig. 4-6). The substrates were hydrolyzed in ^{18}O-water. The signal of 181.06 *m/z* $[M-H]^-$ or 205.06 *m/z* $[M+Na]^+$ was observed in all reactions in $H_2{}^{18}O$ while it was not observed in the reaction product in H_2O (Fig. 4-6). The signals of Ara (173.04 *m/z* $[M+Na]^+$), Xyl (149.05 *m/z* $[M-H]^-$), and Glc6*P* (259.02 *m/z* $[M-H]^-$) were also detected although 259.02 *m/z* signal was also confirmed in background signal. The signals of 151.04 *m/z* $[M-H]^-$ and 261.03 *m/z* $[M-H]^-$ were detected in both the reaction samples in H_2O and $H_2{}^{18}O$, these signals were not considered as the enzymatic reaction products. Monoisotopic mass of $[M-H]^-$ of xylose containing ^{18}O (C5H10O4[18O]) is expected to be 151.05, and 151.04 *m/z* was confirmed in background signal, so 151.04 *m/z* is not thought to be the signal of xylose containing ^{18}O. Besides, no significant increase of the intensity of 151.04 *m/z* and 261.03 *m/z* during the reaction was observed. Therefore, an increase in glucose mass indicates incorporation of ^{18}O to D-glucose and the cleavage between Glc C-1 and O-1.

4.3.4. Comparison of enzymatic characteristics of OsTRE1 with dNAtTRE1

Recombinant OsTRE1 was produced in *P. pastoris*. Soluble protein was not obtained when produced in *E. coli* (data not shown). The deduced sequence of the immature protein had the signal sequence of α-factor of yeast and linker (Ile-His) on the N-terminus of OsTRE1 excluding the first methionine and 21 residues (Glu-Gln-Lys-Leu-Ile-Ser-Glu-Glu-Asp-Leu-Asn-Ser-Ala-Val-Asp-His-His-His-His-His-His) on the C-terminus. OsTRE1 was extracellularly produced in *P. pastoris*, and 518 U trehalase activity was obtained from the culture supernatant from 500 mL of the culture broth. Recombinant OsTRE1 was purified by Ni-affinity column chromatography, and 3.2 mg of the purified enzyme was obtained. The specific activity of purified OsTRE1 was 174 U/mg. Purified enzyme showed a single band at 62 kDa in SDS-PAGE analysis in a good agreement with theoretical value of 65 kDa (the

theoretical value was calculated as the mature protein cleaved by Ste13) (Fig. 4-1C). The stable temperature and pH ranges of OsTRE1 were ≤40°C (15 min) and pH 3.8–9.0 (at 4°C for 24 h), respectively. In contrast to dNAtTRE1, OsTRE1 showed a broad single peak in the pH-*v* curve (Fig. 4-4G). OsTRE1 showed hydrolytic activity to trehalose, Glcα1-1αXyl, Glcα1-1αGal, Glcα1-4-L-Ara, and Tre6*P*, as observed in the reactions of dNAtTRE1 (Fig. 4-5). Kinetic parameters of OsTRE1 for trehalose hydrolysis were determined. The k_{cat} and K_m values of OsTRE1 at pH 4.5 were 352 ± 6 s^{-1} and 0.459 ± 0.009 mM, respectively (Table 4-2). This enzyme showed similar relative k_{cat}/K_m to Glcα1-4-L-Ara, Glcα1-1αGal, and Tre6*P* to the dNAtTRE1 at pH 3.7.

4.3.5. Structural analysis of dNAtTRE1

Obtained crystal of substrate-free dNAtTRE1 belonged to space group $P2_12_12_1$ with two monomers in the asymmetric unit. The structure of dNAtTRE1 was determined at 2.1 Å resolution by the molecular replacement method using the structure of EcTre37A (PDB entry, 2JG0) as the search model. Selected crystallographic data and refinement statistics are listed in Table 4-1. Root mean square deviation of Cα of dNAtTRE1 apo structure chain A with the other trehalases are as follows: *E. coli* EcTre37A (PDB entry, 2JF4), 0.866 Å; *E. cloacae* trehalase (PxEclTre, PDB entry, 5Z66), 0.740 Å; and *S. cerevisiae* neutral trehalase (ScNth1, PDB entry, 5N6N, containing N-terminal domain), 3.71 Å. The overall structure of dNAtTRE1 consisted of an N-terminal domain (Lys79–Tyr148, residue number was shown based on the full length of AtTRE1) and the catalytic domain (Glu178–Tyr616) (Fig. 4-7). The catalytic domain of dNAtTRE1 was folded by an $(\alpha/\alpha)_6$-barrel as observed in other GH37 trehalases (Fig. 4-8A). The N-terminal domain, called hood domain, contained four α-helices (Fig. 4-8A). The catalytic domain of dNAtTRE1 possessed a longer α5→α6 loop (Asn315–Pro402) than other loops, containing two α-helices and two β-strands. The putative general acid catalyst Asp380 is situated on this loop. The α11→α12 loop (Ser575–Gly601) covered the substrate binding

site (Fig. 4-8B). This loop contained the putative general base catalyst Glu580. Electron density of glycerol and inorganic phosphate was observed at subsites -1 and +1, respectively (Fig. 4-8B). Glycerol and inorganic phosphate inhibited the dNAtTRE1 reaction. The specific activity decreased dependent on glycerol concentration. In the presence of 20% glycerol, the specific activity was 40.5 U/mg. Besides, the specific activity of dNAtTRE1 increased in the absence of inorganic phospahte. Glycerol is suitably located to form direct hydrogen bond with Asp232. Trp231 likely formed a water-mediate hydrogen bond with the glycerol. Inorganic phosphate is coordinated by Arg277, Arg344, Glu346 and Asp380. Arg344 is possible to form hydrogen bond with Glu595 on α11→α12 loop (Fig. 4-8B). Tyr596 on this loop could also form water mediated hydrogen bond with inorganic phosphate, Na^+, and Asp380. The Na^+ interacts with glycerol located at subsite -1.

To capture the complex of dNAtTRE1 and trehalose, the mutant enzyme of the general acid catalyst Asp380 (D380A) was prepared. This mutant enzyme showed very low activity to 10 mM trehalose, 6.8×10^{-5} U/mg (-7-fold lower than wild type). The structure of the dNAtTRE1 D380A-trehalose complex was determined at 1.8 Å resolution by the molecular replacement method using the structure of substrate-free dNAtTRE1 (Table 4-1, Fig. 4-8C and D). Electron density of two D-glucosyl residues was observed at the active site in chain B. Although electron density for C-1, C-2, C-3, and O-3 of D-glucosyl residue bound to subsite -1 was poor, other atoms of this D-glucosyl residue fitted well to the electron density map when the D-glucosyl residue took $^4C_1$ chair conformation (Fig. 4-8D). The electron density of D-glucosyl residue bond to subsite +1 was clearly observed, and $^4C_1$ conformation was adapted for this residue. Trehalose molecule was not seen on the surface of dNAtTRE1, because α1→α2 loop and α11→α12 loop covered the substrate binding site (Fig. 4-9 A and B).

The general base catalyst Glu580 on α11→α12 loop is located at a suitable position to form hydrogen bond with Tyr596 on the same loop (Fig. 4-8B and C, Fig. 4-9A and B). Electron density of

the water molecule (O), which is coordinated by the Glu580, was located at a distance of 3.5 Å from the C-1 of D-glucosyl residue at subsite -1. The position of this water molecule is suitable for in-line attack to C-1 of the D-glucosyl residue from the other side of its glucosidic linkage in the single displacement mechanism. Thus, this water molecule could serve as the substrate water. This water molecule could also be coordinated by 6-OH group of the D-glucosyl residue at subsite -1. Asp232 on N-terminal part of the 2nd α-helix of the catalytic domain suitably formed hydrogen bonds with 4-OH and 6-OH groups of this D-glucosyl residue. NE1 of Trp231 on N-terminal part of the 2nd α-helix and NE2 of Gln279 on α3→α4 loop could form hydrogen bonds with 4-OH groups of the D-glucosyl residue. The 4- and 6-OH groups of trehalose was well overlapped with the hydroxy groups of the glycerol molecule bound to subsite -1 of the substrate-free structure of the wild type (Fig. 4-8B and C).

In subsite +1, all hydroxy groups of D-glucosyl residue are predicted to participate in the formation of hydrogen bonds: 2-OH, ND2 of Asn268 on α3→α4 loop; 3-OH, OD1 of Asn268 and NH2 of Arg277; 4-OH, NH2 of Arg344 and OE2 of Glu346 on α5→α6 loop; and 6-OH, Arg224 on α1→α2 loop and Glu595 on α11→α12 loop (Fig. 4-7, Fig. 4-8C). Arg224 interacted with Asp102 on the hood domain. Glu595 interacted with Arg344 as well as the substrate-free structure of the wild type. dNAtTRE1 substrate free structure and D380A-trehalose complex are designated as closed-form.

D380A was co-crystalized with Tre6*P*. Obtained crystal belonged to space group $P2_1$ with four monomers (Mol A–Mol D) in the asymmetric unit. The crystal structure was determined at 1.9 Å resolution (Table 4-1). Mol A was in contact with Mol B on the side surface on the 1st α-helix and 11th α-helix sides, and with Mol C on the side surface on the 5th α-helix side. Mol C and Mol D were in contact on the opposite side of the substrate binding site. No electron density of Tre6*P* was observed at the substrate binding site of all the monomers, but electron density which assigned to be glycerol molecules was observed in subsite -1 and +1 (Fig. 4-9C). Glycerol bound to subsite +1 was situated

at the position corresponding to C-2–C-4 of D-glucosyl residue of trehalose bound to dNAtTRE1 D380A. Interestingly, α1→α2 and α11→α12 loops of one monomer (Mol D) took a conformation considerably different from the others (Fig. 4-9C and D), which matched well with the substrate-free structure of wild type and trehalose complex structures of D380A. Because of the difference of structure of these loops, Mol D had slightly opened substrate binding site (this monomer and the others are designated as open-form and closed-form, respectively (Fig. 4-9D). Especially, the side chain of Arg224 on α1→α2 loop pointed in different directions. (Fig.4-9A–D). In closed-form, Arg224 could interact with 6-OH group of D-glucosyl residue at subsite +1 in the complex with trehalose (Fig. 4-9A and B). In open-form, Arg224 flipped away from the substrate binding site (Fig. 4-9C and D). In dNAtTRE1 D380A-trehalose complex, Arg224 could also form salt bridge with Asp102 on the hood domain. Because of this conformational change of Arg224, Asp102 of the open-form apparently did not form salt bridge with Arg224. The NH1 and CD of Arg224 in closed-form is thought to form π-cation and CH/π interaction to Tyr596 on α11→α12 loop, respectively (Fig. 4-9B). Glu595 and Tyr596 on α11→α12 loop in the open-form monomer are not located at the suitable position to form hydrogen bond with 6-OH group of D-glucosyl residue at subsite +1 and the general base catalyst Glu580, respectively. Tyr596 in both closed- and open-form is thought to form CH/π interaction to the CZ of Phe225 (Fig. 4-9B and D). In the interface of α1→α2 and α11→α12 loops, the side chain of Ser223 could interact with the nitrogen and oxygen of the main chain and the side chain (OG1) of Thr600 in the closed-form (Fig. 4-9B), while the nitrogen of the main chain amide and the oxygen of the side chain (OG) of Ser223 could interact with the oxygen and nitrogen of the main chain of Thr600, respectively, in the open form (Fig. 4-9D).

4.3.6. Site-directed mutagenesis at the residues on α1→α2 and α11→α12 loops of dNAtTRE1

The structural analysis of the open-form dNAtTRE1 suggested that conformational change of Asp102,

Arg224 and Glu595. Ala-substituted mutants of these resides, D102A, R224A, and E595A were expected to have open binding site and show the different substrate preference. The preference of these mutants for trehalose and Tre6*P* was compared with the wild type. These mutants showed much lower k_{cat}/K_m to trehalose than the wild type (Table 4-4). k_{cat}/K_m of R224A and E595A to Tre6*P* was similar to that of wild type and higher than that of the wild type, respectively. R224A and E595A showed a much higher preference for Tre6*P* than the wild type (Table 4-4). Unlike the wild type, which showed two peaks in the pH-k_{cat} curve for the hydrolysis of trehalose, these Ala-substituted mutants showed a single peak (Fig. 4-4H, I, and J).

In the interface of α1→α2 and α11→α12 loops, difference of hydrogen bond interactions between Ser223 and Thr600 were observed in the closed- and open-forms. To destabilize and stabilize the closed form, S223G and T600D mutations were introduced, respectively. S223G mutation is to disrupt the hydrogen bond between the side chain of Ser223 and Thr600 observed in the closed form. Asp600 could form an additional hydrogen bond with His579 on α11→α12 loop to stabilize the closed form (Fig. 4-9B). As expected, S223G and T600D showed higher and lower k_{cat}/K_m to Tre6*P* relative to trehalose than the wild type: the relative k_{cat}/K_m of S223G, T600D, and the wild type were 3.21%, 0.00195%, and 0.0208%, respectively (Table 4-4). In T600D, k_{cat}/K_m to trehalose was hardly affected by the mutation, but k_{cat}/K_m to Tre6*P* significantly decreased. These mutant enzymes showed almost single peak in the pH-k_{cat} curve (Fig. 4-4K and L).

4.4. Discussion

Trehalase is a key enzyme for the degradation of trehalose and is distributed to various kinds of living things. Compared with the bacterial and fungal trehalases, functional and structural characteristics of plant enzymes are much less investigated. In this study, the functions and structures of trehalase from *A. thaliana* is analyzed and compared with the enzymes from other origins.

The structure of AtTRE1 is compared with other trehalases (Fig. 4-7 and Fig. 4-10). The primary structure, AtTRE1, OsTRE1, pig trehalase, EcTre37A, PxEclTre and ScNth1 are compared (Fig. 4-7 and Fig. 4-10). AtTRE1 is less similar to ScNth1 than OsTRE1, pig trehalase, EcTre37A, and Px_EclTre. ScNth1 has a more extended region in N-terminus, α1→α2 loop, α6→α7 loop, α11→α12 loop than others. The amino acid residues which interact with trehalose in dNAtTRE1 D380A are well conserved in all trehalases except for Arg 344 and Glu595. In ScNth1, Arg344 corresponds Pro422 (Fig. 4-7). Unlike other trehalases, ScNth1 does not possess the conserved region of α11→α12 loop containing Glu595 (Gly-Gly-Gly-Gly-Glu-Tyr). In the three-dimensional structure, dNAtTRE1 consists of the hood domain and the catalytic domain of $(\alpha/\alpha)_6$-barrel. The hood domain of AtTRE1 is more similar to EcTre37A (Fig. 4-10A) (Gibson et al., 2007). The orientation of hood domain was different from that of ScNth1 (Fig. 4-10A) (Alblova et al., 2017). In ScNth1, the N-terminal domain and 1st α-helix do not match with other trehalases (Fig. 4-7), and the hood domain is inserted between α1→α2 loop. The N-terminal domain of ScNth1 interacts with 14-3-3 protein, which activates the trehalase (Alblova et al., 2017). The residues around substrate binding site are compared among AtTRE1, EcTre37A, and ScNth1. The amino acid residues which interact with trehalose in dNAtTRE1 D380A overlap well with EcTre37A (Fig. 4-10B). The Glu690 and Tyr691 on α11→α12 loop in ScNth1 could be superposed at the Glu595 and Tyr596 in AtTRE1, although it did not align in the primary structure (Fig. 4-7 and Fig. 4-10C). The Arg344 of AtTRE1 is not conserved in ScNth1, and Arg473 in ScNth1 overlapped well to Arg344 of AtTRE1 structurally (Fig. 4-10C). Amino acid residues that are thought to be involved in substrate binding are structurally overlapped with a few exceptions of Arg344 and Glu595 of AtTRE1. Judging from the other structures and amino acid conservation in primary structures of GH37 trehalases, the structural feature is thought to be basically the same in all trehalases.

Analysis of substrate specificity of dNAtTRE1 and OsTRE1 revealed that these enzymes are

highly specific to trehalose but acts slightly on trehalose-like disaccharides: Tre6*P*, Glcα1-1αXyl, Glcα1-1αGal, and Glcα1-4-L-Ara (Table 4-2, Fig. 4-5). The disaccharides are similar in structure as drawn in Fig. 4-5, even a reducing sugar, Glcα1-4-L-Ara α-anomeric configuration in the L-Ara moiety. Glucosidic bond of the compounds are cleaved by the trehalases as indicated in the ^{18}O-incorporration in the glucose released (Fig. 4-6). Therefore, D-glucosyl residues of the disaccharides are considered to be bound to the enzyme in the same manner in subsite -1. Although binding mode of Glcα1-1αGal was not analyzed, D-galactosyl residue is presumably less preferable for binding to subsite -1 than D-glucosyl residue. Based on the structure of dNAtTRE1 D380A-trehalose complex determined in this study (Fig. 4-8), the D-glucose moieties are well interacted with the protein residues not only in subsite -1, but also in subsite +1. Axial 4-OH of D-galactosyl residue is not likely suitable for the formation of hydrogen bond with Asp232 in subsite -1. Taken together, subsite -1 of dNAtTRE1 is thought to be specific to D-glucosyl residue. In EcTre37A, Asp160 (corresponding to Asp232 in AtTRE1) is predicted to make the hydrogen bond network together with 6-OH of trehalose, the catalytic water, Glu496 (general base, Glu580 in AtTRE1) and Tyr512 (Tyr596 in AtTRE1) at subsite -1 (Fig. 4-8 C and Fig. 4-9E) (Gibson et al., 2007). The residues in subsite -1 are conserved well throughout GH37 enzymes, and thus high specificity to D-glucosyl residue in subsite -1 is presumably common feature. In subsite +1, two residues Asn268 and Arg277 are involved in hydrogen bond formation with 2-OH and 3-OH (Fig. 4-8C), as observed in other trehalases (Adhav et al., 2019; Alblova et al., 2017; Gibson et al., 2007). 4-OH has interactions with the same Arg and other two residues (Arg344 and Glu346). 6-OH interacts with Arg224 and Glu595. Substrate specificity of dNAtTRE1 and OsTRE1 is exerted through the interaction of these residues. Unlike subsite -1, subsite +1 of dNAtTRE1 is capable of accepting sugar residues other than D-glucosyl residue. Based on the structures of tested disaccharides, at least, hydrogen bonding interactions involving 4- and 6-OH groups of D-glucosyl residue at subsite +1 are not essential for the

catalysis. The increase of ΔG values ($\Delta\Delta$G) calculated from k_{cat}/K_m values for Glcα1-1αGal and Glcα1-1αXyl in a comparison with trehalose were 8.1 kJ/mol and 9.4 kJ/mol at pH 3.7, respectively; and 6.6 kJ/mol and 7.8 kJ/mol at pH 6.9, respectively. $\Delta\Delta$G for the removal of neutral and charged hydrogen bond donor or acceptor is estimated to be 2–6 kJ/mol and approximately 12 kJ/mol, respectively (Fersht et al., 1985), so these $\Delta\Delta$G values are equivalent to loss of one or two neutral hydrogen bonds. The structure of dNAtTRE1 D380A in complex with trehalose suggests that 4-OH of D-glucosyl residue of trehalose bound to subsite +1 forms hydrogen bond with Arg344 and Glu346, and 6-OH of this sugar residue with Arg224 and Glu595 (Fig. 4-8C). These residues presumably provide neutral hydrogen bond interaction with the D-glucosyl residue in subsite +1.

AtTRE1 had two catalytic states that differed depending on pH. In the analysis of pH dependency for the hydrolysis of trehalose by dNAtTRE1, the pH-k_{cat} curve of this enzyme had two peaks at pH 3.7 and 6.9, while pH-k_{cat}/K_m curve of dNAtTRE1 had a single peak at pH 4.5 (Fig. 4-4 A and B). This result indicates two different ES complexes depending on pH conditions: ES_{acid} with lower pK_{es1} and pK_{es2} and $ES_{neutral}$ with higher pK_{es1} and pK_{es2}. In the reaction with Tre6*P*, dNAtTRE1 showed pH-k_{cat} curve with a single peak at pH 3.9. ES_{acid} could hydrolyzed Tre6*P*. Although a divalent negative charge of Tre6*P* at pH 6.9 might be one reason why AtTRE1 showed low activity to Tre6*P* in $ES_{neutral}$ (the pK_a of Tre6*P* is expected to be around 6–7 based on that of Glc6*P* in various conditions (Cowan, 1991; Koban et al., 2004)), in ES_{acid}, the subsite is required to have more space than for binding to D-glucosyl residue to bind to 6-phospho-D-glucosyl residue in subsite +1. Structural analysis of AtTRE1 D380A crystallized in the presence of Tre6*P* showed that this enzyme could take two structures with largely different conformations of α1→α2 and α11→α12 loops and the hood domain: open-form and closed-form (Fig. 4-9). In the substrate-free structure of the wild type (closed-form), the substrate binding site matched well to the D380A-trehalose complex (Fig. 4-8B and C). Glu595 on the α11→α12 loop interacted with Arg344. Tyr596 on the α11→α12 loop interacted with

Asp380 and inorganic phosphate *via* a water molecule. This hydrogen-bond network would account for the fact that the AtTRE1 wild type showed closed-form even in the absence of trehalose in the substrate binding site. This prediction is consistent with the results that the activity of AtTRE1 decreased in the presence of inorganic phosphate and glycerol. Besides, Tyr 596 also interacted with Arg224 and Glu580 (base). However, the interaction between Glu580 (base) and Tyr596 disappeared in open-form (Fig. 4-9). This interaction would change the dissociation state of the catalytic base. ES_{acid} with lower pK_{es1} and pK_{es2} might be formed by the disturbance of the interaction of Glu580 (base) and Tyr596 in open-form.

The open-form is judged to be preferable to act on Tre6*P*. In the closed-form, Arg224 and Glu595 probably cause steric hindrance upon binding to 6-phospho-glucosyl residue of Tre6*P*, and the closed-form enzyme should be inactive against Tre6*P*. In open-form, Arg224 and Glu595 were located apart from the substrate binding site to open the space for a bulky chemical group at the C-6 position. Analysis of the mutant enzyme revealed that AtTRE1 preferred Tre6*P* when it had an open substrate binding site. Based on the known structure (Adhav et al., 2019; Gibson et al., 2007) and D380A-trehalose complex (Fig. 4-8C), the closed-type substrate binding site was formed by α1→α2 and α11→α12 loops. The interaction between Arg224 and Tyr596 is required for the α1→α2 loop to close. The interaction between Arg344 and Glu595 is required for the α11→α12 loops to close. Substitution of these residues with Ala significantly enhanced preference for Tre6*P* (Table 4-4). R224A lost the interaction between Arg224 and Tyr596, and E595A lost it between Arg344 and Glu595. Therefore, these mutants could not close these two loops and are expected to have an open substrate binding site. ES_{acid} is judged to take a structure favorable for binding to Tre6*P* and have an open and wider substrate binding site similar to the open-form.

Comparison of the structures of open- and closed-form dNAtTRE1 indicates that the pair of atoms forming hydrogen bond between Ser223 and Thr600 was different (Fig. 4-9B, D, and E). Since

S223G mutation enhanced the preference for Tre6*P*, S223G is thought to form more open-form than the wild type. The side chain of Ser223 is presumably important for the stabilization of the closed-form. On the other hand, introduction of Asp to the position of Thr600 reduced the preference for the Tre6*P* without loss of activity to trehalose. As Asp at the Thr600 position could form additional hydrogen bond with His579 on the same loop to stabilize the closed-form, T600D presumably predominantly form the closed-form, which is not suitable for the reaction with Tre6*P*. The fact that these mutant enzymes showed almost single peak in the pH-k_{cat} curve (Fig. 4-4K and L) supports the interpretation that these mutant enzymes predominantly form only one ES complex. The switch of the interaction between Ser223 and Thr600 might be important for the interconversion of the closed-form and open-form. For the reasons above, it was suggested that a closed structure unsuitable for Tre6*P* was formed at the neutral pH, and α1→α2 and α11→α12 loops structurally changed to form an open and wider substrate binding site that could allow the phosphoryl group of Tre6*P* at the acidic pH.

Comparison of 380 sequences of trehalases from various organisms showed that Ser223 and Thr600 are conserved well only in plant trehalases (Fig. 4-9F), containing AtTRE1 and OsTRE1 which showed Tre6*P*-hydrolyzing activity. These plant enzymes might also be able to take the open-form to act on Tre6*P* as dNAtTRE1. The lack of activity of the bacterial and animal trehalases to Tre6*P* might be due to the lack of these residues to take the open form.

Table 4-1. Summary of crystallization conditions, data collection, and refinement statistics.

		dNAtTRE1	D380A-trehalose	D380A-Tre6P
PDBID		7E9U	7EAW	7E9X
Data collection	Beam line	BL-41XU at SPring-8	BL-41XU at SPring-8	BL-5A at Photon Factory
	Space group	P 21 21 21	P 21 21 21	P 1 21 1
	Unit cell parameters a, b, c (Å), α, β, γ, (˚)	54.981 129.813 155.802 90 90 90	52.671 104.507 237.842 90 90 90	54.657 129.647 151.141 90 91.027 90
	Wavelength	1.0	1.0	1.0
	Resolution range	48.22–2.1 (2.175–2.1)	48.16–1.8 (1.864–1.8)	41.55–1.881 (1.949–1.881)
	Total reflections	488469 (76850)	1196340 (196415)	1158019 (169902)
	Unique reflections	125588 (6482)	122983 (19210)	169902 (27135)
	Completeness (%)	99.6 (98.6)	98.7 (96.4)	99.8 (99.1)
	Redundancy	3.9 (3.8)	9.7 (10.2)	6.82 (6.72)
	Mean I/sigma(I)	12.33 (1.50)	14.45 (3.87)	14.34 (1.96)
	R-meas (%)[a]	7.5 (85.7)	13.9 (68.9)	9.0 (91.7)
	CC1/2	99.9 (85.9)	99.5 (92.4)	99.9 (83.8)
Refinement				
	Reflections used in refinement	65799 (6447)	121493 (11893)	169813 (16726)
	Reflections used for R-free	1990 (196)	2000 (196)	1998 (195)
	R-work[b]	0.2090 (0.3108)	0.2280 (0.2508)	0.1932 (0.3100)
	R-free[c]	0.2580 (0.3578)	0.2581 (0.2843)	0.2450 (0.3679)
	Number of non-hydrogen atoms	8936	9842	18502
	macromolecules	8655	8937	17496
	ligands	30	64	48
	solvent	251	841	958
	Protein residues	1079	1116	2187
	RMS(bonds)	0.008	0.008	0.008
	RMS(angles)	1.19	1.29	1.16
	Ramachandran favored (%)	95.96	97.11	96.71
	Ramachandran allowed (%)	3.95	2.71	3.10
	Ramachandran outliers (%)	0.09	0.18	0.19
	Rotamer outliers (%)	0.21	0.51	0.16
	Clashscore	6.89	3.89	3.32
	Average B-factor	51.20	25.21	35.37
	macromolecules	51.29	24.72	35.30
	ligands	47.68	22.89	34.94
	solvent	48.34	30.59	36.63

Values in parentheses are for the highest resolution shell. [a] R-meas = Σ_{hkl} $\{N(hkl)/[N(hkl) - 1]\}^{1/2}$ $\Sigma_i|_i(hkl)$ - <I(hkl)>|/Σ_{hkl} $\Sigma iIi(hkl)$, where <$I(hkl)$> and $N(hkl)$ are the mean intensity of a set of equivalent reflections and the multiplicity respectively. [b] R-work = Σ_{hkl} ||Fobs| - |F_{calc}||/Σ_{hkl}|F_{obs}|. [c] R-free was calculated for a5% randomly selected test sets that were not used in the refinement.

Table 4-2. Kinetic parameters of plant trehalases to various oligosaccharides.

	AtTRE1 (pH 3.7)				AtTRE1 (pH 6.9)				OsTRE1			
	k_{cat}	K_m	k_{cat}/K_m		k_{cat}	K_m	k_{cat}/K_m		k_{cat}	K_m	k_{cat}/K_m	
	s^{-1}	mM	$s^{-1}mM^{-1}$	%	s^{-1}	mM	$s^{-1}mM^{-1}$	%	s^{-1}	mM	$s^{-1}mM^{-1}$	%
Trehalose	274 ± 3	2.44 ± 0.06	112	100	134 ± 1	1.08 ± 0.05	127	100	352 ± 6	0.459 ± 0.009	767	100
Tre6*P*	1.27 ± 0.032	15.4 ± 0.443	0.0825	0.073	N.D.	N.D.	0.00385	0.003	1.00 ± 0.02	4.22 ± 0.31	0.237	0.031
Glcα1-4-L-Ara	11.7 ± 0.1	2.49 ± 0.327	4.70	4.17	21.3 ± 0.2	1.15 ± 0.10	18.5	15.1	45.2 ± 1.2	1.28 ± 0.12	35.3	4.6
Glcα1-1αGal	126 ± 10	26.4 ± 2.5	4.77	4.23	147 ± 6	14.7 ± 1.2	10.0	8.11	201 ± 14	4.91 ± 0.77	40.9	5.4
Glcα1-1αXyl	27.6 ± 0.3	9.42 ± 0.24	2.93	2.6	13.8 ± 0.4	2.24 ± 0.22	6.16	4.98	N.A.	N.A.	N.A.	N.A.

N.D., not determined. N.A., not analyzed. The data are presented as the means of triplicate experiments with standard deviations.

Table 4-3 The reaction velocity of various trehalases to 10 mM substrates at pH 5.0 at 37°C.

	Trehalose μmol/min/mg	Tre6*P* μmol/min/mg	Tre6*P*/Trehalose %
dNAtTRE1	110	0.303	0.275
EcTre37A	412	0.0285	0.00692
pig trehalase*	1.07	$<1.7\times10^{-4}$	<0.0159

* at pH 5.5

Table 4-4 Kinetic parameters of dNAtTRE1 wild type, dNAtTRE1 mutants, and OsTRE1 to trehalose and Tre6*P*.

Enzyme	Trehalose			Tre6*P*			k_{cat}/K_m ratio of Tre6*P*/Trehalose
	k_{cat}	K_m	k_{cat}/K_m	k_{cat}	K_m	k_{cat}/K_m	
	s^{-1}	mM	s^{-1} mM^{-1}	s^{-1}	mM	s^{-1} mM^{-1}	%
Wild type	110 ± 13.5	0.338 ± 0.008	325 ± 43.8	0.630 ± 0.053	9.31 ± 0.55	0.0675 ± 0.0016	0.0208
D102A	5.32 ± 0.23	3.18 ± 0.42	1.69 ± 0.15	0.0092 ± 0.0004	21.2 ± 2.1	0.00044 ± 0.00003	0.0260
S223G	15.5 ± 1.3	2.77 ± 0.41	5.67 ± 0.54	1.48 ± 0.15	8.17 ± 1.14	0.182 ± 0.007	3.21
R224A	0.674 ± 0.023	4.07 ± 0.24	0.166 ± 0.004	0.094 ± 0.000	1.78 ± 0.02	0.0526 ± 0.0006	31.7
E595A	1.23 ± 0.05	1.23 ± 0.16	1.01 ± 0.11	0.750 ± 0.077	3.72 ± 0.97	0.201 ± 0.079	20
T600D	286 ± 8	0.719 ± 0.008	398 ± 8	0.429 ± 0.008	11.9 ± 0.5	0.00775 ± 0.0001	0.00195
OsTRE1	352 ± 6	0.459 ± 0.009	767 ± 6	1.00 ± 0.02	4.22 ± 0.309	0.240 ± 0.012	0.0313

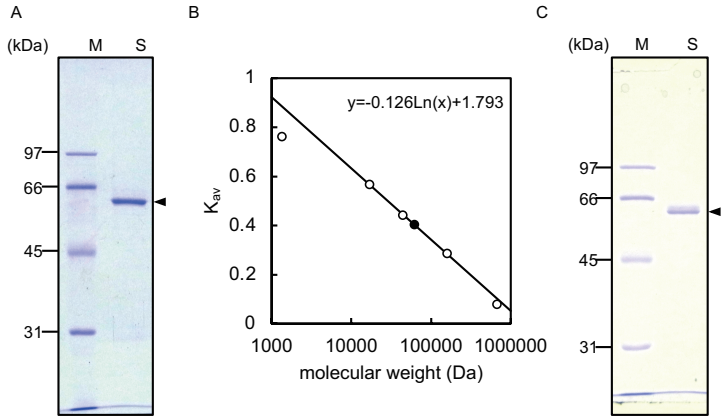

Fig. 4-1. SDS-PAGE analysis of purified recombinant trehalases.

One microgram of purified dNAtTRE1 (A) and OsTRE1 (C) was analyzed by SDS-PAGE. Estimated molecular mass of dNAtTRE1 and OsTRE1 indicated by an arrow is 63 kDa and 62 kDa, respectively. Panel B showed the gel-filtration column chromatography (Superdex200 10/300 GL, 1.0 cm i.d.×30 cm, 24 mL) of marker proteins [Thyroglobulin (bovine), 670 kDa, 9.3 mL; γ-globulin (bovine), 158 kDa, 12.6 mL; Ovalbumin, 44 kDa, 15.1 mL; Myoglobin (horse), 17 kDa, 17.1 mL; Vitamin B12, 1.4 kDa, 20.2 mL] and dNAtTRE1 (398 μg). Void volume was 8.0 mL. K_{av} = (Elution volume – Void volume)/(24-Void volume).

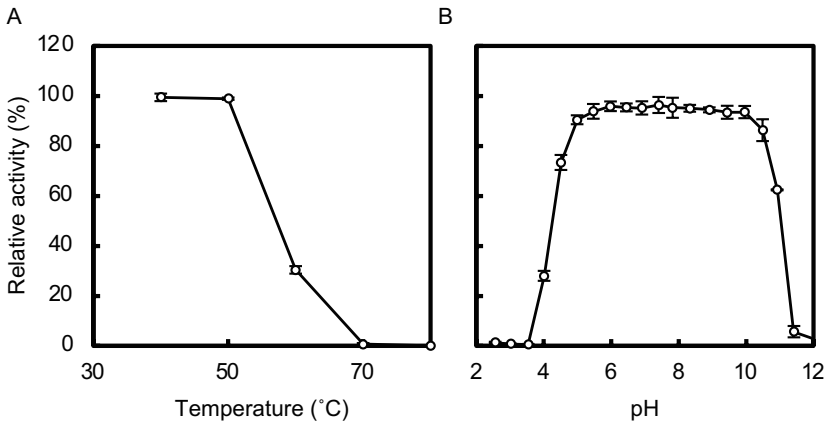

Fig. 4-2 Temperature stability and pH stability of dNAtTRE1.

Panel A showed residual activities were measured after the incubation at indicated temperatures at pH 6.5 for 15 min. Panel B showed pH stability at 4°C using Briton-Robinson buffer (pH 2.5–12). Residual activities after incubation at various pH at 4°C for 24 h are shown. Data and error bar are means and standard deviation of triplicate experiments, respectively.

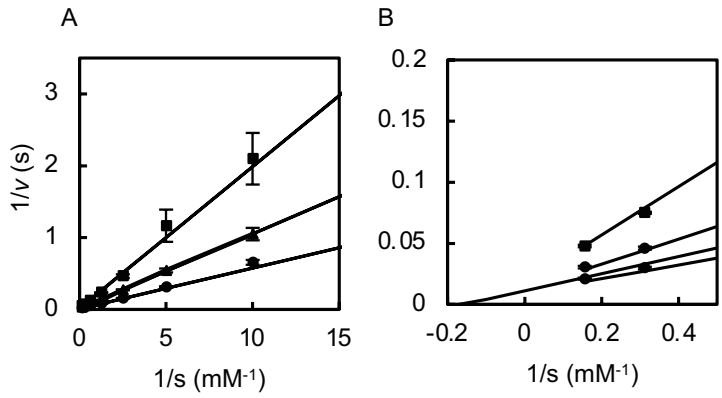

Fig. 4-3. 1/s-1/*v* plots for the inhibition of dNAtTRE1 by Tris with varying trehalose concentrations.

The velocity of dNAtTRE1 in the presence of 5, 10, and 20 mM Tris was analyzed. (A) 1/s-1/*v* plots are shown, and (B) is the enlarged view of (A). Filled circles, filled triangles, and filled squares show velocities with 5, 10, and 20 mM Tris, respectively. The kinetic constants derived from these lines are k_{cat}=143 ± 2 s^{-1}, K_s = 1.39 ± 0.03 mM, K'_s = 19.1 ± 7.1 mM, K_i=1.03 ± 0.09 mM, and K'_i=13.8 ± 4.1 mM. Data are means of triplicate experiments with standard deviations in three independent reactions.

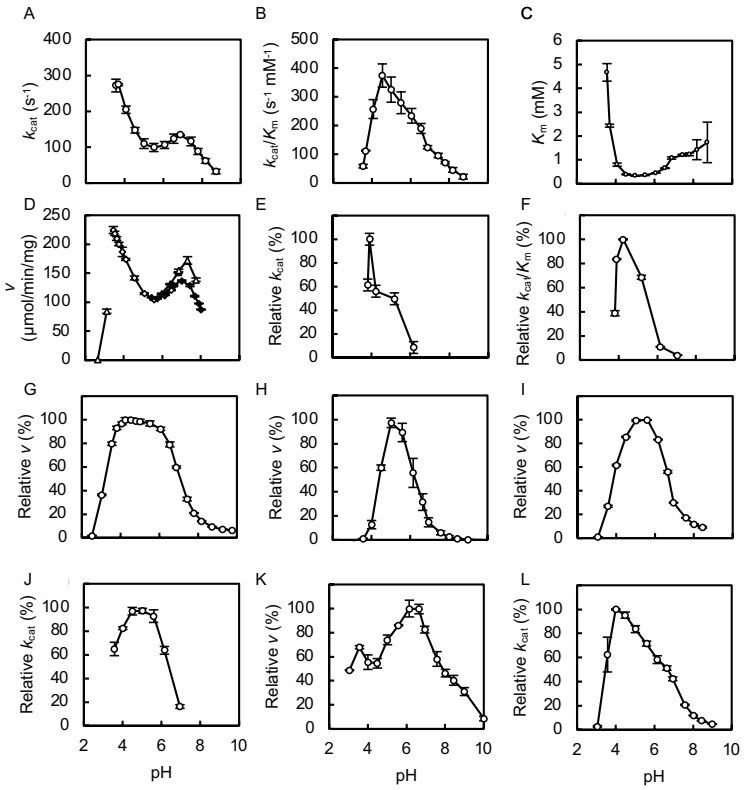

Fig. 4-4. pH-dependency of kinetic parameters of dNAtTRE1.

Panels A–C showed pH-k_{cat}, pH-k_{cat}/K_m and pH-K_m curves for the hydrolysis of trehalose by wild-type dNAtTRE1, respectively. D, pH activity curve of wild-type dNAtTRE1 using each buffer below. Open triangle, glycine-HCl buffer (pH 2.7–3.1); open diamond, sodium acetate buffer (pH 3.5–6.1); filled diamond, MES-NaOH buffer (pH 6.0–6.8); open triangle, HEPES-NaOH buffer (pH 6.9–7.8). filled triangle, sodium phosphate buffer (pH 5.4–8.0). E, and F, pH-k_{cat} and pH-k_{cat}/K_m curves for the hydrolysis of Tre6*P* by dNAtTRE1 respectively. G, pH-*v* curves for the hydrolysis of trehalose by OsTRE1. Panels H–L show relative pH-k_{cat} curves of D102A (H), R224A (I), E595A (J), S223G (K), and T600D (L). In panel G, H, I, and K, the reaction velocity to 10 mM trehalose at 37°C was regarded as k_{cat} because this substrate concentration is fully higher than the K_m value for trehalose. Data and error bar are means and standard deviation of triplicate experiments, respectively.

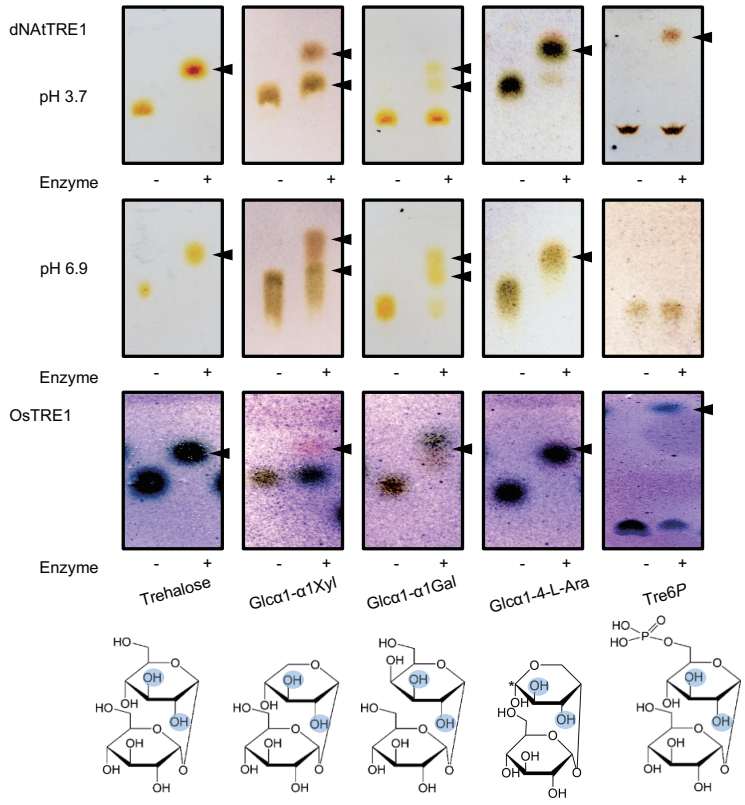

Fig. 4-5. TLC analysis of hydrolysis reaction catalyzed by dNAtTRE1 and OsTRE1.

To assess the hydrolytic activity of dNAtTRE1 and OsTRE1, these enzymes were incubated with 10 mM each substrate in 100 mM Briton-Robinson buffer (pH 3.6 and pH 6.9) for dNAtTRE1 or 100 mM sodium acetate buffer (pH 4.5) for OsTRE1 at 37°C for 24 h. The reactions were performed with (plus) or without (minus) the enzyme. Arrow heads indicate the reaction products. Chemical structures of the substrates used are shown below the figures. Glcα1-4-L-Ara is drawn here with an asterisk showing anomeric C-1 of L-Ara moiety. For the analysis of the reaction products from trehalose, Glcα1-1αXyl, and Glcα1-1αGal, 2-propanol: 1-butanol: water = 2: 2: 1 (v/v/v) was used as developing solvent; for the reaction product from Glcα1-4-L-Ara, isopropanol: acetone: 0.1 M lactic acid = 4: 4: 2 (v/v/v) was used; and for the products from the other substrates, acetonitrile: ethyl acetate: 1-propanol: water = 85: 20: 50: 60 (v/v/v/v) was used.

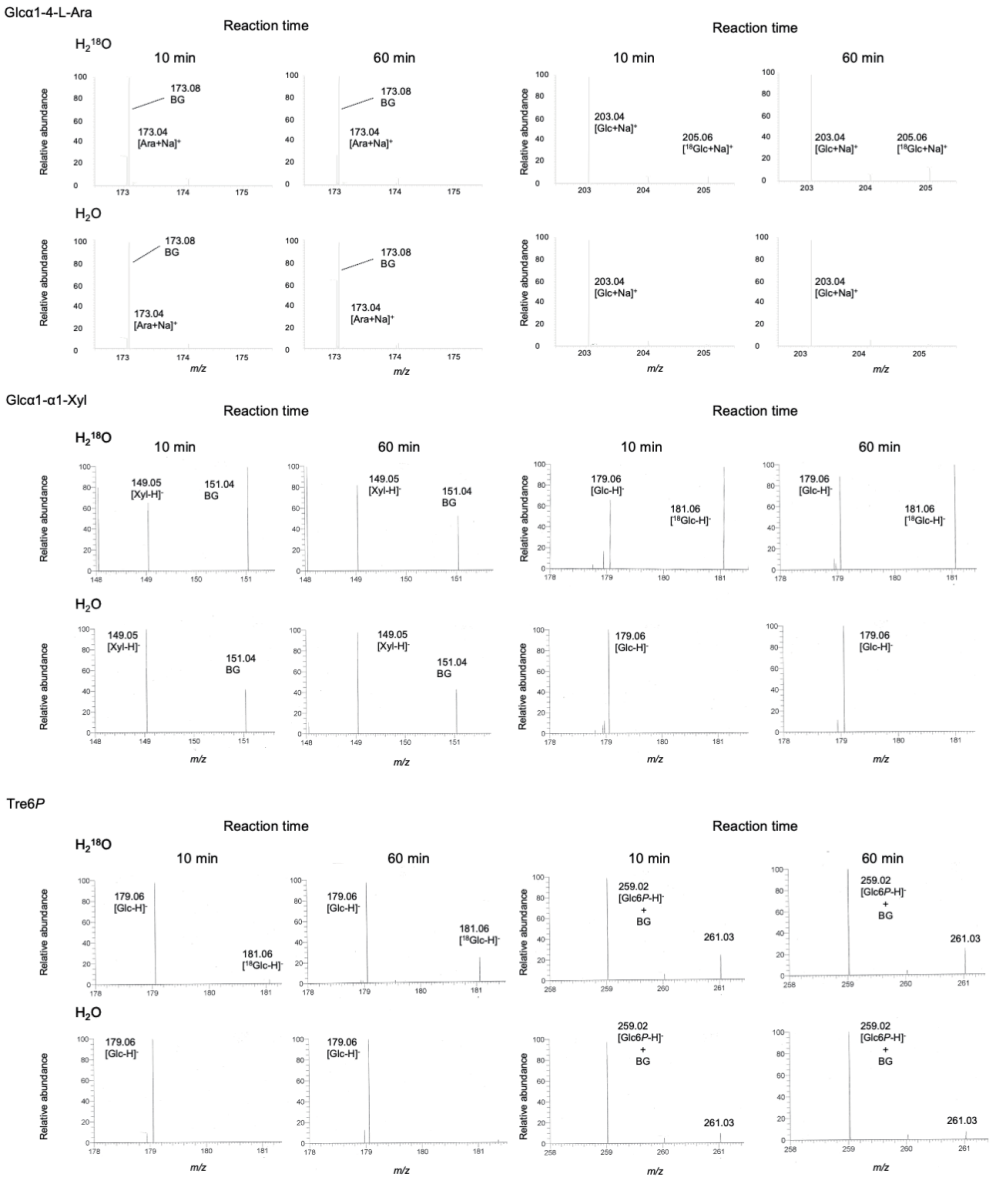

Fig. 4-6. Mass spectra of the hydrolytic reaction products in H_2O and $H_2{}^{18}O$.

dNAtTRE1 was incubated with 10 mM each substrate in the presence or absence of $H_2{}^{18}O$. The mass spectra of the produced monosaccharides are shown.

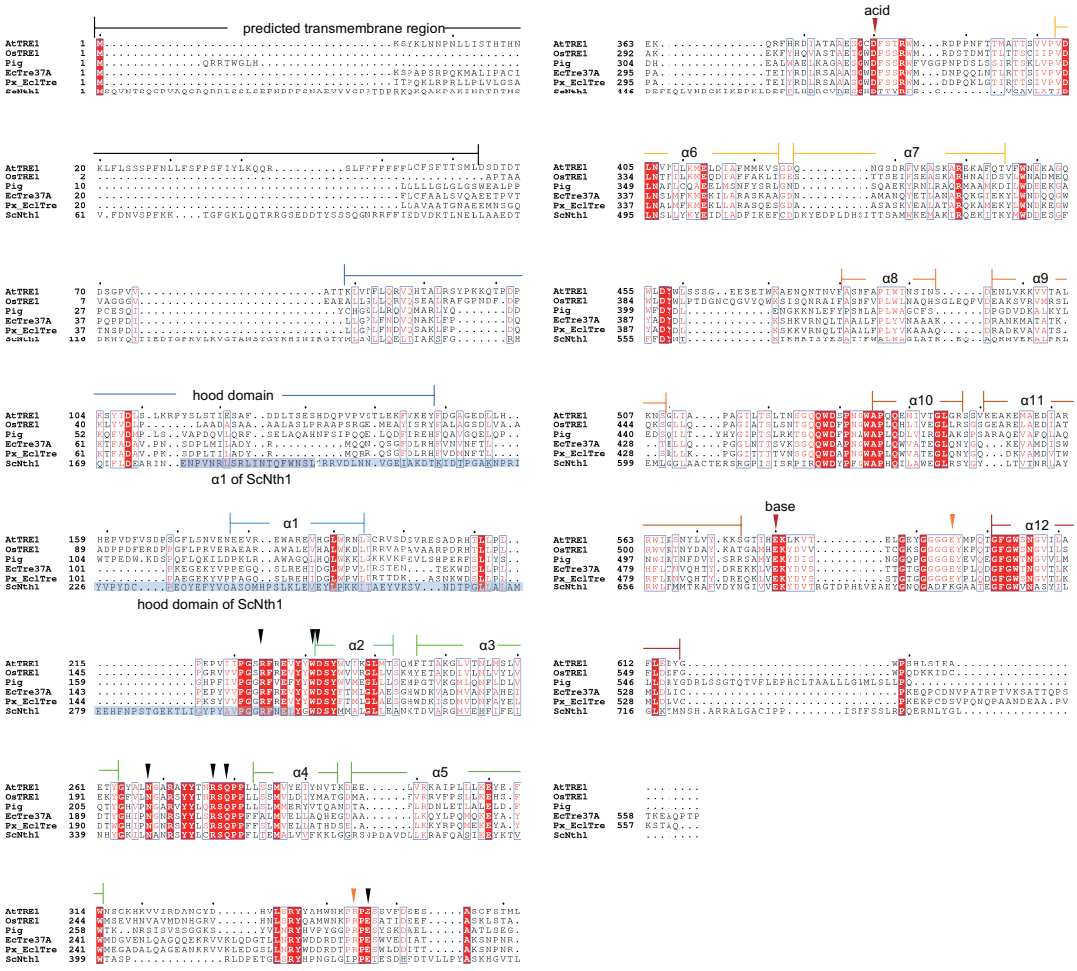

Fig. 4-7 Alignment of primary structure of trehalases

Multiple alignment of the amino acid sequences of AtTRE1, OsTRE1, pig trehalase, EcTre37A, Px_EclTre, and ScNth1 was made by MAFFT v7 with automatic method (Katoh et al., 2019). Secondary structure of AtTRE1 is shown on the top of sequences. Based on the known structure (Gibson et al., 2007), residues responsible for the catalysis and substrate-binding are shown by inverted arrowheads (red: catalytic residues, black: substrate binding, orange: substrate binding, but not conserved in all trehalase). The sequence of 1st α-helix and hood domain of ScNth1 are shaded.

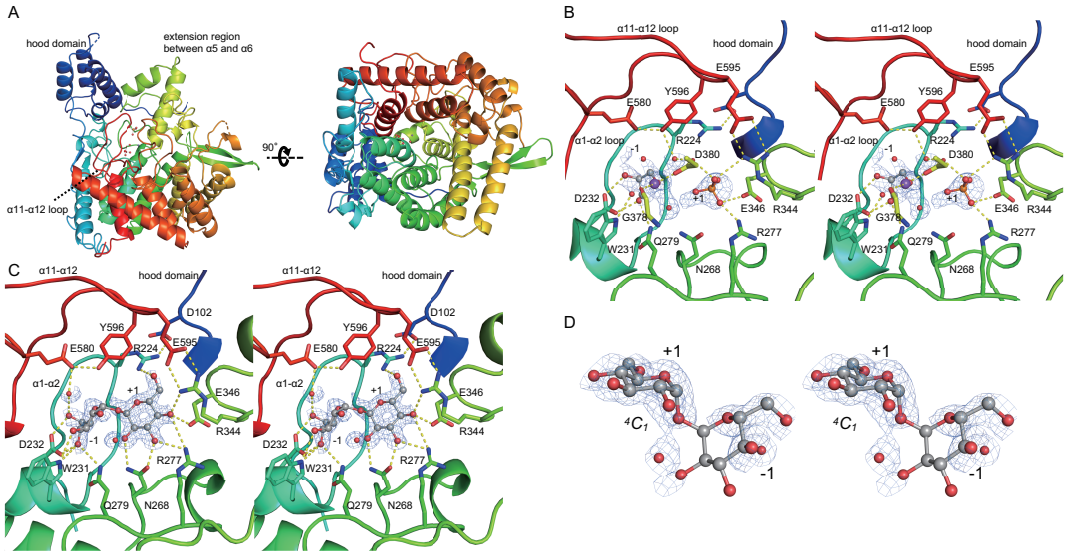

Fig. 4-8. Structure of the dNAtTRE1 apo and dNAtTRE1 D380A with trehalose complex.

A, Two views of the structure of the dNAtTRE1 substrate-free structure. The structure is shown as cartoons and colored rainbow (N: blue-C: red). B, Stereo view of dNAtTRE1 substrate-free structure (wall-eyed stereo). A F_o-F_c electron density map of the bound glycerol, inorganic phosphate, and sodium ion (purple sphere) are shown in light blue mesh at 3.5 σ. Predicted hydrogen bonds are indicated by dashed lines. C, the structure of D380A in complex with trehalose (wall-eyed stereo). A F_o-F_c electron density map of the bound trehalose is shown in light blue mesh at 3.5 σ. Trehalose is shown as ball and stick representation. D, Enlarged view of the trehalose (gray) in dNAtTRE1.

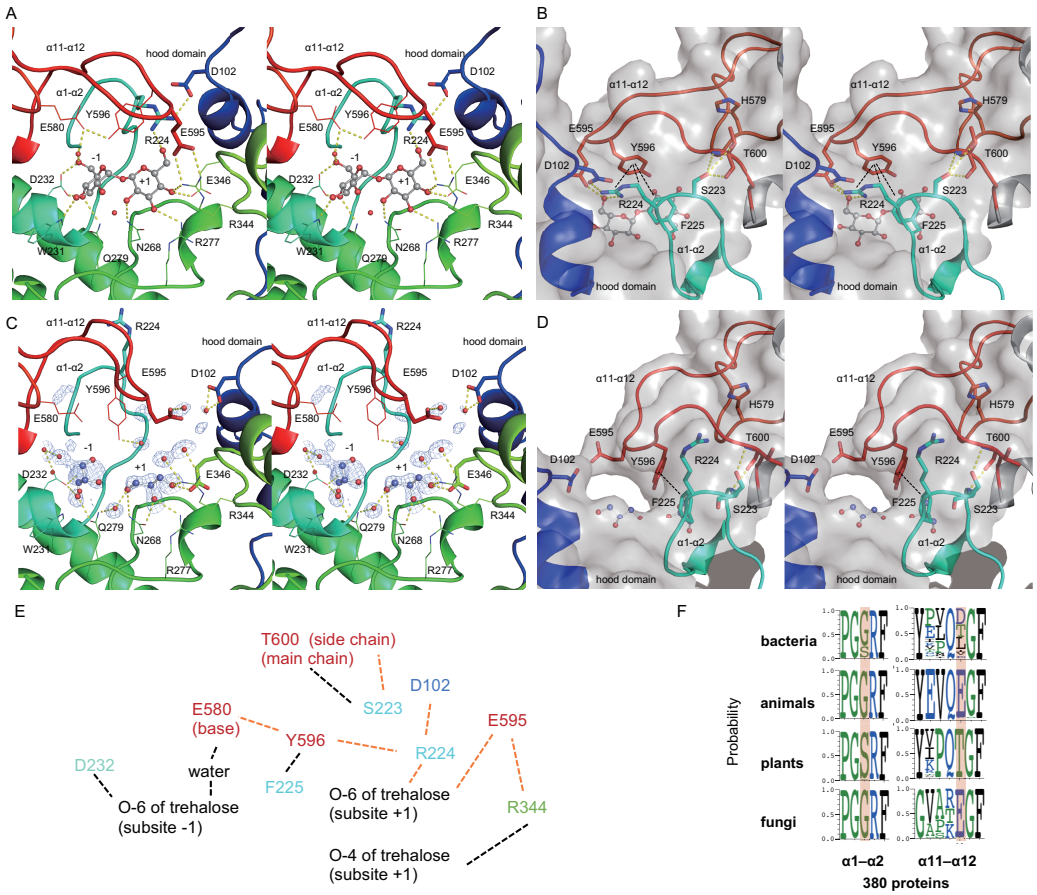

Fig. 4-9. Structures of distorted D380A.

Structures of dNAtTRE1 D380A in closed- (A and B) and open-(C and D) forms are shown. Panels A and C show the close-up view of the substrate binding site of closed- and open-forms, respectively. Trehalose bound to the closed-form is superimposed to the open-form. Panels B and D show surface models of closed- and open-forms, respectively. Glycerol molecules bound to the open-form are shown in purple. A F_o-F_c electron density map of the bound glycerol is shown in light blue mesh at 3.0 σ. Panel E showed the schematic drawing of substrate binding. The colors of letters are corresponding to the structure colored rainbow (N: blue-C: red) as Fig. 4-7. Dashed line shows the interaction. Orange lines show the interaction thought to be disappeared in open-form. Panel F showed Web logo analysis of trehalases of various organisms. The conserved amino acid residues on α1→α2 loop and α11→α12 loop in 380 sequences of trehalases were shown. The residues corresponding to Ser223 and Thr600 of AtTRE1 are shown in red shade. Web logo was generated using WebLogo 3 (Crooks et al., 2004).

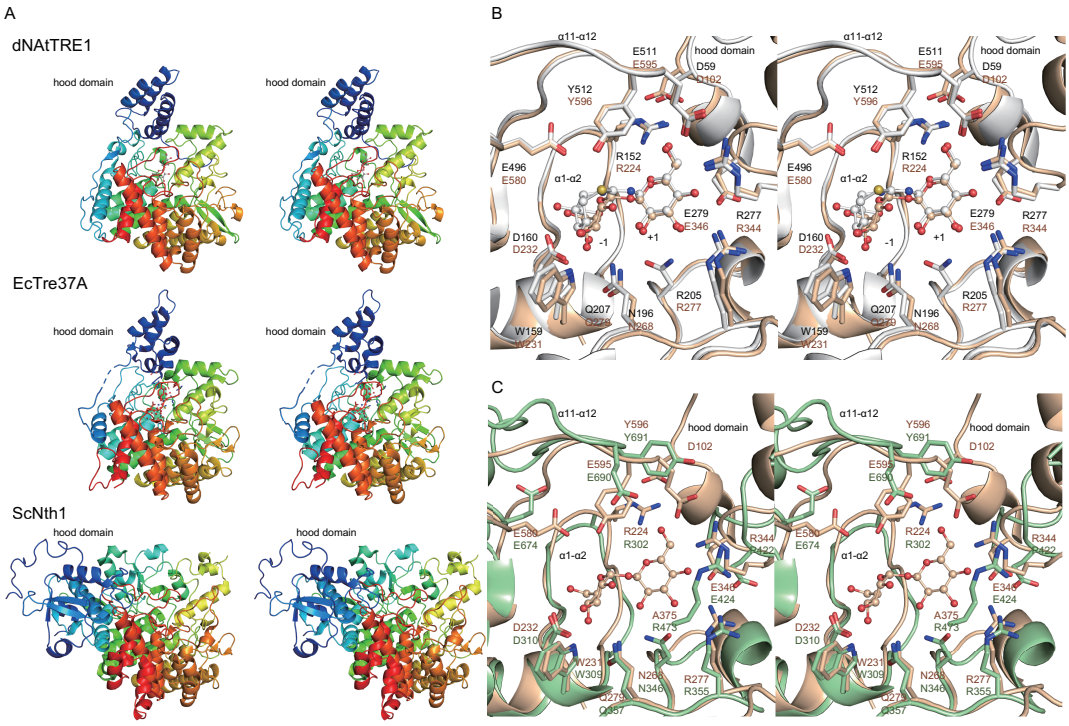

Fig 4-10 Comparison of three-dimensional structure of trehalases.

Stereo view of dNAtTRE1, EcTre37A (PDB entry: 2JG0) (Gibson et al., 2007), ScNth1 (5N6N) (Alblova et al., 2017). Panel A showed whole structures of trehalases (N: blue-C: red). Panel B showed the superposed view of the substrate binding site of dNAtTRE1 (brown) and EcTre37A (white). Panel C showed the superposed view of the substrate binding site of dNAtTRE1 (brown) and ScNth1 (green).

5. General discussion

In plants, Tre6*P* and trehalose levels are controlled by TPS, TPP, and trehalase. In contrast to prokaryotes, which have various metabolic pathways for trehalose synthesis and degradation, eukaryotes generally have only the TPS-TPP pathway for the synthesis and the trehalase pathway for the degradation (Avonce et al., 2006). Especially in plants, the endogenous amount of Tre6*P* and trehalose is small, but small changes of these levels have a great impact on growth, development, and stress response (Van Dijken et al., 2004; Griffiths et al., 2016; Wahl et al., 2013; Yadav et al., 2014). In other words, the TPS-TPP pathway and trehalase pathway are responsible for regulation various physiological states of plants. Numerous number of isozymes for the trehalose synthesis in higher plants are thought to regulate the level of trehalose related sugars (Lunn et al., 2014). This interpretation explain various phenotypic changes observed in overexpressors and gene-deficient mutants of TPS, TPP, and trehalase (Eastmond et al., 2002; Van Houtte et al., 2013; Krasensky et al., 2014; Lin et al., 2019, 2020; Tian et al., 2019; Wang et al., 2020). Despite the physiological importance of the trehalose-related enzymes, their enzymatic functions and structures have been scarcely understood thus far. For precise functional and structural analysis of the enzymes, Tre6*P* and its derivatives are required abundantly.

In this study, the availability of trehalose-related saccharides Tre6*P* and some trehalose analogues, which has been a bottleneck in the analysis of trehalose-metabolizing enzymes, was improved by establishing an efficient synthesis of the compounds using phosphorylase and other enzymes. Using synthesized trehalose analogs such as Glcα1-1αMan6*P* and Glcα1-1αGal the plant trehalose metabolizing enzymes were characterized comprehensively. In the synthesis of Tre6*P*, synthesis of trehalose analogs using TPS has been difficult, because the TPS shows high substrate specificity and uses nucleotide sugar which is difficult to use in large amount as sugar doner. In contrast to TPS reaction, the utilization of reverse phosphorolysis catalyzed by prokaryotic

phosphorylases enabled the synthesis of trehalose-related oligosaccharides from abundant sugars. In chapters 2 and 4, various trehalose analogs have been synthesized by utilizing TrePP, TP and MP. Using Glcα1-1αMan6*P*, an analog of Tre6*P*, TPP was shown to be specific to disaccharide phosphates with an α1-1α linkage (D-glucosyl residue was important for catalysis), and the importance of 2-OH group of D-glucosyl residues of Tre6*P* for the catalysis was evaluated (Fig. 3-6). For trehalase, substrate recognition mechanisms in subsites -1 and +1 was discussed separately by using Glcα1-1αXyl, Glcα1-1αGal, Glcα1-4-L-Ara, and Tre6*P*, although contribution of these subsites for the reaction with trehalose was unclear. Besides, kinetic analysis of the reactions with Glcα1-1αXyl, Glcα1-1αGal, Glcα1-4-L-Ara, and Tre6*P* has emphasized the existence of the two states of complex of AtTRE1 with substrate. Increasing the variety of compounds may allow for a more detailed functional analysis of the enzyme. Another Tre6*P* analog, Glcα1-1αGal6*P* could also be synthesized through the reverse phosphorolysis of LlTrePP, although reaction velocity for the reverse phosphorolysis with Gal6*P* was very low. It may be challenging, but isotopically labeled Tre6*P*, which would be helpful for tracing metabolites, might be produced by using ^{13}C-labeled maltose and ^{32}P-labeled inorganic phosphate, for instance, as substrates.

Another difficulty in studying plant trehalose metabolism is arisen from the difficulty to determine whether Tre6*P* or trehalose causes phenotypic changes in various mutants. In most papers, the phenotypic changes caused by change of trehalose-related compounds are discussed based on the change of the expression level of the genes encoding TPS, TPP, and trehalase. However, the relationship between the endogenous amount of trehalose-related compounds and the expression level of the genes encoding the trehalose metabolizing enzymes is ambiguous, because enzymatic function of these enzymes was unclear. In this study, the enzymatic characteristics of ten AtTPPs and AtTRE1 were revealed. Degree of Tre6*P* synthesis, trehalose synthesis, and trehalose degradation could be evaluated using the expression levels and activities of AtTPS1, AtTPPs, and AtTRE1 as indicators.

The k_{cat}/K_m values were used as an indicator of activity to low-concentration substrates, because the physiological concentrations of both Tre6*P* and trehalose are small in plants. Since AtTPS1 is thought to be the major TPS responsible for Tre6*P* synthesis (Delorge et al., 2015; Eastmond et al., 2002; Fichtner et al., 2020), tps score is made based on only *AtTPS1* expression level, although *A. thaliana* has multiple TPS isozymes (Eq. 5-1). Transcript abundance of *AtTPS1*, *AtTPPs*, and *AtTRE1* in various tissues and developmental stages based on Affymetrix ATH1 array data from Schmid *et al*. (Schmid et al., 2005) were extracted from the ePlant database (bar.utoronto.ca/eplant). The arbitrary score obtained by multiplying the expression level by k_{cat}/K_m of each TPP and AtTRE1 is set as tpp score (tpp score is the sum of the values for AtTPPA–AtTPPJ) (Eq. 5-2) and tre score (Eq. 5-3), respectively. tpp'-Score was calculated only from the gene expression level.

$$\text{tps score} = Ex_{AtTPS1} \quad \text{(Eq. 5-1)}$$

$$\text{tpp score} = \sum_{n=\text{A}}^{J} Ex_{AtTPPn} \times k_{\text{cat}}/K_{m\ \text{AtTPP}n} \quad \text{(Eq. 5-2)}$$

$$\text{tre score} = Ex_{AtTRE1} \times k_{\text{cat}}/K_{m\ \text{AtTRE1}} \quad \text{(Eq. 5-3)}$$

$$\text{tpp}' \text{ score} = \sum_{n=\text{A}}^{J} Ex_{AtTPPn} \quad \text{(Eq. 5-4)}$$

Ex is the transcription abundance (absolute expression level extracted from the ePlant database). The scores were standardized to have an average of 0 and a variance of 1, respectively (Z value) for the comparison of the scores.

$$Z_{lm} = \frac{score_{lm} - \mu_l}{\sigma_l} \quad \text{(Eq. 5-5)}$$

m is sample type. *l* is the enzyme type. μ is the means of score. σ is the standard deviation of score. Comparing the Z_{tpp} from activity and expression level and the $Z_{tpp'}$ only from the expression level, the Z_{tpp} was slightly higher in the leaves and lower in the flowers and silique than Z_{tpp} (Fig. 5-1 and Fig. 5-2). This difference is presumably arisen from the localization of the isozymes with high activity. AtTPPA, AtTPPF, AtTPPG, and AtTPPH, showing high k_{cat}/K_m values, are expressed abundantly in the leaves and slightly in flowers and siliques (Table 3-3, Fig. 3-1). Z_{tpp} was thought to be suitable for

the estimation of levels of Tre6*P* and trehalose because some AtTPPs with no or low activity such as AtTPPI and AtTPPJ can be omitted. The balance between Tre6*P* and trehalose in tissues is discussed based on Z_{tps}, Z_{tpp}, and Z_{tre}. The Z_{tps} and Z_{tpp} are high and low, respectively, at the shoot apex, suggesting that Tre6*P* is increasing (Fig. 5-1, Fig. 5-2). This estimation is consistent well with the finding of Wahl *et al*. (Wahl et al., 2013) that the amount of Tre6*P*, important for flowering, increases during flowering in shoot apical meristems. In roots, the Z_{tpp} is higher than Z_{tps} and Z_{tre} suggesting that the amount of Tre6*P* decreases and trehalose accumulates. In the leaves and stems, Z_{tps}, $Z_{tpp,}$ and Z_{tre} are low, and thus Tre6*P* and trehalose contents in leaves and stems are thought to be low. In most parts of flowers, Z_{tps} and Z_{tpp} are low, and Z_{tre} is dominant. There is a tendency to avoid the accumulation of trehalose. Consistent with these estimations, Muller *et al*. reported that root contains trehalose more than flower, stem, and leaf (Müller et al., 2001). Since the evaluation based on the score calculated in this study are consistent well with the amount of Tre6*P* and trehalose reported in the previous study (Müller et al., 2001; Wahl et al., 2013), it can be inferred which of trehalose and Tre6*P* is dominant by comparing Z_{tps}, Z_{tpp}, and Z_{tre}.

Pollen and developing silique showed characteristic scores. In pollen, Z_{tpp} is particularly dominant, and Z_{tps} and Z_{tre} are small (Fig. 5-2). Accumulation of trehalose is assumed. It is known that trehalase is expressed, when pollen germinates and elongates pollen tube in *Solanum pimpinellifolium*, *Hemerocallis minor*, *Galtonia candican*s, *Camellia japonica*, and *Lathyrus odoratus*, and trehalose is used as an energy source (Gussin et al., 1969). It is considered that trehalose synthesis is strengthened at pollen for storing trehalose as an energy source. In developing siliques, the Z_{tps} and Z_{tre} are high, but the Z_{tpp} values are small. It is assumed that the trehalose metabolism shifts toward Tre6*P* synthesis and is controlled to avoid trehalose accumulation. Since Tre6*P* is essential for embryogenesis occurred in developing siliques (Eastmond et al., 2002; Schluepmann et al., 2003), it is considered to prevent the decrease of Tre6*P* concentration.

The contribution of trehalose metabolism in guard cells is discussed. Guard cells are responsible for stomatal closure regulated by ABA. Since stomata closure is weakened in both *AtTPPs* and *AtTRE1* gene-deficient mutants, trehalose metabolism in guard cells is considered to have physiological significance in opening and closing stomata. The Tre6*P* and trehalose balance is evaluated using the score calculated in the same manner as described above from the transcript abundance of *AtTPS1*, *AtTPPs*, and *AtTRE1* in mesophyll cells and guard cells based on Affymetrix ATH1 array data from Yang *et al*. (Yang et al., 2008) (Fig. 5-3). The three Z scores are not changed by ABA in mesophyll cells, but the scores drastically changed in guard cells. Z_{tps} score is high in the absence of ABA (JS34), while Z_{tpp} and Z_{tre} are high in the presence of ABA (JS33). It suggested that Tre6*P* is accumulated constantly in guard cells, but it is degraded into D-glucose by TPP and trehalase in response to ABA. Thus, trehalose is not predicted to accumulate and not to be responsible for stomatal closing. Since Tre6*P* negatively regulates sucrose level, in response to ABA, decreased Tre6*P* increases sucrose level, and sucrose might be used as energy for stomatal closing.

The balance between Tre6*P* and trehalose in various stress responses is inferred from the scores. Z_{tps}, Z_{tpp}, and Z_{tre} are calculated in the same manner as described above based on the information in the database of changes of expression at the root and aboveground parts along with stress responses (Kilian et al., 2007) (Fig. 5-4–Fig. 5-8). The untreated stress score grown under the same conditions is subtracted because the amount of Tre6*P* changes circadianly. In the above-ground part, Z_{tps} increases just after all the stresses. Then Z_{tpp} increases except for the response to osmotic and drought stresses. Osmotic and drought stress would cause the accumulation of Tre6*P* (Fig. 5-5 and Fig. 5-7). Trehalose is thought to be accumulated in response to other stresses, because Z_{tre} did not increase clearly (Fig. 5-4–Fig. 5-8). In root, Z_{tre} is dominant generally, and Z_{tps} is low constantly (Fig. 5-4–Fig. 5-8). Besides, Z_{tpp} is high in the response to cold and salt stress (Fig. 5-4 and Fig. 5-6). Therefore, trehalose metabolism in the root is thought to be shifted to the trehalose decomposition. In the case of wounding

(Fig. 5-8), the change in Z_{tps} increases 3 hours after wounding treatment. Then the Z_{tpp} increased at 12 h. The response was slower than the response to other stresses. After that, the Z_{tre} is small, so trehalose is thought to be accumulated. This is consistent with the fact that trehalose increases through damage by feeding (Brodmann et al., 2002; Hodge et al., 2013; Singh and Shah, 2012).

It has become possible to explain trehalose metabolism in plants by focusing on trehalose-related enzymes' functions in detail. Since there are multiple TPPs and they are widely expressed in various tissues and situations, it was difficult to determine the ability of Tre6*P* degradation. By combining TPP activities of *A. thaliana* and expression level of the genes, it became possible to infer changes in trehalose metabolism more sophisticatedly. It will also be more accurate to evaluate the trehalose metabolism if the activity of plant TPSs would be available. Although Z_{tps} was calculated only from the expression of the gene encoding predominant TPS, AtTPS1, a more precise prediction of trehalose metabolism would be possible by combining the activity of TPS isozymes. Since recombinant AtTPS1 was not produced in *E. coli* and *S. cerevisiae* (data not shown), the expression system suitable for the plant enzymes is necessary.

In this study, the fact that AtTRE1 can decompose Tre6*P* is revealed, but it is unclear whether this has physiological significance. AtTRE1 is localized in the cell membrane, and it is unknown whether the catalytic domain faces the apoplast side or the intracellular side. Tre6*P* is shown to be localized in the nucleus because the main Tre6*P* synthase AtTPS1 is localized in the nucleus (Fichtner et al., 2020). Complementary experiments with *AtTRE1*-deficient *A. thaliana* mutants are appropriate for clarifying the physiological significance of AtTRE1's Tre6*P*-degrading activity. *AtTRE1*-deficient mutants have weaker stomatal closure and are more susceptible to drought stress, but the introduction of the *AtTRE1* gene eliminates this defect (Van Houtte et al., 2013). In this study, mutant enzymes having higher and lower preference for Tre6*P* over trehalose (E595A and T600D, respectively) were successfully generated. By introducing these AtTRE1 mutants into *AtTRE1*-deficient *A. thaliana*

plants and examining the phenotype, the physiological significance of Tre6*P*-degrading activity by AtTRE1 would be clarified.

I hope that the study based on the enzyme functions and structures will contribute to understanding more detailed trehalose-metabolic mechanism.

A

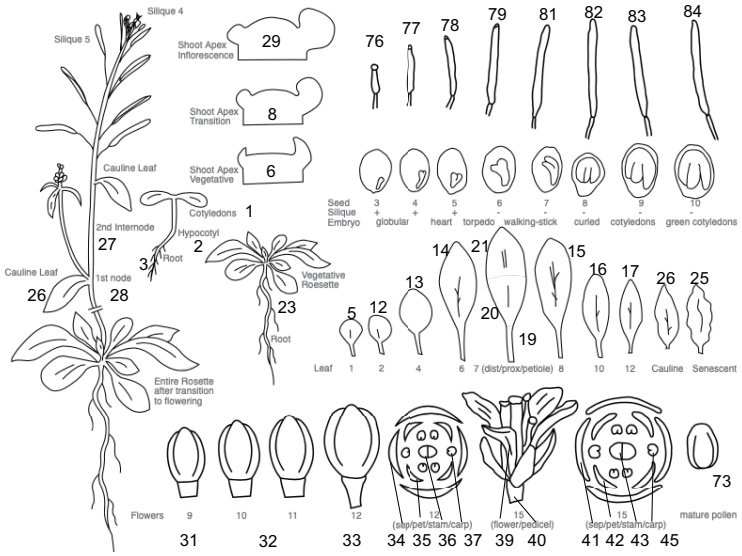

B

tps value	tpp value	tre value	Tre6*P* level evaluation	Trehalose level evaluation
				+
				+
			+	−
			+	
			+	+
			+	−
			+	−
			+	
			−	
			−	+
			−	+
				−
				+
			+	−
			+	−
			+	
			−	−
			−	+
			−	+
			−	−
			−	
			−	+
				−
				−

Fig. 5-1 Schematic diagram of *A. thaliana* tissue, and heatmap of tables.

A, The tissue of *A. thaliana* is shown schematically. The image was is taken from ePlant database (bar.utoronto.ca/eplant). The numbers indicate the ATGE numbers in Fig. 5-2. B, The color coding of the heatmap and the expected amount of Tre6*P* and trehalose are shown schematically. The higher and lower Z value than median is shown in blue and red, respectively.

ATGE	tissue	day-old	Z_{tps}	Z_{tpp}	Z_{tre}	$Z_{tpp'}$
1	cotyledons	7	-0.69	-0.288	-0.553	-0.298
2	hypocotyl	7	1.02	-0.317	-0.912	-0.288
3	root	7	-0.41	0875	-0.856	0.628
5	leaf	7	-0.02	-0.247	-0.642	-0.353
6	shoot apex vegetative	7	1.81	-0.24	-0.867	-0.387
8	shoot apex transition	14	2.41	-0.418	-0.703	-0.532
9	root	17	-0.77	0.307	-0.787	0.192
12	leaf	17	-1.15	-0.187	-0.654	-0.291
13	leaf	17	-1.11	-0.182	-0.665	-0.314
14	leaf	17	-1.04	-0.09	-0.663	-0.24
15	leaf	17	-0.8	-0.156	-0.742	-0.311
16	leaf	17	-0.34	-0.184	-0.701	-0.326
17	leaf	17	0.18	-0.251	-0.732	-0.357
19	petiole	17	-0.27	-0.141	-0.795	-0.293
20	distal half	17	-0.53	-0.099	-0.705	-0.252
21	proximal half	17	-0.41	-0.117	-0.588	-0.237
23	entire rosette after transition to flowering	22	-0.56	-0.296	-0.704	-0.364
25	senescent	35	-1.29	-0.457	-0.431	-0.351
26	cauline	more than21	0	-0.421	-0.28	-0.4
27	2nd internode	more than21	-1.3	0.31	-0.818	0.454
28	1st node	more than21	0.09	0.24	-0.822	0.16
29	shoot apex inflorescence	21	1.01	-0.38	-0.618	-0.409
31	flower	more than21	0.22	-0.373	-0.568	-0.441
32	flower	more than21	0.1	-0.391	-0.376	-0.455
33	flower	more than21	0.29	-0.171	-0.101	-0.226
34	flower	more than21	-0.35	-0.389	0.625	-0.217
35	flower	more than21	-1.33	-0.152	-0.8	-0.028
36	flower	more than21	-0.69	1.75	-0.011	1.408
37	flower	more than21	1.46	-0.152	0.223	-0.177
39	flower	more than21	034	-0.185	0.69	-0.12
40	flower	more than21	-0.94	-0.306	-0.744	-0.258
41	flower	more than21	-0.85	-0.422	2.41	-0.078
42	flower	more than21	-0.92	-0.282	2.287	-0.134
43	flower	more than21	-0.48	1.309	0.48	1.056
45	flower	more than21	1.34	-0.179	1.041	-0.23
73	mature pollen	42	-1.21	5.963	-0.494	6.134
76	silique	56	-0.33	0.002	1.347	-0.008
77	silique	56	0.16	-0.292	1.043	-0.249
78	silique	56	0.31	-0.474	0.408	-0.489
79	silique	56	0.82	-0.44	1.305	-0.389
81	silique	56	1.54	-0.354	1.686	-0.07
82	silique	56	2.07	-0.499	2.206	-0.261
83	silique	56	1.74	-0.435	2.281	0346
84	silique	56	1.51	-0.436	1.331	-0.125
89	vegetative rosette	14	-0.63	-0.354	-0.765	-0.419

Fig. 5-2 Heatmap of tps, tpp, and tre scores in various tissues at different growth stage.

The higher and lower Z value than median of all z value (-0.285) is shown in blue and red, respectively, in gradation. ATGE follows the sample name of Schmid *et al.* (Schmid et al., 2005). The numbers correspond to the tissue numbers in Fig. 5-1.

A

sample	tissue	treatment	treatment_2	Z_{tps}	Z_{tpp}	Z_{tre}
JS88	mesophyll cell	100μM ABA		-0.516	-0.92	-0.821
JS36	mesophyll cell	100 μM ABA	actinomycin and cordycepin	-0.485	-1.058	-0.988
JS87	mesophyll cell	without ABA		-0.516	-0.88	-0.847
JS35	mesophyll cell	without ABA	actinomycin and cordycepin	-0.503	-0.974	-1.01
JS85	guard cell	100μM ABA		-0.448	1.025	0.593
JS33	guard cell	100 μM ABA	actinomycin and cordycepin	0.306	1.56	1.884
JS86	guard cell	without ABA		-0.394	0.782	0.643
JS34	guard cell	without ABA	actinomycin and cordycepin	2.555	0.466	0.545

B

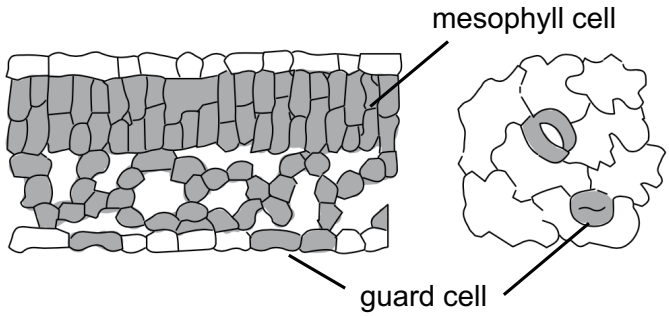

Fig. 5-3 Heatmap of tps, tpp, and tre scores in mesophyll cells and guard cells.

A, The higher and lower Z value than median of all z value (-0.467) is shown in blue and red, respectively, in gradation. Actinomycin D and cordycepin were inhibitor of transcription and translation, and were added during protoplast isolation (Yang et al., 2008). B, The types of leaf cells are shown schematically. The image was is taken from ePlant database (bar.utoronto.ca/eplant).

sample	treatment	tissue	time	replication	Z_{tps}	Z_{tpp}	Z_{tre}
AtGen_6_1121	cold (4˚C)	roots	0.5 h	rep1	0.522	0.393	-0.592
AtGen_6_1122	cold (4˚C)	roots	0.5 h	rep2	-0.753	0.093	0.204
AtGen_6_1221	cold (4˚C)	roots	1.0 h	rep1	0.082	-0.256	-0.698
AtGen_6_1222	cold (4˚C)	roots	1.0 h	rep2	-1.088	-0.420	0.802
AtGen_6_1321	cold (4˚C)	roots	3.0 h	rep1	-0.753	0.698	0.563
AtGen_6_1322	cold (4˚C)	roots	3.0 h	rep2	0.486	1.189	0.093
AtGen_6_1421	cold (4˚C)	roots	6.0 h	rep1	0.437	-0.251	-0.244
AtGen_6_1422	cold (4˚C)	roots	6.0 h	rep2	0.673	-0.915	0.487
AtGen_6_1521	cold (4˚C)	roots	12.0 h	rep1	-1.511	0.704	0.750
AtGen_6_1522	cold (4˚C)	roots	12.0 h	rep2	-1.745	0.989	0.744
AtGen_6_1621	cold (4˚C)	roots	24.0 h	rep1	0.246	0.269	0.614
AtGen_6_1622	cold (4˚C)	roots	24.0 h	rep2	0.205	0.044	0.648
AtGen_6_1111	cold (4˚C)	shoots	0.5 h	rep1	0.966	0.464	-0.238
AtGen_6_1112	cold (4˚C)	shoots	0.5 h	rep2	2.658	0.439	-1.985
AtGen_6_1211	cold (4˚C)	shoots	1.0 h	rep1	2.865	0.980	-1.898
AtGen_6_1212	cold (4˚C)	shoots	1.0 h	rep2	2.184	1.697	-2.145
AtGen_6_1311	cold (4˚C)	shoots	3.0 h	rep1	0.767	5.109	-0.316
AtGen_6_1312	cold (4˚C)	shoots	3.0 h	rep2	1.070	4.384	-0.588
AtGen_6_1411	cold (4˚C)	shoots	6.0 h	rep1	1.968	1.524	-0.628
AtGen_6_1412	cold (4˚C)	shoots	6.0 h	rep2	1.509	1.605	0.048
AtGen_6_1511	cold (4˚C)	shoots	12.0 h	rep1	0.372	0.243	0.301
AtGen_6_1512	cold (4˚C)	shoots	12.0 h	rep2	0.529	0.056	-0.217
AtGen_6_1611	cold (4˚C)	shoots	24.0 h	rep1	0.483	-0.863	-0.140
AtGen_6_1612	cold (4˚C)	shoots	24.0 h	rep2	0.390	-0.847	-0.226

Fig. 5-4 Heatmap of tps, tpp, and tre scores in response to cold stress.

The higher and lower Z value than median of all z value (-0.0825) is shown in blue and red, respectively, in gradation. Sample name follows those of Kilian *et al*. (Kilian et al., 2007). In brief, plant material from 18 day old wild-type *A. thaliana* Col-0 plants was analyzed. The seeds were sown on rafts in MS-Agar-media. After 2 days in the cold room (4°C, dark), the plants were transferred to a long day chamber. At day 11, the rafts were transferred in MS-liquid-media. The plants were grown under long day conditions with 16/8 h light/dark, 24°C, 50% humidity and 150 µEinstein cm^2 s^{-1} light intensity. Plants were kept on crushed ice in cold chamber (4°C).

sample	treatment	tissue	time	replication	Z_{tps}	Z_{tpp}	Z_{tre}
AtGen_6_2121	osmotic stress	roots	0.5 h	rep1	0.451	-0.255	0.736
AtGen_6_2122	osmotic stress	roots	0.5 h	rep2	-1.126	-0.410	0.059
AtGen_6_2221	osmotic stress	roots	1.0 h	rep1	-0.131	-1.389	-0.229
AtGen_6_2222	osmotic stress	roots	1.0 h	rep2	-0.690	-1.707	0.216
AtGen_6_2321	osmotic stress	roots	3.0 h	rep1	-0.559	-0.547	2.658
AtGen_6_2322	osmotic stress	roots	3.0 h	rep2	-1.190	-0.612	2.627
AtGen_6_2421	osmotic stress	roots	6.0 h	rep1	0.070	-1.016	1.725
AtGen_6_2422	osmotic stress	roots	6.0 h	rep2	-0.136	-0.936	2.144
AtGen_6_2521	osmotic stress	roots	12.0 h	rep1	-2.110	0.224	1.797
AtGen_6_2522	osmotic stress	roots	12.0 h	rep2	-1.902	0.160	3.381
AtGen_6_2621	osmotic stress	roots	24.0 h	rep1	-0.085	-0.285	2.662
AtGen_6_2622	osmotic stress	roots	24.0 h	rep2	-0.326	-0.381	1.727
AtGen_6_2111	osmotic stress	shoots	0.5 h	rep1	-0.108	-0.182	0.438
AtGen_6_2112	osmotic stress	shoots	0.5 h	rep2	0.587	-0.317	-1.120
AtGen_6_2211	osmotic stress	shoots	1.0 h	rep1	1.325	-0.812	-0.854
AtGen_6_2212	osmotic stress	shoots	1.0 h	rep2	1.795	-0.433	-1.818
AtGen_6_2311	osmotic stress	shoots	3.0 h	rep1	-0.983	-0.181	-0.235
AtGen_6_2312	osmotic stress	shoots	3.0 h	rep2	-0.172	0.162	0.088
AtGen_6_2411	osmotic stress	shoots	6.0 h	rep1	0.240	-0.193	0.690
AtGen_6_2412	osmotic stress	shoots	6.0 h	rep2	0.077	-0.025	1.392
AtGen_6_2511	osmotic stress	shoots	12.0 h	rep1	-0.395	-0.683	-0.435
AtGen_6_2512	osmotic stress	shoots	12.0 h	rep2	-0.489	-0.872	0.380
AtGen_6_2611	osmotic stress	shoots	24.0 h	rep1	0.489	-1.111	-0.797
AtGen_6_2612	osmotic stress	shoots	24.0 h	rep2	0.268	-0.907	-0.565

Fig. 5-5 Heatmap of tps, tpp, and tre scores in response to osmotic stress.

The higher and lower Z value than median of all z value (-0.0825) is shown in blue and red, respectively, in gradation. Sample name follows those of Kilian *et al*. (Kilian et al., 2007). The growth condition was same as Fig. 5-4. Plants were transferred to the media containing 300 mM mannitol (osmotic stress treatment).

sample	treatment	tissue	time	replication	Z_{tps}	Z_{tpp}	Z_{tre}
AtGen_6_3121	salt stress	roots	0.5 h	rep1	-0.260	0.646	1.655
AtGen_6_3122	salt stress	roots	0.5 h	rep2	-1.065	0.479	0.206
AtGen_6_3221	salt stress	roots	1.0 h	rep1	-0.615	0.283	0.013
AtGen_6_3222	salt stress	roots	1.0 h	rep2	-0.991	0.048	0.838
AtGen_6_3321	salt stress	roots	3.0 h	rep1	-0.712	-0.083	1.609
AtGen_6_3322	salt stress	roots	3.0 h	rep2	-1.227	-0.216	3.927
AtGen_6_3421	salt stress	roots	6.0 h	rep1	0.407	0.341	2.952
AtGen_6_3422	salt stress	roots	6.0 h	rep2	-0.031	0.169	3.041
AtGen_6_3521	salt stress	roots	12.0 h	rep1	-2.224	0.557	3.547
AtGen_6_3522	salt stress	roots	12.0 h	rep2	-1.760	0.902	1.104
AtGen_6_3621	salt stress	roots	24.0 h	rep1	-0.352	-0.199	1.227
AtGen_6_3622	salt stress	roots	24.0 h	rep2	-1.103	0.144	1.421
AtGen_6_3111	salt stress	shoots	0.5 h	rep1	-0.146	0.451	0.110
AtGen_6_3112	salt stress	shoots	0.5 h	rep2	1.101	-0.089	-1.709
AtGen_6_3211	salt stress	shoots	1.0 h	rep1	1.615	0.236	-1.826
AtGen_6_3212	salt stress	shoots	1.0 h	rep2	2.390	0.342	-1.893
AtGen_6_3311	salt stress	shoots	3.0 h	rep1	0.644	0.654	-0.264
AtGen_6_3312	salt stress	shoots	3.0 h	rep2	0.801	1.095	-0.879
AtGen_6_3411	salt stress	shoots	6.0 h	rep1	0.461	1.075	-0.566
AtGen_6_3412	salt stress	shoots	6.0 h	rep2	1.297	1.375	0.399
AtGen_6_3511	salt stress	shoots	12.0 h	rep1	-0.360	0.070	-0.307
AtGen_6_3512	salt stress	shoots	12.0 h	rep2	-0.793	-0.082	-0.774
AtGen_6_3611	salt stress	shoots	24.0 h	rep1	1.175	-0.442	-1.312
AtGen_6_3612	salt stress	shoots	24.0 h	rep2	0.728	-0.300	-1.090

Fig. 5-6 Heatmap of tps, tpp, and tre scores in response to salt stress.

The higher and lower Z value than median of all z value (-0.0825) is shown in blue and red, respectively, in gradation. Sample name follows those of Kilian *et al*. (Kilian et al., 2007). The growth condition was same as Fig. 5-4. Plants were transferred to the media containing 150 mM NaCl (salt stress treatment).

sample	treatment	tissue	time	replication	Z_{tps}	Z_{tpp}	Z_{tre}
AtGen_6_4721	drought stress	roots	0.25 h	rep1	0.037	-1.310	1.489
AtGen_6_4722	drought stress	roots	0.25 h	rep2	-1.298	-1.297	0.208
AtGen_6_4121	drought stress	roots	0.5 h	rep1	-0.298	-0.658	-0.744
AtGen_6_4122	drought stress	roots	0.5 h	rep2	-0.549	-0.984	0.022
AtGen_6_4221	drought stress	roots	1.0 h	rep1	-0.689	-0.802	-0.238
AtGen_6_4222	drought stress	roots	1.0 h	rep2	-0.841	-0.748	0.160
AtGen_6_4321	drought stress	roots	3.0 h	rep1	-0.126	-0.292	-0.518
AtGen_6_4322	drought stress	roots	3.0 h	rep2	-0.569	-0.216	1.294
AtGen_6_4421	drought stress	roots	6.0 h	rep1	-2.202	0.209	0.273
AtGen_6_4422	drought stress	roots	6.0 h	rep2	-2.361	-0.282	1.794
AtGen_6_4521	drought stress	roots	12.0 h	rep1	0.542	-0.918	0.787
AtGen_6_4522	drought stress	roots	12.0 h	rep2	0.573	-0.847	0.162
AtGen_6_4621	drought stress	roots	24.0 h	rep1	-0.781	-0.438	0.952
AtGen_6_4622	drought stress	roots	24.0 h	rep2	-0.104	-0.329	-1.514
AtGen_6_4711	drought stress	shoots	0.25 h	rep1	2.749	-0.035	-1.743
AtGen_6_4712	drought stress	shoots	0.25 h	rep2	2.322	0.633	-1.624
AtGen_6_4111	drought stress	shoots	0.5 h	rep1	0.174	-0.545	-0.271
AtGen_6_4112	drought stress	shoots	0.5 h	rep2	0.502	-0.489	-1.088
AtGen_6_4211	drought stress	shoots	1.0 h	rep1	0.968	-0.584	-0.953
AtGen_6_4212	drought stress	shoots	1.0 h	rep2	0.966	-0.598	0.208
AtGen_6_4311	drought stress	shoots	3.0 h	rep1	-0.449	0.501	-0.152
AtGen_6_4312	drought stress	shoots	3.0 h	rep2	-0.353	-0.012	0.219
AtGen_6_4411	drought stress	shoots	6.0 h	rep1	-0.232	-0.555	0.237
AtGen_6_4412	drought stress	shoots	6.0 h	rep2	-0.495	0.027	0.202
AtGen_6_4511	drought stress	shoots	12.0 h	rep1	-2.194	-1.063	0.043
AtGen_6_4512	drought stress	shoots	12.0 h	rep2	-2.354	-1.303	0.072
AtGen_6_4611	drought stress	shoots	24.0 h	rep1	2.125	-0.289	-1.069
AtGen_6_4612	drought stress	shoots	24.0 h	rep2	2.611	-0.269	-0.471

Fig. 5-7 Heatmap of tps, tpp, and tre scores in response to drought stress.

The higher and lower Z value than median of all z value (-0.0825) is shown in blue and red, respectively, in gradation. Sample name follows those of Kilian *et al*. (Kilian et al., 2007). The growth condition was same as Fig. 5-4. As drought stress treatment, plants were exposed to the air stream for 15 min with loss of app.10% fresh weight.

sample	treatment	tissue	time	replication	Z_{tps}	Z_{tpp}	Z_{tre}
AtGen_6_8723	wounding stress	roots	0.25 h	rep1	0.968	-0.166	-0.297
AtGen_6_8724	wounding stress	roots	0.25 h	rep2	-0.473	-0.660	-0.440
AtGen_6_8124	wounding stress	roots	0.5 h	rep1	-0.314	-0.942	0.215
AtGen_6_8126	wounding stress	roots	0.5 h	rep2	-0.642	-1.410	0.046
AtGen_6_8224	wounding stress	roots	1.0 h	rep1	0.454	-1.070	-0.481
AtGen_6_8225	wounding stress	roots	1.0 h	rep2	-0.047	-1.135	0.037
AtGen_6_8324	wounding stress	roots	3.0 h	rep1	0.237	-1.116	-0.431
AtGen_6_8325	wounding stress	roots	3.0 h	rep2	0.361	-1.364	0.647
AtGen_6_8423	wounding stress	roots	6.0 h	rep1	-1.125	-0.854	0.760
AtGen_6_8424	wounding stress	roots	6.0 h	rep2	-1.617	-0.896	0.773
AtGen_6_8524	wounding stress	roots	12.0 h	rep1	-0.108	0.021	0.860
AtGen_6_8525	wounding stress	roots	12.0 h	rep2	-0.494	-0.131	0.684
AtGen_6_8621	wounding stress	roots	24.0 h	rep2	-0.199	-0.666	1.222
AtGen_6_8622	wounding stress	roots	24.0 h	rep2	0.816	-0.690	-0.113
AtGen_6_8712	wounding stress	shoots	0.25 h	rep2	0.257	-0.784	-1.182
AtGen_6_8715	wounding stress	shoots	0.25 h	rep1	0.485	-0.535	-1.839
AtGen_6_8111	wounding stress	shoots	0.5 h	rep1	0.158	-0.427	0.717
AtGen_6_8112	wounding stress	shoots	0.5 h	rep2	0.394	0.115	0.197
AtGen_6_8211	wounding stress	shoots	1.0 h	rep1	0.232	-0.070	-0.737
AtGen_6_8214	wounding stress	shoots	1.0 h	rep2	0.032	-0.018	0.452
AtGen_6_8313	wounding stress	shoots	3.0 h	rep1	1.779	-0.149	1.182
AtGen_6_8314	wounding stress	shoots	3.0 h	rep2	2.279	-0.208	-0.371
AtGen_6_8411	wounding stress	shoots	6.0 h	rep1	0.022	-1.493	0.222
AtGen_6_8412	wounding stress	shoots	6.0 h	rep2	-0.387	-1.594	0.279
AtGen_6_8511	wounding stress	shoots	12.0 h	rep1	-2.051	1.502	0.694
AtGen_6_8512	wounding stress	shoots	12.0 h	rep2	-2.014	1.532	-0.237
AtGen_6_8611	wounding stress	shoots	24.0 h	rep1	0.621	-0.274	-1.357
AtGen_6_8612	wounding stress	shoots	24.0 h	rep2	0.738	-0.303	-0.874

Fig. 5-8 Heatmap of tps, tpp, and tre scores in response to wounding stress.

The higher and lower Z value than median of all z value (-0.0825) is shown in blue and red, respectively, in gradation. Sample name follows those of Kilian *et al*. (Kilian et al., 2007). The growth condition was same as Fig. 5-4. The wounding treatment was performed by injuring the leaves by 3 consecutive applications of a custom-made pin-tool consisting of 16 needles.

6. References

Adams, P.D., Afonine, P. V., Bunkóczi, G., Chen, V.B., Davis, I.W., Echols, N., Headd, J.J., Hung, L.W., Kapral, G.J., Grosse-Kunstleve, R.W., McCoy, A.J., Moriarty, N.W., Oeffner, R., Read, R.J., Richardson, D.C., Richardson, J.S., Terwilliger, T.C., and Zwart, P.H. (2010). PHENIX: a comprehensive Python-based system for macromolecular structure solution. Acta Crystallogr. D. Biol. Crystallogr. *66*, 213–221.

Adhav, A., Harne, S., Bhide, A., Giri, A., Gayathri, P., and Joshi, R. (2019). Mechanistic insights into enzymatic catalysis by trehalase from the insect gut endosymbiont *Enterobacter cloacae*. FEBS J. *286*, 1700–1716.

Aisaka, K., Masuda, T., and Chikamune, T. (1996). Properties of maltose phosphorylase from *Propionibacterium freudenreichii*. J. Ferment. Bioeng. *82*, 171–173.

Aisaka, K., Masuda, T., Chikamune, T., and Kamitori, K. (1998). Purification and characterization of trehalose phosphorylase from *Catellatospora ferruginea*. Biosci. Biotechnol. Biochem. *62*, 782–787.

Alblova, M., Smidova, A., Docekal, V., Vesely, J., Herman, P., Obsilova, V., and Obsil, T. (2017). Molecular basis of the 14-3-3 protein-dependent activation of yeast neutral trehalase Nth1. Proc. Natl. Acad. Sci. U. S. A. *114*, E9811–E9820.

Aleshin, A., Golubev, A., Firsov, L.M., and Honzatko, R.B. (1992). Crystal structure of glucoamylase from *Aspergillus awamori* var. X100 to 2.2-Å resolution. J. Biol. Chem. *267*, 19291–19298.

Aleshin, A.E., Firsov, L.M., and Honzatko, R.B. (1994). Refined structure for the complex of acarbose with glucoamylase from *Aspergillus awamori* var. X100 to 2.4-A resolution. J. Biol. Chem. *269*, 15631–15639.

Allen, K.N., and Dunaway-Mariano, D. (2004). Phosphoryl group transfer: evolution of a catalytic scaffold. Trends Biochem. Sci. *29*, 495–503.

Andersson, U., Levander, F., and Rådström, P. (2001). Trehalose-6-phosphate phosphorylase is part of a novel metabolic pathway for trehalose utilization in *Lactococcus lactis*. J. Biol. Chem. *276*, 42707–42713.

Ashby, J.H., Clarke, H.B., Crook, E.M., and Datta, S.P. (1955). Thermodynamic quantities for the

dissociation equilibria of biologically important compounds. 4. The second acid dissociation of glucose 1-phosphoric acid. Biochem. J. *59*, 203–208.

Avonce, N., Leyman, B., Mascorro-Gallardo, J.O., Van Dijck, P., Thevelein, J.M., and Iturriaga, G. (2004). The *Arabidopsis* trehalose-6-P synthase *AtTPS1* gene is a regulator of glucose, abscisic acid, and stress signaling. Plant Physiol. *136*, 3649–3659.

Avonce, N., Mendoza-Vargas, A., Morett, E., and Iturriaga, G. (2006). Insights on the evolution of trehalose biosynthesis. BMC Evol. Biol. *6*, 109.

Avonce, N., Wuyts, J., Verschooten, K., Vandesteene, L., and Van Dijck, P. (2010). The *Cytophaga hutchinsonii* ChTPSP: First characterized bifunctional TPS-TPP protein as putative ancestor of all eukaryotic trehalose biosynthesis proteins. Mol. Biol. Evol. *27*, 359–369.

Barrozo, A., Liao, Q., Esguerra, M., Marloie, G., Florián, J., Williams, N.H., and Kamerlin, S.C.L. (2018). Computer simulations of the catalytic mechanism of wild-type and mutant β-phosphoglucomutase. Org. Biomol. Chem. *16*, 2060–2073.

Belocopitow, E., and Maréchal, L.R. (1974). Metabolism of trehalose in *Euglena gracilis*. Partial purification and some properties of phosphoglucomutase acting on beta-glucose 1-phosphate. Eur. J. Biochem. *46*, 631–637.

Benaroudj, N., Lee, D.H., and Goldberg, A.L. (2001). Trehalose accumulation during cellular stress protects cells and cellular proteins from damage by oxygen radicals. J. Biol. Chem. *276*, 24261–24267.

Blázquez, M.A., Lagunas, R., Gancedo, C., and Gancedo, J.M. (1993). Trehalose-6-phosphate, a new regulator of yeast glycolysis that inhibits hexokinases. FEBS Lett. *329*, 51–54.

Blázquez, M.A., Santos, E., Flores, C.L., Martínez-Zapater, J.M., Salinas, J., and Gancedo, C. (1998). Isolation and molecular characterization of the *Arabidopsis TPS1* gene, encoding trehalose-6-phosphate synthase. Plant J. *13*, 685–689.

Bock, K., and Pedersen, C. (1974). A study of ^{13}CH coupling constants in hexopyranoses. J. Chem. Soc., Perkin Trans. 2 *2*, 293–297.

Bonini, B.M., Van Dijck, P., and Thevelein, J.M. (2004). Trehalose metabolism: enzymatic pathways and

physiological functions. In Biochemistry and Molecular Biology, (Berlin, Heidelberg: Springer Berlin Heidelberg), pp. 291–332.

Boos, W., Ehmann, U., Bremer, E., Middendorf, A., and Postma, P. (1987). Trehalase of *Escherichia coli*. Mapping and cloning of its structural gene and identification of the enzyme as a periplasmic protein induced under high osmolarity growth conditions. J. Biol. Chem. *262*, 13212–13218.

Boos, W., Ehmann, U., Forkl, H., Klein, W., Rimmele, M., and Postma, P. (1990). Trehalose transport and metabolism in *Escherichia coli*. J. Bacteriol. *172*, 3450–3461.

Booth, I.R. (1985). Regulation of cytoplasmic pH in bacteria. Microbiol. Rev. *49*, 359–378.

Bradford, M.M. (1976). A rapid and sensitive method for the quantitation of microgram quantities of protein utilizing the principle of protein-dye binding. Anal. Biochem. *72*, 248–254.

Brodmann, A., Schuller, A., Ludwig-Müller, J., Aeschbacher, R.A., Wiemken, A., Boller, T., and Wingler, A. (2002). Induction of trehalase in Arabidopsis plants infected with the trehalose-producing pathogen *Plasmodiophora brassicae*. Mol. Plant. Microbe. Interact. *15*, 693–700.

Burroughs, A.M., Allen, K.N., Dunaway-Mariano, D., and Aravind, L. (2006). Evolutionary genomics of the HAD superfamily: understanding the structural adaptations and catalytic diversity in a superfamily of phosphoesterases and allied enzymes. J. Mol. Biol. *361*, 1003–1034.

Cabib, E., and Leloir, L.F. (1958). The biosynthesis of trehalose phosphate. J. Biol. Chem. *231*, 259–275.

Cao, Y., Wang, Y., Dai, B., Wang, B., Zhang, H., Zhu, Z., Xu, Y., Cao, Y., Jiang, Y., and Zhang, G. (2008). Trehalose is an important mediator of Cap1p oxidative stress response in *Candida albicans*. Biol. Pharm. Bull. *31*, 421–425.

Chaen, H., Nakada, T., Nishimoto, T., Kuroda, N., Fukuda, S., Sugimoto, T., Kurimoto, M., and Tsujisaka, Y. (1999a). Purification and characterization of thermostable trehalose phosphorylase from *Thermoanaerobium brockii*. J. Appl. Glycosci *46*, 399–405.

Chaen, H., Yamamoto, T., Nishimoto, T., Nakada, T., Fukuda, S., Sugimoto, T., Kurrimoto, M., and Tsujisaka, Y. (1999b). Purification and characterization of a novel phosphorylase, kojibiose phosphorylase, from *Thermoanaerobium brockii*. J. Appl. Glycosci *46*, 423–429.

Chen, V.B., Arendall, W.B., Headd, J.J., Keedy, D.A., Immormino, R.M., Kapral, G.J., Murray, L.W., Richardson, J.S., and Richardson, D.C. (2010). *MolProbity*: all-atom structure validation for macromolecular crystallography. Acta Crystallogr. D. Biol. Crystallogr. *66*, 12–21.

Claeys, H., Vi, S.L., Xu, X., Satoh-Nagasawa, N., Eveland, A.L., Goldshmidt, A., Feil, R., Beggs, G.A., Sakai, H., Brennan, R.G., Lunn, J.E., and Jackson, D. (2019). Control of meristem determinacy by trehalose 6-phosphate phosphatases is uncoupled from enzymatic activity. Nat. Plants *5*, 352–357.

Cleland, W.W. (1963). The kinetics of enzyme-catalyzed reactions with two or more substrates or products. II. Inhibition: nomenclature and theory. Biochim. Biophys. Acta *67*, 173–187.

Coutinho, P.M., Deleury, E., Davies, G.J., and Henrissat, B. (2003). An evolving hierarchical family classification for glycosyltransferases. J. Mol. Biol. *328*, 307–317.

Cowan, J.A. (1991). Metallobiochemistry of magnesium. Coordination complexes with biological substrates: site specificity, kinetics and thermodynamics of binding, and implications for activity. Inorg. Chem *30*, 2740–2747.

Crooks, G.E., Hon, G., Chandonia, J.M., and Brenner, S.E. (2004). WebLogo: a sequence logo generator. Genome Res. *14*, 1188–1190.

Cross, M., Rajan, S., Chekaiban, J., Saunders, J., Hamilton, C., Kim, J.S., Coster, M.J., Gasser, R.B., and Hofmann, A. (2017a). Enzyme characteristics of pathogen-specific trehalose-6-phosphate phosphatases. Sci. Rep. *7*, 2015.

Cross, M., Lepage, R., Rajan, S., Biberacher, S., Young, N.D., Kim, B.N., Coster, M.J., Gasser, R.B., Kim, J.S., and Hofmann, A. (2017b). Probing function and structure of trehalose-6-phosphate phosphatases from pathogenic organisms suggests distinct molecular groupings. FASEB J. *31*, 920–926.

Cross, M., Biberacher, S., Park, S., Rajan, S., Korhonen, P., Gasser, R.B., Kim, J., Coster, M.J., and Hofmann, A. (2018). Trehalose 6-phosphate phosphatases of *Pseudomonas aeruginosa*. FASEB J. *32*, 5470–5482.

Dahl, M.K. (2006). Enzyme IIGlc contributes to trehalose metabolism in *Bacillus subtilis*. FEMS Microbiol. Lett. *148*, 233–238.

Dahlqvist, A., Jensen, A.T., Marcker, K., and Dodson, R.M. (1960). Characterization of hog intestinal trehalase. Acta Chem. Scand. *14*, 9–16.

Dangl, J.L., and Jones, J.D. (2001). Plant pathogens and integrated defence responses to infection. Nature *411*, 826–833.

Davies, G., and Henrissat, B. (1995). Structures and mechanisms of glycosyl hydrolases. Structure *3*, 853–859.

Delorge, I., Figueroa, C.M., Feil, R., Lunn, J.E., and Van Dijck, P. (2015). Trehalose-6-phosphate synthase 1 is not the only active TPS in *Arabidopsis thaliana*. Biochem. J. *466*, 283–290.

De Smet, K.A.L., Weston, A., Brown, I.N., Young, D.B., and Robertson, B.D. (2000). Three pathways for trehalose biosynthesis in mycobacteria. Microbiology *146*, 199–208.

De Virgilio, C., Bürckert, N., Bell, W., Jenö, P., Boller, T., and Wiemken, A. (1993). Disruption of *TPS2*, the gene encoding the 100-kDa subunit of the trehalose-6-phosphate synthase/phosphatase complex in *Saccharomyces cerevisiae*, causes accumulation of trehalose-6-phosphate and loss of trehalose-6-phosphate phosphatase activity. Eur. J. Biochem. *212*, 315–323.

Doi, J., Yokoigawa, K., Isobe, Y., and Kawai, H. (1998). Trehalose 6-phosphate production with energy coupling fermentation by yeast cells. Biosci. Biotechnol. Biochem. *62*, 735–739.

Dubois, M., Gilles, K.A., and Hamilton, J.K. (1956). Colorimetric method for determination of sugars and related substances. Anal. Chem. *28*, 350–356.

Eastmond, P.J., Van Dijken, A.J.H., Spielman, M., Kerr, A., Tissier, A.F., Dickinson, H.G., Jones, J.D.G., Smeekens, S.C., and Graham, I.A. (2002). Trehalose-6-phosphate synthase 1, which catalyses the first step in trehalose synthesis, is essential for *Arabidopsis* embryo maturation. Plant J. *29*, 225–235.

Egloff, M., Uppenberg, J., Haalck, L., and van Tilbeurgh, H. (2001). Crystal structure of maltose phosphorylase from *Lactobacillus brevis*: unexpected evolutionary relationship with glucoamylases. Structure *9*, 689–697.

Elbein, A.D. (1974). The metabolism of α,α-trehalose. Adv. Carbohydr. Chem. Biochem. *30*, 227–256.

Emsley, P., and Cowtan, K. (2004). *Coot*: model-building tools for molecular graphics. Acta Crystallogr. D. Biol. Crystallogr. *60*, 2126–2132.

Farelli, J.D., Galvin, B.D., Li, Z., Liu, C., Aono, M., Garland, M., Hallett, O.E., Causey, T.B., Ali-Reynolds, A., Saltzberg, D.J., Carlow, C.K.S., Dunaway-Mariano, D., and Allen, K.N. (2014). Structure of the trehalose-6-phosphate phosphatase from *Brugia malayi* reveals key design principles for anthelmintic drugs. PLoS Pathog. *10*, e1004245.

Fersht, A.R., Shi, J.P., Knill-Jones, J., Lowe, D.M., Wilkinson, A.J., Blow, D.M., Brick, P., Carter, P., Waye, M.M., and Winter, G. (1985). Hydrogen bonding and biological specificity analysed by protein engineering. Nature *314*, 235–238.

Fichtner, F., Barbier, F.F., Feil, R., Watanabe, M., Annunziata, M.G., Chabikwa, T.G., Höfgen, R., Stitt, M., Beveridge, C.A., and Lunn, J.E. (2017). Trehalose 6-phosphate is involved in triggering axillary bud outgrowth in garden pea (*Pisum sativum L.*). Plant J. *92*, 611–623.

Fichtner, F., Olas, J.J., Feil, R., Watanabe, M., Krause, U., Hoefgen, R., Stitt, M., and Lunn, J.E. (2020). Functional features of TREHALOSE-6-PHOSPHATE SYNTHASE1, an essential enzyme in *Arabidopsis*. Plant Cell *32*, 1949–1972.

Figueroa, C.M., Feil, R., Ishihara, H., Watanabe, M., Kölling, K., Krause, U., Höhne, M., Encke, B., Plaxton, W.C., Zeeman, S.C., Li, Z., Schulze, W.X., Hoefgen, R., Stitt, M., and Lunn, J.E. (2016). Trehalose 6-phosphate coordinates organic and amino acid metabolism with carbon availability. Plant J. *85*, 410–423.

Frison, M., Parrou, J.L., Guillaumot, D., Masquelier, D., François, J., Chaumont, F., and Batoko, H. (2007). The *Arabidopsis thaliana* trehalase is a plasma membrane-bound enzyme with extracellular activity. FEBS Lett. *581*, 4010–4016.

Gao, Y., Saburi, W., Taguchi, Y., and Mori, H. (2019). Biochemical characteristics of maltose phosphorylase MalE from *Bacillus* sp. AHU2001 and chemoenzymatic synthesis of oligosaccharides by the enzyme. Biosci. Biotechnol. Biochem. *83*, 2097–2109.

Garg, A.K., Kim, J., Owens, T.G., Ranwala, A.P., Choi, Y. Do, Kochian, L. V, and Wu, R.J. (2002). Trehalose accumulation in rice plants confers high tolerance levels to different abiotic stresses. Proc. Natl. Acad. Sci. U. S. A. *99*, 15898–15903.

Gibson, R.P., Lloyd, R.M., Charnock, S.J., and Davies, G.J. (2002). Characterization of *Escherichia coli* OtsA, a trehalose-6-phosphate synthase from glycosyltransferase family 20. Acta Crystallogr. Sect. D Biol. Crystallogr. *58*, 349–351.

Gibson, R.P., Gloster, T.M., Roberts, S., Warren, R.A.J., Storch de Gracia, I., García, A., Chiara, J.L., and Davies, G.J. (2007). Molecular basis for trehalase inhibition revealed by the structure of trehalase in complex with potent inhibitors. Angew. Chem. Int. Ed. Engl. *46*, 4115–4119.

Glazener, J.A., Orlandi, E.W., and Baker, C.J. (1996). The active oxygen response of cell suspensions to incompatible bacteria is not sufficient to cause hypersensitive cell death. Plant Physiol. *110*, 759–763.

Gómez, L.D., Gilday, A., Li, Y., Graham, I.A., and Go, L.D. (2006). Delayed embryo development in the *ARABIDOPSIS TREHALOSE-6-PHOSPHATE SYNTHASE 1* mutant is associated with altered cell wall structure, decreased cell division and starch accumulation. Plant J. *46*, 69–84.

González, M.I., Blázquez, M.A., Gancedo, C., Stucka, R., and Feldmann, H. (1992). Molecular cloning of *CIF1*, a yeast gene necessary for growth on glucose. Yeast *8*, 183–192.

Griffiths, C.A., Sagar, R., Geng, Y., Primavesi, L.F., Patel, M.K., Passarelli, M.K., Gilmore, I.S., Steven, R.T., Bunch, J., Paul, M.J., and Davis, B.G. (2016). Chemical intervention in plant sugar signalling increases yield and resilience. Nature *540*, 574–578.

Gussin, A.E.S., McCormack, J.H., Waung, L.Y. Lo, and Gluckin, D.S. (1969). Trehalase: a new pollen enzyme. Plant Physiol. *44*, 1163–1168.

Gutierrez, C., Ardourel, M., Bremer, E., Middendorf, A., Boos, W., and Ehmann, U. (1989). Analysis and DNA sequence of the osmoregulated *treA* gene encoding the periplasmic trehalase of *Escherichia coli* K12. Mol. Gen. Genet. *217*, 347–354.

Halford, N.G., and Grahame Hardie, D. (1998). SNF1-related protein kinases: global regulators of carbon metabolism in plants? Plant Mol. Biol. *37*, 735–748.

Hanahan, D. (1983). Studies on transformation of *Escherichia coli* with plasmids. J. Mol. Biol. *166*, 557–580.

Hartwell, J., Gill, A., Nimmo, G.A., Wilkins, M.B., Jenkins, G.I., and Nimmo, H.G. (1999).

Phosphoenolpyruvate carboxylase kinase is a novel protein kinase regulated at the level of expression. Plant J. *20*, 333–342.

Hehre, E.J., Sawai, T., Brewer, C.F., Nakano, M., and Kanda, T. (1982). Stereocomplementary hydrolytic and glucosyl transfer reactions with α- and β-D-glucosyl fluoride. Biochemistry *21*, 3090–3097.

Henrissat, B., and Davies, G. (1997). Structural and sequence-based classification of glycoside hydrolases. Curr. Opin. Struct. Biol. *7*, 637–644.

Hey, A.E., and Elbein, A.D. (1968). Partial prufication and properties of a trehalase from *Streptomyces hygroscopicus*. J. Bacteriol. *96*, 105–110.

Hidaka, M., Honda, Y., Kitaoka, M., Nirasawa, S., Hayashi, K., Wakagi, T., Shoun, H., and Fushinobu, S. (2004). Chitobiose phosphorylase from *Vibrio proteolyticus*, a member of glycosyl transferase family 36, has a clan GH-L-like $(\alpha/\alpha)_6$ barrel fold. Structure *12*, 937–947.

Hodge, S., Ward, J.L., Beale, M.H., Bennett, M., Mansfield, J.W., and Powell, G. (2013). Aphid-induced accumulation of trehalose in *Arabidopsis thaliana* is systemic and dependent upon aphid density. Planta *237*, 1057–1064.

Hokse, H. (1983). Purification of α-D-glucose-1-phosphate. Starch - Stärke *35*, 101–102.

Horlacher, R., Uhland, K., Klein, W., Ehrmann, M., and Boos, W. (1996). Characterization of a cytoplasmic trehalase of *Escherichia coli*. J. Bacteriol. *178*, 6250–6257.

Huber, J.L., Hite, D.R.C., Outlaw, W.H., and Huber, S.C. (1991). Inactivation of highly activated spinach leaf sucrose-phosphate synthase by dephosphorylation. Plant Physiol. *95*, 291–297.

Islam, M.O., Kato, H., Shima, S., Tezuka, D., Matsui, H., and Imai, R. (2019). Functional identification of a rice trehalase gene involved in salt stress tolerance. Gene *685*, 42–49.

Kabsch, W. (2010). *XDS*. Acta Crystallogr. Sect. D Biol. Crystallogr. *66*, 125–132.

Kamogawa, A., Yokobayashi, K., and Fukui, T. (1973). Purification and properties of maltose phosphorylase from *Lactobacillus brevis*. Agric. Biol. Chem. *37*, 2813–2819.

Kato, M., Miura, Y., Kettoku, M., Shindo, K., Iwamatsu, A., and Kobayashi, K. (1996a). Purification and characterization of new trehalose-producing enzymes isolated from the hyperthermophilic archae, *Sulfolobus solfataricus* KM1. Biosci. Biotechnol. Biochem. *60*, 546–550.

Kato, M., Miura, Y., Kettoku, M., Komeda, T., Iwamatsu, A., and Kobayashi, K. (1996b). Reaction mechanism of a new glycosyltrehalose-hydrolyzing enzyme isolated from the hyperthermophilic archaeum, *Sulfolobus solfataricus* KM1. Biosci. Biotechnol. Biochem. *60*, 925–928.

Katoh, K., Rozewicki, J., and Yamada, K.D. (2019). MAFFT online service: multiple sequence alignment, interactive sequence choice and visualization. Brief. Bioinform. *20*, 1160–1166.

Kilian, J., Whitehead, D., Horak, J., Wanke, D., Weinl, S., Batistic, O., D'Angelo, C., Bornberg-Bauer, E., Kudla, J., and Harter, K. (2007). The AtGenExpress global stress expression data set: protocols, evaluation and model data analysis of UV-B light, drought and cold stress responses. Plant J. *50*, 347–363.

Kim, T.K., Jang, J.H., Cho, H.Y., Lee, H.S., and Kim, Y.W. (2010). Gene cloning and characterization of a trehalose synthase from *Corynebacterium glutamicum* ATCC13032. Food Sci Biotechnol *19*, 565–569.

Kim, Y., Yakunin, A.F., Kuznetsova, E., Xu, X., Pennycooke, M., Gu, J., Cheung, F., Proudfoot, M., Arrowsmith, C.H., Joachimiak, A., Edwards, A.M., and Christendat, D. (2004). Structure- and function-based characterization of a new phosphoglycolate phosphatase from *Thermoplasma acidophilum*. J. Biol. Chem. *279*, 517–526.

Kizawa, H., Miyagawa, K., and Sugiyama, Y. (1995). Purification and characterization of trehalose phosphorylase from *Micrococcus varians*. Biosci. Biotechnol. Biochem. *59*, 1908–1912.

Klutts, S., Pastuszak, I., Edavana, V.K., Thampi, P., Pan, Y.T., Abraham, E.C., Carroll, J.D., and Elbein, A.D. (2003). Purification, cloning, expression, and properties of mycobacterial trehalose-phosphate phosphatase. J. Biol. Chem. *278*, 2093–2100.

Koban, A., Geipel, G., Roßberg, A., and Bernhard, G. (2004). Uranium(VI) complexes with sugar phosphates in aqueous solution. Radiochim. Acta *92*, 903–908.

Kobayashi, K., Kato, M., Miura, Y., Kettoku, M., Komeda, T., and Iwamatsu, A. (1996a). Gene analysis of trehalose-producing enzymes from hyperthermophilic archaea in *Sulfolobales*. Biosci. Biotechnol.

Biochem. *60*, 1720–1723.

Kobayashi, K., Kato, M., Miura, Y., Kettoku, M., Komeda, T., and Iwamatsu, A. (1996b). Gene cloning and expression of new trehalose-producing enzymes from the hyperthermophilic archaeum *Sulfolobus solfataricus* KM1. Biosci. Biotechnol. Biochem. *60*, 1882–1885.

Kobayashi, K., Komeda, T., Miura, Y., Kettoku, M., and Kato, M. (1997). Production of trehalose from starch by novel trehalose-producing enzymes from *Sulfolobus solfataricus* KM1. J. Ferment. Bioeng. *83*, 296–298.

Koonin, E. V., and Tatusov, R.L. (1994). Computer analysis of bacterial haloacid dehalogenases defines a large superfamily of hydrolases with diverse specificity. Application of an iterative approach to database search. J. Mol. Biol. *244*, 125–132.

Kormish, J.D., and McGhee, J.D. (2005). The *C. elegans* lethal gut-obstructed *gob-1* gene is trehalose-6-phosphate phosphatase. Dev. Biol. *287*, 35–47.

Korte, J., Alber, M., Trujillo, C.M., Syson, K., Koliwer-Brandl, H., Deenen, R., Köhrer, K., DeJesus, M.A., Hartman, T., Jacobs, W.R., Bornemann, S., Ioerger, T.R., Ehrt, S., and Kalscheuer, R. (2016). Trehalose-6-phosphate-mediated toxicity determines essentiality of OtsB2 in *Mycobacterium tuberculosis In Vitro* and in Mice. PLOS Pathog. *12*, e1006043.

Krasensky, J., Broyart, C., Rabanal, F.A., and Jonak, C. (2014). The redox-sensitive chloroplast trehalose-6-phosphate phosphatase AtTPPD regulates salt stress tolerance. Antioxid. Redox Signal. *21*, 1289–1304.

Kushwaha, S., Singh, P.K., Rana, A.K., and Misra-Bhattacharya, S. (2011). Cloning, expression, purification and kinetics of trehalose-6-phosphate phosphatase of filarial parasite *Brugia malayi*. Acta Trop. *119*, 151–159.

Kuznetsova, E., Proudfoot, M., Gonzalez, C.F., Brown, G., Omelchenko, M. V, Borozan, I., Carmel, L., Wolf, Y.I., Mori, H., Savchenko, A. V, Arrowsmith, C.H., Koonin, E. V, Edwards, A.M., and Yakunin, A.F. (2006). Genome-wide analysis of substrate specificities of the *Escherichia coli* haloacid dehalogenase-like phosphatase family. J. Biol. Chem. *281*, 36149–36161.

Laemmli, U.K. (1970). Cleavage of structural proteins during assembly of head of bacteriophage-T4.

Nature *227*, 680–685.

Lama, L., Nicolaus, B., Trincone, A., Morzillo, P., De Rosa, M., and Gambacorta, A. (1990). Starch conversion with immobilized thermophilic archaebacterium *Sulfolobus solfataricus*. Biotechnol. Lett. *12*, 431–432.

Lee, J.H., Tsuji, M., Nakamura, M., Nishimoto, M., Okuyama, M., Mori, H., Kimura, A., Matsui, H., and Chiba, S. (2001). Purification and identification of the essential ionizable groups of honeybee, *Apis mellifera* L., trehalase. Biosci. Biotechnol. Biochem. *65*, 2657–2665.

Lee, S.S., Hong, S.Y., Errey, J.C., Izumi, A., Davies, G.J., and Davis, B.G. (2011). Mechanistic evidence for a front-side, S_Ni-type reaction in a retaining glycosyltransferase. Nat Chem Biol *7*, 631–638.

Lemieux, R.U., and Bauer, H.F. (1954). A chemical synthesis of D-trehalose. Can. J. Chem. *32*, 340–344.

Leyman, B., Van Dijck, P., and Thevelein, J.M. (2001). An unexpected plethora of trehalose biosynthesis genes in *Arabidopsis thaliana*. Trends Plant Sci. *6*, 510–513.

Lin, Q., Yang, J., Wang, Q., Zhu, H., Chen, Z., Dao, Y., and Wang, K. (2019). Overexpression of the trehalose-6-phosphate phosphatase family gene *AtTPPF* improves the drought tolerance of *Arabidopsis thaliana*. BMC Plant Biol. *19*, 381.

Lin, Q., Wang, S., Dao, Y., Wang, J., and Wang, K. (2020). *Arabidopsis thaliana* trehalose-6-phosphate phosphatase gene *TPPI* enhances drought tolerance by regulating stomatal apertures. J. Exp. Bot. *71*, 4285–4297.

Liu, C., and Mariano, P.S. (2015). An improved method for the large scale preparation of α,α′-trehalose-6-phosphate. Tetrahedron Lett. *56*, 3008–3010.

Lombard, V., Golaconda Ramulu, H., Drula, E., Coutinho, P.M., and Henrissat, B. (2014). The carbohydrate-active enzymes database (CAZy) in 2013. Nucleic Acids Res. *42*, 490–495.

Lowry, O.H., and Lopez, J.A. (1946). The determination of inorganic phosphate in the presence of labile phosphate esters. J. Biol. Chem. *162*, 421–428.

Lu, Z., Dunaway-Mariano, D., and Allen, K.N. (2005). HAD superfamily phosphotransferase substrate

diversification: structure and function analysis of HAD subclass IIB sugar phosphatase BT4131. Biochemistry *44*, 8684–8696.

Lunn, J.E. (2007). Gene families and evolution of trehalose metabolism in plants. Funct. Plant Biol. *34*, 550–563.

Lunn, J.E., Feil, R., Hendriks, J.H.M., Gibon, Y., Morcuende, R., Osuna, D., Scheible, W.R., Carillo, P., Hajirezaei, M.R., and Stitt, M. (2006). Sugar-induced increases in trehalose 6-phosphate are correlated with redox activation of ADPglucose pyrophosphorylase and higher rates of starch synthesis in *Arabidopsis thaliana*. Biochem. J. *397*, 139–148.

Lunn, J.E., Delorge, I., Figueroa, C.M., Van Dijck, P., and Stitt, M. (2014). Trehalose metabolism in plants. Plant J. *79*, 544–567.

Mach, H., Volkin, D.B., Burke, C.J., and Middaugh, C.R. (1995). Ultraviolet absorption spectroscopy. In Methods in Molecular Biology, B.A. Shirley, ed. (New Jersey: Humana Press), pp. 91–114.

Maeo, K., Tokuda, T., Ayame, A., Mitsui, N., Kawai, T., Tsukagoshi, H., Ishiguro, S., and Nakamura, K. (2009). An AP2-type transcription factor, WRINKLED1, of *Arabidopsis thaliana* binds to the AW-box sequence conserved among proximal upstream regions of genes involved in fatty acid synthesis. Plant J. *60*, 476–487.

Marechal, L.R., and Belocopitow, E. (1972). Metabolism of trehalose in *Euglena gracilis*. J. Biol. Chem. *247*, 3223–3228.

Martins, M.C.M., Hejazi, M., Fettke, J., Steup, M., Feil, R., Krause, U., Arrivault, S., Vosloh, D., Figueroa, C.M., Ivakov, A., Yadav, U.P., Piques, M., Metzner, D., Stitt, M., and Lunn, J.E. (2013). Feedback inhibition of starch degradation in *Arabidopsis* leaves mediated by trehalose 6-phosphate. Plant Physiol. *163*, 1142–1163.

Maruta, K., Mitsuzumi, H., Nakada, T., Kubota, M., Chaen, H., Fukuda, S., Sugimoto, T., and Kurimoto, M. (1996). Cloning and sequencing of a cluster of genes encoding novel enzymes of trehalose biosynthesis from thermophilic archaebacterium *Sulfolobus acidocaldarius*. Biochim. Biophys. Acta *1291*, 177–181.

McCarter, J.D., and Withers, S.G. (1994). Mechanisms of enzymatic glycoside hydrolysis. Curr. Opin.

Struct. Biol. *4*, 885–892.

McCoy, A.J., Grosse-Kunstleve, R.W., Adams, P.D., Winn, M.D., Storoni, L.C., and Read, R.J. (2007). *Phaser* crystallographic software. J Appl Crystallogr *40*, 658–674.

Miao, Y., Tenor, J.L., Toffaletti, D.L., Washington, E.J., Liu, J., Shadrick, W.R., Schumacher, M.A., Lee, R.E., Perfect, J.R., and Brennan, R.G. (2016). Structures of trehalose-6-phosphate phosphatase from pathogenic fungi reveal the mechanisms of substrate recognition and catalysis. Proc. Natl. Acad. Sci. U. S. A. *113*, 7148–7153.

Miranda, J.A., Avonce, N., Suárez, R., Thevelein, J.M., Van Dijck, P., and Iturriaga, G. (2007). A bifunctional TPS-TPP enzyme from yeast confers tolerance to multiple and extreme abiotic-stress conditions in transgenic *Arabidopsis*. Planta *226*, 1411–1421.

Mittenbühler, K., and Holzer, H. (1988). Purification and characterization of acid trehalase from the yeast suc2 mutant. J. Biol. Chem. *263*, 8537–8543.

Miwa, I., Okuda, J., Maeda, K., and Okuda, G. (1972). Mutarotase effect on colorimetric determination of blood glucose with β-D-glucose oxidase. Clin. Chim. Acta *37*, 538–540.

Moore, S., and Stein, W.H. (1948). Photometric ninhydrin method for use in the chromatography of amino acids. J. Biol. Chem. *176*, 367–388.

Mori, H., Lee, J.H., Okuyama, M., Nishimoto, M., Ohguchi, M., Kim, D., Kimura, A., and Chiba, S. (2009). Catalytic reaction mechanism based on α-secondary deuterium isotope effects in hydrolysis of trehalose by european honeybee trehalase. Biosci. Biotechnol. Biochem. *73*, 2466–2473.

Müller, J., Aeschbacher, R., Wingler, A., Boller, T., and Wiemken, A. (2001). Trehalose and trehalase in *Arabidopsis*. Plant Physiol. *125*, 1086–1093.

Murao, S., Nagano, H., Ogura, S., and Nishino, T. (1985). Enzymatic synthesis of trehalose from maltose. Agric. Biol. Chem. *49*, 2113–2118.

Nakada, T., Maruta, K., Mitsuzumi, H., Kubota, M., Chaen, H., Sugimoto, T., Kurimoto, M., and Tsujisaka, Y. (1995a). Purification and characterization of a novel enzyme, maltooligosyl trehalose trehalohydrolase, from *Arthrobacter* sp. Q36. Biosci. Biotechnol. Biochem. *59*, 2215–2218.

Nakada, T., Maruta, K., Tsusaki, K., Kubota, M., Chaen, H., Sugimoto, T., Kurimoto, M., and Tsujisaka, Y. (1995b). Purification and properties of a novel enzyme, maltooligosyl trehalose synthase, from *Arthrobacter* sp. Q36. Biosci. Biotechnol. Biochem. *59*, 2210–2214.

Nakai, H., Baumann, M.J., Petersen, B.O., Westphal, Y., Schols, H., Dilokpimol, A., Hachem, M.A., Lahtinen, S.J., Duus, J.Ø., and Svensson, B. (2009). The maltodextrin transport system and metabolism in *Lactobacillus acidophilus* NCFM and production of novel α-glucosides through reverse phosphorolysis by maltose phosphorylase. FEBS J. *276*, 7353–7365.

Nakai, H., Dilokpimol, A., Hachem, M.A., and Svensson, B. (2010). Efficient one-pot enzymatic synthesis of α-(1→4)-glucosidic disaccharides through a coupled reaction catalysed by *Lactobacillus acidophilus* NCFM maltose phosphorylase. Carbohydr. Res. *345*, 1061–1064.

Navon, G., Shulman, R.G., Yamane, T., Eccleshall, T.R., Lam, K.B., Baronofsky, J.J., and Marmur, J. (1979). Phosphorus-31 nuclear magnetic resonance studies of wild-type and glycolytic pathway mutants of *Saccharomyces cerevisiae*. Biochemistry *18*, 4487–4499.

Ni, M., and Yu, J.H. (2007). A novel regulator couples sporogenesis and trehalose biogenesis in *Aspergillus nidulans*. PLoS One *2*, 1–9.

Nihira, T., Nakai, H., Chiku, K., and Kitaoka, M. (2012). Discovery of nigerose phosphorylase from *Clostridium phytofermentans*. Appl. Microbiol. Biotechnol. *93*, 1513–1522.

Nihira, T., Saito, Y., Chiku, K., Kitaoka, M., and Nakai, H. (2013). Potassium ion-dependent trehalose phosphorylase from halophilic *Bacillus selenitireducens* MLS10. FEBS Lett. *587*, 3382–3386.

Nishimoto, T., Nakano, M., Ikegami, S., Chaen, H., Fukuda, S., Sugimoto, T., Kurimoto, M., and Tsujisaka, Y. (1995). Existence of a novel enzyme converting maltose into trehalose. Biosci. Biotechnol. Biochem. *59*, 2189–2190.

Nishimoto, T., Nakano, M., Nakada, T., Chaen, H., Fukuda, S., Sugimoto, T., Kurimoto, M., and Tsujisaka, Y. (1996). Purification and properties of a novel enzyme, trehalose synthase, from *Pimelobacter* sp. R48. Biosci. Biotechnol. Biochem. *60*, 640–644.

O'Leary, B., Park, J., and Plaxton, W.C. (2011). The remarkable diversity of plant PEPC (phosphoenolpyruvate carboxylase): recent insights into the physiological functions and post-translational

controls of non-photosynthetic PEPCs. Biochem. J. *436*, 15–34.

Pace, C.N., Vajdos, F., Fee, L., Grimsley, G., and Gray, T. (1995). How to measure and predict the molar absorption coefficient of a protein. Protein Sci. *4*, 2411–2423.

Pan, Y.T., Koroth Edavana, V., Jourdian, W.J., Edmondson, R., Carroll, J.D., Pastuszak, I., and Elbein, A.D. (2004). Trehalose synthase of *Mycobacterium smegmatis*: purification, cloning, expression, and properties of the enzyme. Eur. J. Biochem. *271*, 4259–4269.

Postma, P.W., Keizer, H.G., and Koolwijk, P. (1986). Transport of trehalose in *Salmonella typhimurium*. J. Bacteriol. *168*, 1107–1111.

Pramanik, M.H.R., and Imai, R. (2005). Functional identification of a trehalose 6-phosphate phosphatase gene that is involved in transient induction of trehalose biosynthesis during chilling stress in rice. Plant Mol. Biol. *58*, 751–762.

Purvis, J.E., Yomano, L.P., and Ingram, L.O. (2005). Enhanced trehalose production improves growth of *Escherichia coli* under osmotic stress. Appl. Environ. Microbiol. *71*, 3761–3769.

Puttikamonkul, S., Willger, S.D., Grahl, N., Perfect, J.R., Movahed, N., Bothner, B., Park, S., Paderu, P., Perlin, D.S., and Cramer, R.A. (2010). Trehalose 6-phosphate phosphatase is required for cell wall integrity and fungal virulence but not trehalose biosynthesis in the human fungal pathogen *Aspergillus fumigatus*. Mol. Microbiol. *77*, 891–911.

Qu, Q., Lee, S.J., and Boos, W. (2004). TreT, a novel trehalose glycosyltransferring synthase of the hyperthermophilic archaeon *Thermococcus litoralis*. J. Biol. Chem. *279*, 47890–47897.

Ramon, M., De Smet, I., Vandesteene, L., Naudts, M., Leyman, B., Van Dijck, P., Rolland, F., Beeckman, T., and Thevelein, J.M. (2009). Extensive expression regulation and lack of heterologous enzymatic activity of the Class II trehalose metabolism proteins from *Arabidopsis thaliana*. Plant, Cell Environ. *32*, 1015–1032.

Richards, A.B., Krakowka, S., Dexter, L.B., Schmid, H., Wolterbeek, A.P.M., Waalkens-Berendsen, D.H., Shigoyuki, A., and Kurimoto, M. (2002). Trehalose: a review of properties, history of use and human tolerance, and results of multiple safety studies. Food Chem. Toxicol. *40*, 871–898.

Rimmele, M., and Boos, W. (1994). Trehalose-6-phosphate hydrolase of *Escherichia coli*. J. Bacteriol. *176*, 5654–5664.

Robinson, O., Dylus, D., and Dessimoz, C. (2016). Phylo.io : interactive viewing and comparison of large phylogenetic trees on the web. Mol. Biol. Evol. *33*, 2163–2166.

Romero, C., Bellés, J.M., Vayá, J.L., Serrano, R., and Culiáñez-Macià, F.A. (1997). Expression of the yeast trehalose-6-phosphate synthase gene in transgenic tobacco plants: pleiotropic phenotypes include drought tolerance. Planta *201*, 293–297.

Rønnow, T.E.C.L., Meldal, M., and Bock, K. (1994). Gram-scale synthesis of α,α-trehalose 6-monophosphate and α,α-trehalose 6,6′-diphosphate. Carbohydr. Res. *260*, 323–328.

Rye, C.S., and Withers, S.G. (2000). Glycosidase mechanisms. Curr. Opin. Chem. Biol. *4*, 573–580.

Ryu, S.I., Park, C.S., Cha, J., Woo, E.J., and Lee, S.B. (2005). A novel trehalose-synthesizing glycosyltransferase from *Pyrococcus horikoshii*: molecular cloning and characterization. Biochem. Biophys. Res. Commun. *329*, 429–436.

Sambrook, J., and Russell, D.W. (2001). Molecular cloning: a laboratory manual. (Cold spring harbor laboratory press), pp. 1–32–1–34.

Sasajima, K., Kawachi, T., Sato, S., and Sugimura, T. (1975). Purification and properties of α,α-trehalase from the mucosa of rat small intestine. Biochim. Biophys. Acta - Enzymol. *403*, 139–146.

Satoh-Nagasawa, N., Nagasawa, N., Malcomber, S., Sakai, H., and Jackson, D. (2006). A trehalose metabolic enzyme controls inflorescence architecture in maize. Nature *441*, 227–230.

Schägger, H., Cramer, W.A., and Vonjagow, G. (1994). Analysis of molecular masses and oligomeric states of protein complexes by blue native electrophoresis and isolation of membrane protein complexes by two-dimensional native electrophoresis. Anal. Biochem. *217*, 220–230.

Schluepmann, H., Pellny, T., van Dijken, A., Smeekens, S., and Paul, M. (2003). Trehalose 6-phosphate is indispensable for carbohydrate utilization and growth in *Arabidopsis thaliana*. Proc. Natl. Acad. Sci. U. S. A. *100*, 6849–6854.

Schmid, M., Davison, T.S., Henz, S.R., Pape, U.J., Demar, M., Vingron, M., Schölkopf, B., Weigel, D., and Lohmann, J.U. (2005). A gene expression map of *Arabidopsis thaliana* development. Nat. Genet. *37*, 501–506.

Schöck, F., and Dahl, M.K. (1996). Analysis of DNA flanking the *treA* gene of *Bacillus subtilis* reveals genes encoding a putative specific enzyme IITre and a potential regulator of the trehalose operon. Gene *175*, 59–63.

Seifried, A., Schultz, J., and Gohla, A. (2013). Human HAD phosphatases: structure, mechanism, and roles in health and disease. FEBS J. *280*, 549–571.

Shi, Y., Sun, H., Wang, X., Jin, W., Chen, Q., Yuan, Z., and Yu, H. (2019). Physiological and transcriptomic analyses reveal the molecular networks of responses induced by exogenous trehalose in plant. PLoS One *14*, e0217204.

Shibuya, T., and Izawa, S. (2016). Manufacturing method of powder containg α,α-crystalline trehalose dihydrate (Japan)., JP2017063791A.

Shima, S., Matsui, H., Tahara, S., and Imai, R. (2007). Biochemical characterization of rice trehalose-6-phosphate phosphatases supports distinctive functions of these plant enzymes. FEBS J. *274*, 1192–1201.

Singh, V., and Shah, J. (2012). Tomato responds to green peach aphid infestation with the activation of trehalose metabolism and starch accumulation. Plant Signal. Behav. *7*, 605–607.

Sinnott, M.L. (1990). Catalytic mechanism of enzymic glycosyl transfer. Chem. Rev. *90*, 1171–1202.

Steiner, A., and Cori, C.F. (1935). The preparation and determination of trehalose in yeast. Science *82*, 422–423.

Stewart, L.C., Richtmyer, N.K., and Hudson, C.S. (1950). The preparation of trehalose from yeast. J. Am. Chem. Soc. *72*, 2059–2061.

Su, W., Huber, S.C., and Crawford, N.M. (1996). Identification in vitro of a post-translational regulatory site in the hinge 1 region of *Arabidopsis* nitrate reductase. Plant Cell *8*, 519–527.

Suzuki, M., Kaneda, K., Nakai, Y., Kitaoka, M., and Taniguchi, H. (2009). Synthesis of cellobiose from

starch by the successive actions of two phosphorylases. N. Biotechnol. *26*, 137–142.

Taguchi, Y., Saburi, W., Imai, R., and Mori, H. (2017). Evaluation of acceptor selectivity of *Lactococcus lactis* ssp. *lactis* trehalose 6-phosphate phosphorylase in the reverse phosphorolysis and synthesis of a new sugar phosphate. Biosci. Biotechnol. Biochem. *81*, 1512–1519.

Taguchi, Y., Saburi, W., Imai, R., and Mori, H. (2020). Efficient one-pot enzymatic synthesis of trehalose 6-phosphate using GH65 α-glucoside phosphorylases. Carbohydr. Res. *488*, 107902.

Tian, L., Xie, Z., Lu, C., Hao, X., Wu, S., Huang, Y., Li, D., and Chen, L. (2019). The trehalose-6-phosphate synthase TPS5 negatively regulates ABA signaling in *Arabidopsis thaliana*. Plant Cell Rep. *38*, 869–882.

Tsusaki, K., Nishimoto, T., Nakada, T., Kubota, M., Chaen, H., Sugimoto, T., and Kurimoto, M. (1996). Cloning and sequencing of trehalose synthase gene from *Pimelobacter* sp. R48. Biochim. Biophys. Acta *1290*, 1–3.

Vandesteene, L., Ramon, M., Le Roy, K., Van Dijck, P., and Rolland, F. (2010). A single active trehalose-6-P synthase (TPS) and a family of putative regulatory TPS-like proteins in *Arabidopsis*. Mol. Plant *3*, 406–419.

Van Dijck, P., Mascorro-gallardo, J.O., Bus, M.D.E., Royackers, K., Iturriaga, G., and Thevelein, J.M. (2002). Truncation of *Arabidopsis thaliana* and *Selaginella lepidophylla* trehalose-6-phosphate synthase unlocks high catalytic activity and supports high trehalose levels on expression in yeast. Biochem. J. *71*, 63–71.

Van Dijken, A.J.H., Schluepmann, H., and Smeekens, S.C.M. (2004). *Arabidopsis* trehalose-6-phosphate synthase 1 is essential for normal vegetative growth and transition to flowering. Plant Physiol. *135*, 969–977.

Van Heerden, J.H., Wortel, M.T., Bruggeman, F.J., Heijnen, J.J., Bollen, Y.J.M., Planqué, R., Hulshof, J., O'Toole, T.G., Wahl, S.A., and Teusink, B. (2014). Lost in transition: start-up of glycolysis yields subpopulations of nongrowing cells. Science *343*, 1245114.

Van Houtte, H., Vandesteene, L., López-Galvis, L., Lemmens, L., Kissel, E., Carpentier, S., Feil, R., Avonce, N., Beeckman, T., Lunn, J.E., and Van Dijck, P. (2013). Overexpression of the trehalase gene

AtTRE1 leads to increased drought stress tolerance in *Arabidopsis* and is involved in abscisic acid-induced stomatal closure. Plant Physiol. *161*, 1158–1171.

Vogel, G., Müller, J., Vogel, G., Aeschbacher, R.A., Mu, J., Boller, T., and Wiemken, A. (1998). Trehalose-6-phosphate phosphatases from *Arabidopsis thaliana*: identification by functional complementation of the yeast tps2 mutant. Plant Cell *13*, 673–683.

Wahl, V., Ponnu, J., Schlereth, A., Arrivault, S., Langenecker, T., Franke, A., Feil, R., Lunn, J.E., Stitt, M., and Schmid, M. (2013). Regulation of flowering by trehalose-6-phosphate signaling in *Arabidopsis thaliana*. Science *339*, 704–707.

Wang, J.W., Czech, B., and Weigel, D. (2009). miR156-Regulated SPL transcription factors define an endogenous flowering pathway in *Arabidopsis thaliana*. Cell *138*, 738–749.

Wang, W., Chen, Q., Xu, S., Liu, W., Zhu, X., and Song, C. (2020). Trehalose-6-phosphate phosphatase E modulates ABA-controlled root growth and stomatal movement in *Arabidopsis*. J. Integr. Plant Biol. *62*, 1518–1534.

Wildberger, P., Pfeiffer, M., Brecker, L., Rechberger, G.N., Birner-Gruenberger, R., and Nidetzky, B. (2015). Phosphoryl transfer from α-D-glucose 1-phosphate catalyzed by *Escherichia coli* sugar-phosphate phosphatases of two protein superfamily types. Appl. Environ. Microbiol. *81*, 1559–1572.

Winter, D., Vinegar, B., Nahal, H., Ammar, R., Wilson, G. V., and Provart, N.J. (2007). An "electronic fluorescent pictograph" browser for exploring and analyzing large-scale biological data sets. PLoS One *2*, e718.

Yadav, U.P., Ivakov, A., Feil, R., Duan, G.Y., Walther, D., Giavalisco, P., Piques, M., Carillo, P., Hubberten, H.M., Stitt, M., and Lunn, J.E. (2014). The sucrose-trehalose 6-phosphate (Tre6P) nexus: specificity and mechanisms of sucrose signalling by Tre6P. J. Exp. Bot. *65*, 1051–1068.

Yamaguchi, A., Wu, M.F., Yang, L., Wu, G., Poethig, R.S., and Wagner, D. (2009). The microRNA-regulated SBP-Box transcription factor SPL3 is a direct upstream activator of *LEAFY*, *FRUITFULL*, and *APETALA1*. Dev. Cell *17*, 268–278.

Yang, H.L., Liu, Y.J., Wang, C.L., and Zeng, Q.Y. (2012). Molecular evolution of trehalose-6-phosphate synthase (TPS) gene family in *Populus*, *Arabidopsis* and rice. PLoS One *7*, e42438.

Yang, Y., Costa, A., Leonhardt, N., Siegel, R.S., and Schroeder, J.I. (2008). Isolation of a strong *Arabidopsis* guard cell promoter and its potential as a research tool. Plant Methods *4*, 6.

Yoshida, M., Nakamura, N., and Horikoshi, K. (1997). Production of trehalose from starch by maltose phosphorylase and trehalose phosphorylase from a strain of *Plesiomonas*. Starch - Stärke *49*, 21–26.

Yoshida, M., Nakamura, N., and Horikoshi, K. (1998). Production of trehalose by a dual enzyme system of immobilized maltose phosphorylase and trehalose phosphorylase. Enzyme Microb. Technol. *22*, 71–75.

Zang, B., Li, H., Li, W., Deng, X.W., and Wang, X. (2011). Analysis of trehalose-6-phosphate synthase (TPS) gene family suggests the formation of TPS complexes in rice. Plant Mol. Biol. *76*, 507–522.

Zhai, Z., Liu, H., and Shanklin, J. (2017). Phosphorylation of WRINKLED1 by KIN10 results in its proteasomal degradation, providing a link between energy homeostasis and lipid biosynthesis. Plant Cell *29*, 871–889.

Zhai, Z., Keereetaweep, J., Liu, H., Feil, R., Lunn, J.E., and Shanklin, J. (2018). Trehalose 6-phosphate positively regulates fatty acid synthesis by sabilizing WRINKLED1. Plant Cell *30*, 2616–2627.

Zhang, G., Dai, J., Wang, L., Dunaway-Mariano, D., Tremblay, L.W., and Allen, K.N. (2005). Catalytic cycling in β-phosphoglucomutase: a kinetic and structural analysis. Biochemistry *44*, 9404–9416.

Zhang, Y., Primavesi, L.F., Jhurreea, D., Andralojc, P.J., Mitchell, R.A.C., Powers, S.J., Schluepmann, H., Delatte, T., Wingler, A., and Paul, M.J. (2009). Inhibition of SNF1-related protein kinase1 activity and regulation of metabolic pathways by trehalose-6-phosphate. Plant Physiol. *149*, 1860–1871.

ACKNOWLEDGEMENTS

First of all, I would like to express my sincere gratitude to my first advisor, Professor Haruhide Mori for his kindly suggestion throughout my project and giving me words of encouragement supervision. Besides, I deeply appreciate Associate Professor Wataru Saburi for guidance and his help in progressing my research.

I would also like to thank Professor Haruhide Mori, Professor Atsushi Yokota, Professor Hideyuki Matsuura, and Associate Professor Wataru Saburi for their guidance and encouragement in preparing this paper. I would like to thank Dr. Ryozo Imai, principal researcher, Institute of Agrobiological Science, National Agriculture and Food Research Organization, for his advice on the execution of research on plants. Regarding the X-ray crystal structure analysis of proteins, I would like to thank Professor Min Yao and Assistant Professor Jian Yu, Faculty of Advanced Life Science, Hokkaido University for their advice. I would like to thank Dr. Eri Fukushi, GC-MS & NMR Room, Research Faculty of Agriculture, Hokkaido University for her cooperation in the measurement of NMR. I would like to express our gratitude to Mr. Tomohiro Hirose, Instrumental Analysis Division, Global Facility Center, Creative Research Institution, Hokkaido University for performing ESI-MS analysis using Thermo Scientific Exactive and providing insight and expertise that greatly assisted the research. I would like to express our gratitude to Ms. Nozomi Takeda, Instrumental Analysis Division, Global Facility Center, Creative Research Institution, Hokkaido University for performing amino acid analysis using JLC-500/V and L-8900 and providing insight and expertise that greatly assisted the research. I would like to thank Professor Emeritus Hirokazu Matsui of the Research Faculty of Agriculture, Hokkaido University for giving us an opportunity to think deeply about how to live as a researcher. This work was supported by JSPS Grant-in-Aid for JSPS Fellows Grant Number 18J20503.

I would like to express our sincere gratitude to all the graduates and current students of Biochemistry Laboratory, including Dr. Daisuke Tezuka, and Mr. Shu Horikoshi, who helped me technically and mentally in my research and personal life. Finally, I would like to express my deep gratitude to my parents who warmly watched over my student life and supported me financially and mentally.

Yodai Taguchi

謝辞

本研究を遂行するにあたり，研究室配属時より，厳しくも愛のあるご指導をいただきました北海道大学大学院農学研究院　森　春英　教授および佐分利　亘　准教授に深く感謝申し上げます．

また，本論文を作成するにあたり，ご指導，ご鞭撻をいただきました北海道大学大学院農学研究院　森　春英　教授，横田　篤　教授，松浦　英幸　教授，および佐分利　亘　准教授に感謝いたします．

植物に関する研究の遂行には農研機構・生物機能利用研究部門　主席研究員　今井　亮三　博士に多くのご助言を賜りました．厚く御礼申し上げます．

タンパク質の X 線結晶構造解析につきましては，北海道大学大学院先端生命科学研究院生命融合科学コース X 線構造生物学研究室　姚　閔　教授，ならびに于　健　助教に多くのご助言を賜り感謝いたします．

NMR の測定にご協力いただきました北海道大学大学院農学研究院 GC-MS＆NMR 室　福士　江里　博士に感謝いたします．

Thermo Scientific Exactive を使用した ESI-MS 測定を実施していただくとともに、有益なご助言をいただいた北海道大学 創成研究機構 グローバルファシリティセンター 機器分析受託部門 広瀬　知弘　氏に感謝いたします．

JLC-500/V および L-8900 を使用したアミノ酸組成分析を実施していただくとともに、有益なご助言をいただいた北海道大学 創成研究機構 グローバルファシリティセンター 機器分析受託部門 武田　希美　氏に感謝いたします．

研究者としてどう生きるかを深く考えるきっかけを与えてくださった北海道大学大学院農学研究院　松井　博和　名誉教授に感謝申し上げます．

本研究は JSPS 特別研究員奨励費 18J20503 の助成を受けたものです。厚く御礼申し上げます．

研究や私生活でも相談相手になっていただき，精神的に支えてくださった農研機構・生物機能利用研究部門　手塚　大介　博士，北海道大学大学院農学院博士課程2年　堀越　秀　氏をはじめ，生物化学研究室の卒業生と在校生の皆様に心より感謝申し上げます．

最後になりましたが，学生生活を温かく見守り，経済的・精神的に支えてくださった両親に深く感謝いたします．

田口陽大